Chemical looping combustion for coupling with efficient CO_2 capture and utilization: stable oxygen carriers and carbon cycle

Zhang, Y., Han, H., Zhu, N., Che, Y., Zhang, X., Xue, Y., Deng, J., Wu, C., Wang, H., Chen, Y., & Yi, S. (2025). Chemical looping combustion for coupling with efficient CO_2 capture and utilization: stable oxygen carriers and carbon cycle. *Industrial and Engineering Chemistry Research*. Advance online publication. https://doi.org/10.1021/acs.iecr.4c03713

Published in:
Industrial and Engineering Chemistry Research

Document Version:
Publisher's PDF, also known as Version of record

I&EC research
Industrial & Engineering Chemistry Research

pubs.acs.org/IECR
Review

Chemical Looping Combustion for Coupling with Efficient CO_2 Capture and Utilization: Stable Oxygen Carriers and Carbon Cycle

Published as part of Industrial & Engineering Chemistry Research special issue "2024 Class of Influential Researchers".

Yanan Zhang, Hongjing Han, Nini Zhu, Yu Che, Xiaodan Zhang, Yan Xue, Jitong Deng, Chunfei Wu, Haiying Wang, Yanguang Chen,* and Shouliang Yi*

Cite This: https://doi.org/10.1021/acs.iecr.4c03713

ABSTRACT: The capture of CO_2 with chemical looping combustion (CLC) offers a novel approach to significantly reduce carbon emissions while simultaneously utilizing captured CO_2 as a valuable resource by leveraging its inherent CO_2 separation capability. The separation of CO_2 in CLC technology achieves low-cost CO_2 capture through the utilization of highly efficient oxygen carriers (OC), enabling the coupling of CO_2 capture with subsequent hydrogenation reactions for high-value-added chemical production. This review comprehensively summarizes the principle of the CLC technology, the current status of OC research, and the potential for CO_2 capture in chemical synthesis, providing theoretical insights into the feasibility of activating and utilizing CO_2 within practical industrial processes. The stable OC brought about excellent properties and higher application value in the long term operation. The careful selection of a stable OC and the rational design of oxygen vacancies are the keys to enable this technology; however, further research is needed to develop a highly efficient and stable OC to optimize the CO_2 capture efficiency and product yields while elucidating the underlying reaction mechanisms.

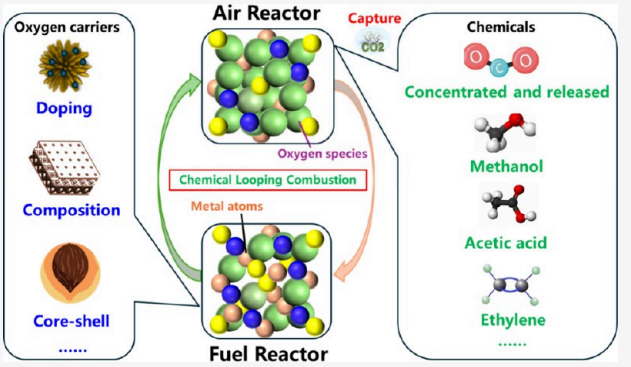

1. INTRODUCTION

The emissions of CO_2 have increased dramatically in recent years with the increase of industry and the combustion of fossil fuels (coal, oil, and natural gas). In 2023, the emission amount of CO_2 related to global energy had increased by 1.1%, that is, by 410 million tons, which reached a higher record of 37.4 billion tons. Of this, the emission amount caused by the combustion of coal accounted for >65% of the total emissions in 2023, as shown in Figure 1.[1,2] CO_2, as one of the major greenhouse gases, has been receiving worldwide attention due to global warming and its massive emissions. The United Nations Environment Program (UNEP) report showed that the global average temperature will rise by at least 2 °C by 2050 without any measurements.[3] To avoid this, the "low carbon economy" is proposed to reduce emissions from sources, with the goal that the emissions of greenhouse gases (such as CO_2) would be reduced by at least 50% by 2050, compared to 1990.[4] On the other hand, it is possible to reduce the concentration of CO_2 in the atmosphere by capturing and storing CO_2 and transforming it using chemical methods. Hence, Carbon Capture, Utilization and Storage (CCUS) has become the most economical and feasible way to reduce large-scale greenhouse gas emissions and minimize global warming in the future. This technology can realize the end-end emission reduction treatment of industrial exhaust gases and is anticipated to reach the net-zero emission of CO_2 by utilizing fossil energy, which has been considered an effective method for reducing CO_2.

For the CCUS technology, the cost of carbon capture occupies 70% of the total cost of CCUS.[5] Moreover, the efficiency of carbon capture and its economic benefits are crucial to CCUS technology. Thus, the core of the CCUS technology is CO_2 capture, and CO_2 capture technology exerts an important role in carbon neutralization and carbon peaking. Based on the CO_2 capture processes, CO_2 capture technologies in Figure 2 primarily include precombustion capture, oxygen-enriched combustion capture, postcombustion capture, and chemical looping combustion (CLC) capture, *etc.*[6] Post-combustion capture refers to capturing the CO_2 in the

Received: October 2, 2024
Revised: January 3, 2025
Accepted: January 6, 2025

https://doi.org/10.1021/acs.iecr.4c03713
Ind. Eng. Chem. Res. XXXX, XXX, XXX−XXX

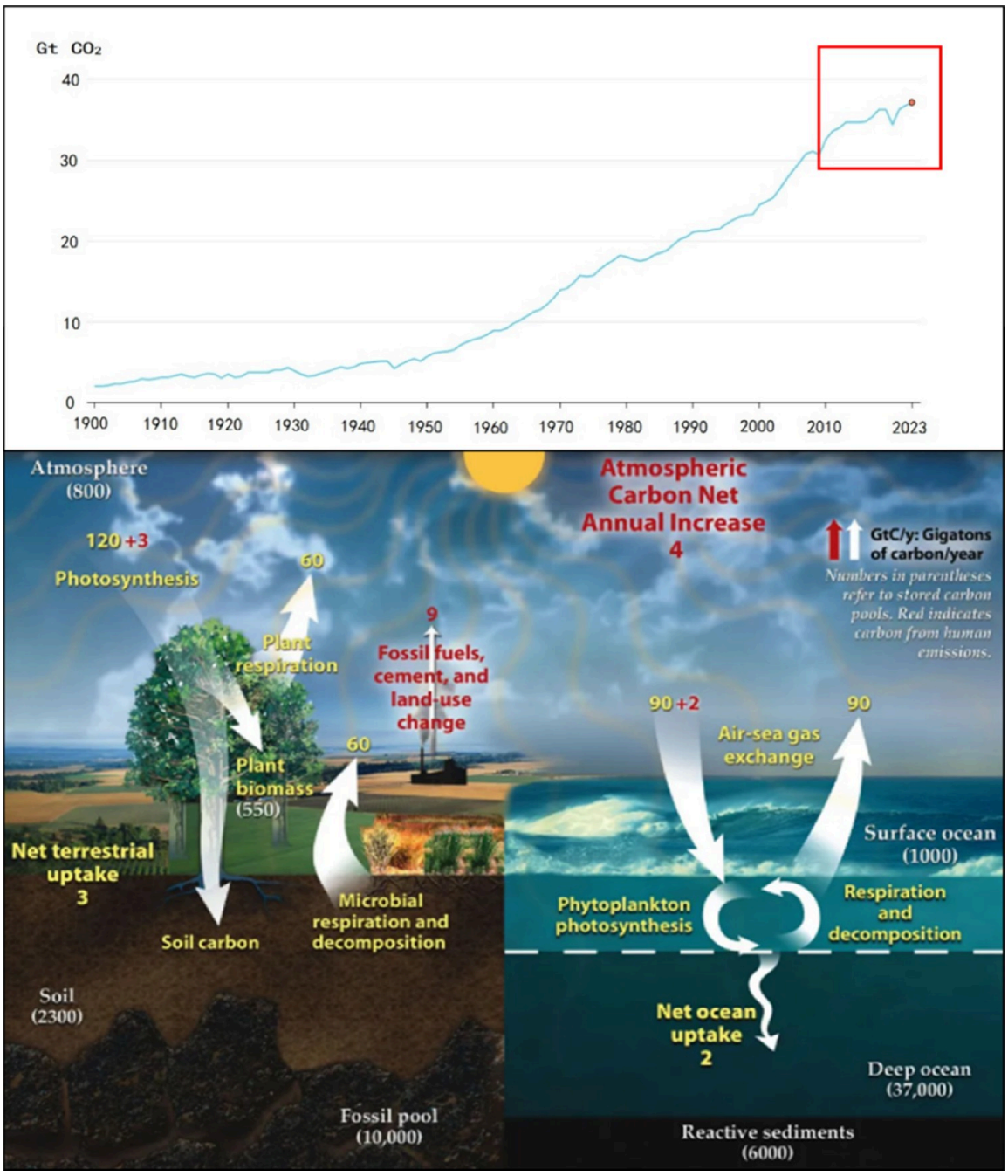

Figure 1. Circular path and magnitude of carbon in the Earth and the global energy-related CO_2 emissions in 1900−2023. (The red part is part of the emissions under human influence, the yellow part is the carbon cycle flux in nature, and the white number represents the stored carbon in one billion tons of carbon elements.)

products before releasing it into the atmosphere.[7] At present, the commonly employed method is the employment of renewable solvents (such as monoethanolamine, MEA) to remove CO_2 from the waste gas, which is a relatively simple process. However, due to a large amount of N_2, the concentration of CO_2 in the waste gas is greatly diluted, causing an increase in the energy and cost consumed for CO_2 capture. The precombustion capture technology is the separation of CO_2 from fuel or fuel conversion gas before fuel combustion. The technology requires higher gas pressure, higher CO_2 concentration, and lower impurities, which are mainly utilized in Integrated Gasification Combined Cycle (IGCC) power generation plants. However, this technology is associated with lower efficiencies. The oxygen-enriched combustion capture employs a higher fraction of oxygen to capture CO_2 during the combustion. However, more oxygen is required, and the cost of oxygen production is much higher with explosive danger. Compared with the above-mentioned three technologies, the CLC capture is a novel CO_2 capture means and is considered a promising approach to reduce the cost of capturing CO_2. Since the CLC capture does not require air separation for O_2 production, a higher concentration of CO_2 without N_2 can be produced directly, and a significant reduction in the energy consumption and the cost of CO_2 capture is achieved.

https://doi.org/10.1021/acs.iecr.4c03713
Ind. Eng. Chem. Res. XXXX, XXX, XXX−XXX

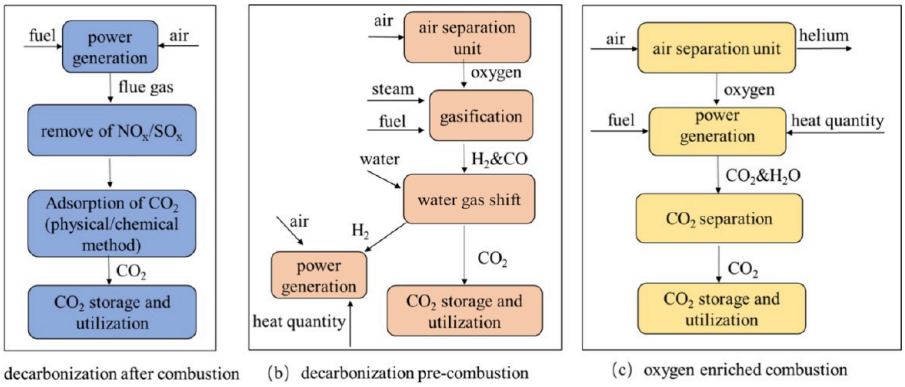

Figure 2. Process of three CCUS technologies.

The "chemical looping" was first proposed by Richter and Knoche in 1983 to improve the combustion efficiency in the power plants.[8] Due to the urgent demand for carbon peak and carbon neutrality, the CLC technology has been in-depth investigated. The CLC technology is a novel generation of combustion technology, which utilizes the lattice oxygen of the oxygen carriers (OCs) instead of the gaseous oxygen in the air to achieve *in situ* carbon capture in the combustion process, and has the advantages of high combustion efficiency and CO_2 internal separation characteristics. Over the past decade, it has emerged as an innovative technology for CO_2 capture and carbon cycle,[9] as illustrated by more than 5000 publications to date. Currently, the study of CLC technology has accumulated massive work and significant insights for further development in the CO_2 capture. Generally, the CLC technology can accomplish the inherent carbon capture with the employment of the OC solid-phase materials,[10] which are substitutes for gaseous oxygen or air in the combustion of carbonaceous fuels. However, two major limitations in current research are identified as follows: 1) the poor stability of the OCs makes it easier to generate the deposition carbon and the weak cyclic stability restricts the large-scale application to some degree, coupled with the absence of effective strategies for their design and optimization, 2) the insufficient understanding of reaction intermediates and OCs without the advanced measurement technology has considerably impeded the progress, and 3) the implementation and universality of efficient CO_2 capture technologies are due to the restriction of the technology cost, the technology maturity, and lower market acceptance. Especially, for the actual industrial production, the OCs with favorable stability and excellent properties are extremely required, and the design of OCs can be achieved via the *in situ* stabilization, the establishment of special structure, and the introduction of composite materials, which are favorable for the transfer and transportation of active oxygen species. This review is focused on the application of CLC technology as a generalized strategy for process enhancement, particularly in the efficient capture of CO_2 and various other applications through the concept of chemical looping and carbon cycling. This approach offers considerable benefits including improved efficiency, energy savings, reduced emissions, and cost-effectiveness. This work aims to examine the design principles of stable OCs or redox catalysts utilized in the CLC reaction process alongside the development of effective CO_2 capture technologies and carbon cycling methodologies.

2. FUNDAMENTAL ASPECTS OF CHEMICAL LOOPING COMBUSTION

2.1. Chemical Looping Combustion: The General Reaction Process and Mechanism. The CLC technology has fundamentally changed the combustion method and the concept of fuel utilization. Its technical principle is illustrated in Figure 3. Unlike the traditional combustion methods, the

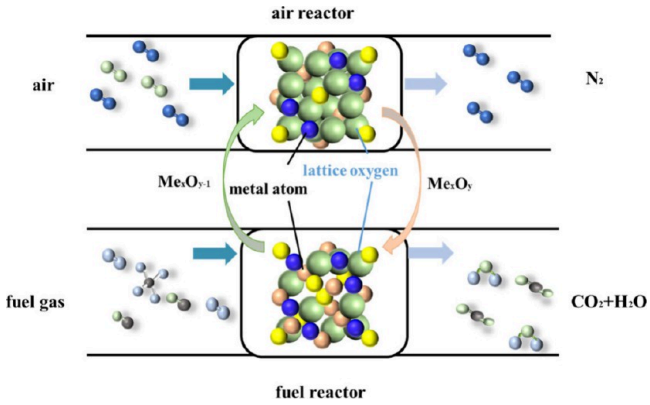

Figure 3. Scheme of the CLC technology.

basic feature of the CLC technology is the combustion process conducted in a fuel reactor (FR) and an air reactor (AR) employing the OC.[11] Meanwhile, CLC technology is not consistent with the conventional combustion method. The basic feature of CLC technology is the oxygen transfer by alternating cycles of the OCs from FR and AR. First, the OC (Me_xO_y) reacts with the fuel (C_nH_{2m}) in the FR, and the Me_xO_y is converted to Me_xO_{y-1}, while the fuel is changed to form the CO_2 and H2O. A high concentration of CO_2 can be obtained from the off gas of the flame retardant by simple condensation. Subsequently, the reduced OC is separated from the residue and fed to the AR for oxidative regeneration and heat generation. The oxidized and regenerated OC are then fed into the FR for the next reduction−oxidation cycle. In the CLC process, the fuel does not contact directly with the atmosphere. However, the lattice oxygen for the fuel combustion is delivered through the OC,[12] which avoids the separation of CO_2 and N_2 in the atmosphere. The produced CO_2 is not diluted by airborne N_2, thus enabling energy-free internal separation of CO_2 in the FR. The chemical reactions occurring are shown in eqs 1 and 2:

https://doi.org/10.1021/acs.iecr.4c03713
Ind. Eng. Chem. Res. XXXX, XXX, XXX−XXX

$$(2n + m)Me_xO_y + C_nH_{2m} \rightarrow (2n + m)Me_xO_{y-1} + nCO_2 + mH_2O + Q1 \quad (1)$$

$$2Me_xO_{y-1} + O_2 \rightarrow 2Me_xO_y + Q2 \quad (2)$$

The conventional combustion reaction is shown in eq 3:

$$C_nH_{2m} + \frac{2n + m}{2}O2 \rightarrow nCO_2 + mH_2O + Q3 \quad (3)$$

During the CLC process, an equal amount of fuel is consumed: Q1 + Q2 = Q3; i.e., the total amount of heat emitted by the two-step chemical reaction of fuel has the same magnitude as that released by the conventional combustion. However, the CLC technology changes the way of releasing the chemical energy of fuel into the energy of heat, by orderly releasing the fuel chemical energy, tapping the effective utilization of the chemical energy grade from fuel, and reducing the difference between the chemical energy grade of fuel and the chemical energy grade of heat.[13] Thus, the irreversible loss of the chemical energy releasing process is reduced, and the graded utilization of fuel chemical energy is effectively realized, which has a higher energy conversion efficiency compared with the traditional combustion method. More importantly, during the combustion process, the fuel is not in direct contact with the air. The reaction temperature in the AR is much lower than that of the thermal NO_x (taking the coal fuel for instance), so there is no thermal NO_x generation.[14] In addition, the reaction in the FR reactor is a gas−solid reaction without a flame, so there is no rapid generation of NO_x. Therefore, CLC technology can greatly reduce the generation of NO_x, which is a major breakthrough in solving the environmental pollution problem of NO_x.

The CLC process is initially focused on the gaseous fuels, and when the fuel is solid, the slow rate of diffusion reaction between the solid−solid phases becomes a key limiting factor for the reaction efficiency, as the OC is also a solid material. For improving the system efficiency, a series of CLC technologies have been developed for solid fuels, including three forms of syngas CLC technology (Syngas-CLC), *in situ* gasification CLC technology (iG-CLC), and chemical looping oxygen uncoupling (CLOU).[15−17] Among them, the Syngas-CLC pregasifies solid fuel, and then the generated syngas reacts with the OC in a gas−solid reaction. The gasifying agent and OC are involved in the reactor together for the reaction during the iG-CLC technology, which couples the gasification process with the CLC process in essence. For this technology, the kinetics from the gasification reaction of solid fuel are the key to determining the reaction efficiency. To enhance the combustion effect, the CLOU technique is gradually developed. This process generally employs the metal oxides (CuO or Mn_2O_3) as the OCs, and the lattice oxygen in these OCs will be released as the gaseous oxygen under the conditions of high temperature so that the fuel can be burned in an oxygen environment, which demonstrates excellent fuel conversion and reaction stability in numerous tests.

2.2. Potential Applications of CLC Process. The CLC technology for the CO_2 capture is displayed in Figure S1. The generalized reactions are all facilitated by the OC solid particles, which represents an important underlying feature of most CLC processes.[18] Apart from solid coal, solid biomass is becoming more popular at present. The concept of sustainable development has gradually become an international consensus, and all countries have paid great attention to biomass energy and regarded the development and utilization of biomass energy as an important component of energy strategies. As an important renewable energy source and solid fuel, the systematic utilization of biomass energy technology is now relatively mature, and the relevant research on biomass by the CLC process has also been also increasing. The CLC technology realizes the gasification of biomass via the multistage reactions with high gasification efficiency and high product quality.[19] At the same time, fine regulation of the product can be accomplished through multiple stages, which solves the problem of unstable products by traditional biomass gasification technology. The introduction of the CLC technology during the biomass conversion has the following advantages: 1) the release of lattice oxygen from the OC replaces the oxygen supply role of the conventional gasification media, overcomes the defects associated with the utilization of the conventional gasification media (the dilution of N_2 and high preparation cost), optimizes the gasification system, and reduces the system cost, 2) the OC runs through the heat and mass transfer process, not only circulating the lattice oxygen but also transferring and utilizing the part of heat, which improves the energy efficiency of system, 3) compared with the gaseous molecular oxygen in the conventional gasification medium, the lattice oxygen of the OC is generally weak in the reactivity, which is more conducive to selective oxidation of biomass and pyrolysis intermediates, and improves the quality of the products, and 4) in the middle and late stages with the reducing atmosphere, the OC is generally also equipped with the ability to catalyze the cracking of tars, which reduce the harm of tar formation to the gasification system,[20] and also improve the syngas yield. The potential applications of the CLC process are illustrated in Table 1, and CLC technology exhibits various applications.

Since the solid−solid reaction rate between solid fuel and OC is slow and difficult to carry out completely, while the gas−solid reaction is faster, it is a more natural idea to convert the harder solid−solid reaction to the easier gas−solid reaction and the faster gas−solid reaction is more conducive to the realization of CLC process and the improvement of energy conversion efficiency. Unlike solid fuels, gaseous fuels during the CLC process first undergo adsorption, while the pyrolysis of solid fuels produces small molecules that react in the same way as the gas fuels. The reduced OC is oxidized very rapid in the AR. In contrast, the reaction between the carrier and the fuel in the FR is relatively slow, which acts as a rate-limiting step. Therefore, the reduction reactions between the OCs and various fuels have been systematically investigated to enhance the CLC process and ensure efficient production. In the reported CLC processes, gaseous fuels (such as H_2, CH_4, syngas, *etc.*)[36−38] have been utilized as fuels for CLC reactions. The CLC process of gaseous fuels is generally investigated in the fixed-bed reaction experiments for the synthesis of OCs, including Fe-based, Ca-based, Cu-based, and Ni-based OCs.[39−42] The cyclic redox reactions are conducted to test the stability of the synthesized OCs. Meanwhile, a numerical model is selected, and the kinetic parameters are solved numerically to explore the process. Then, the process is combined with the experimental data to optimize the existing model and gain an in-depth understanding of the CLC reaction mechanism. The study progress of gaseous fuels is relatively slow due to the instability of gases and the operational uncertainty of experimental conditions, while numerical

https://doi.org/10.1021/acs.iecr.4c03713
Ind. Eng. Chem. Res. XXXX, XXX, XXX−XXX

Table 1. Progress on the Employment of OCs in the Study of CLC Technology

Number	Fuel	The type of OCs	Operating variables	The experimental results	References
1	Methane	$LaFeO_3$	Reaction temperature, pressure, the composition of the OCs, and the doping element	The methane conversion and CO selectivity were 95.2% and 85.1% at 850 °C, respectively.	21
2	Methane	$La_{0.6}Ca_{0.4}FeO_3$	Reaction temperature (850 °C), the concentration of CH_4 and CO_2 (5%), and the doping type of OCs (CO, Co, Ni-Co)	Doping the OC with only 5 at % Ni-Co (2.5 at % each) greatly increased the gas conversion by 6 times, compared to the bare OC. The Ni-Co codoped OCs exhibited excellent oxygen stability and carbon resistance at 850 °C, generating a record production of syngas (totaling about 10 mmol/g) and maintaining high activity in 50 oxygen cycles.	22
3	Methane	$CeFeO_3$	Molar ratio of Fe/Ce, reaction time, and cycle stability	$CeFeO_3$ showed the conversion rate (81.3%) of methane, the selectivity (96.6%) of CO, lower temperature sensitivity, and excellent stability in 20 redox cycles.	23
4	Methane	Copper ore, mainly composed of CuO and CuO-Fe_2O_3	Different temperatures and gas concentrations	The activation energy for the reduction of copper ore with CO and H_2 were calculated as 5.08 and 4.28 kJ/mol. The relationship between the concentration of oxygen vacancy and reaction activity was studied, and the redox range was adjusted to enhance the conversion rate and product purity.	24
5	Water hyacinth	Lean iron ore	Reaction temperature and the molar ratio of Fe to raw material	The proportion of syngas was promoted to 74.39%, lower heating value to 11.83 MJ/N m^3 and cold gasification efficiency to 80.94%. With a temperature of 900 °C, the highest H_2/CO ratio of 1.37 of syngas was obtained.	25
6	Coal	$CuFe_2O_4$	Reaction time	The data of reaction products showed that the $CuFe_2O_4$ OC accelerated the gasification reaction rate of coal compared with that of silica sand. Compared with hematite, $CuFe_2O_4$ had higher conversion of carbon, higher gasification efficiency and higher yield of syngas than Cu-based OCs.	26
7	Coal	CaO/Fe_2O_3	Molar ratio of CaO and Fe_2O_3, and the ratio of H_2/CO	The maximum H_2/CO ratio of 4.6 was achieved as well as 1.4 N m^3 syngas/kg coal was yielded in FeCa50 and it could achieve the maximum oxygen loss rate of 1.2×10^{-3} g/s. Compared with $CaFe_3O_5$ and Fe_3O_4, $Ca_2Fe_2O_5$ with oxygen vacancy showed better catalytic activity during the water-gas shift reaction, and the catalytic activity of $Ca_2Fe_2O_5$ was higher than that of $Ca_2Fe_3O_5$ and Fe_3O_4, higher CO conversion and selectivity were obtained.	27
8	Coal	Cu/Fe-based OC	Gasification time, quality of syngas, and gasification rate of coal and carbon	Both activated point oxygen and alkali metals accelerated the conversion of coal/coke, and the coke conversion was related to H_2 yield. The red mud and Cu20Fe80@C OCs were better candidates and the H_2/CO ratios of 4.03 and 2.36 were attained. The cyclic redox tests showed that both Cu20Fe80@C and red mud OCs could maintain a stable syngas yield within the range of 1.25−1.29 and 1.08−1.14 N m^3/kg of coal.	28
9	Coal	Fe-Ni composition OC	Cycle frequency and pyrolysis temperature	Fe-Ni composite OC showed high conversion of carbon and selectivity of synthesis gas during coal-based chemical looping gasification, but the increase of cycle frequency had no obvious effect on it. The gas yield of carbon-OC was lower than that of coal-OC. The carbon conversion of solid fuel gradually decreased and then tended to be stabilized at about64% at ∼100 min	29
10	lignite	Phosphogypsum (PG)-steel slag (SS) composite OC	Reaction condition and process	The OCs prepared by PG and SS increased the utilization of waste and reduced the preparation cost. SS effectively improved the performance of PG-OCs and produced 72.51% H_2-rich syngas at a reaction temperature of ∼1023 K, lignite/OCs mass ratio of 67−150 wt % of SS/OCs mass ratio, and water vapor/OCs mass ratio of 0.6.	30
11	Car paint sludge	Red mud OC (ROC)	Different reaction conditions	The proportion of OC in the red mud played a role during the formation of hydrocarbon, CO, and H_2. Reaction temperature affected the quantity of hydrocarbon in the combustible gas. In the presence of ROC, a large amount of hydrocarbon was produced by the reaction of hydrocarbons, and large amounts of hydrogen and CO were produced by the decomposition of hydrocarbon under the optimal experimental conditions of reaction time of 60 min, reaction temperature of 1000 °C, reaction aeration rate of 2.4 L·h^{-1}, and RM−OC addition ratio of 2:1, the gas productions of CO, CH_4, and H_2 could reach 0.16 L·g^{-1}, 0.09 L·g^{-1} and 0.37 L·g^{-1}.	31
12	Coal and rice husk	5% Co_3O_4/CaO OC	CLG of coal, water vapor chemical looping cogasification of coal and rice husk, and chemical looping gasification of coal and rice husk	The gas products were higher than those from water vapor gasification, and the yields of gas products from chemical looping cogasification (CLCG) were also higher than those from water vapor cogasification or CLG alone. At the conditions of 950 °C, OC/mixed feedstocks = 1, S/MF = 4, and CaO/OC = 0.75, the H_2/CO product ratio of the syngas was in the range of 1.84−1.93.	32
13	Rice husk and coal	Iron ore	The ratio of oxygen to carbon ratio, reaction temperature, the flow rate of water vapor, and rice husk admixture	Max CCE: 88.16%; Max GE: 49.23%; Max GY: 1.14 N m^3/kg. The addition of coal reduces ash deposition at the oxygen/carbon ratio of 0.2, the reactor temperature of 900 °C, the steam flow rate of 0.125 g/min, and the rice husk blending ratio of 50% were achieved.	33
14	Biomass	Manganese ore	Effective air ratio, temperature, and fuel flow	High fuel flow and high temperatures favored syngas production for complete conversion of substance C3 was achieved at the temperature of 850−900 °C and the fuel flow rates of 0.6−3 L·min^{-1}.	34
15	Sawdust	30% Al_2O_3/$BaFe_2O_4$ OC	OC and biomass mixing mode, ratio of OC and	High temperatures and steam feed rates were favorable for hydrogen-rich syngas, but too much could cause H_2/CO values to drop. The hydrogen-enriched syngas was obtained when O/B was 0.6 and steam volume fraction of 33.6% at 850 °C, which exhibited good regeneration properties.	35

https://doi.org/10.1021/acs.iecr.4c03713
Ind. Eng. Chem. Res. XXXX, XXX, XXX−XXX

Table 1. continued

Number	Fuel	The type of OCs	Operating variables	The experimental results	References
			biomass (O/B), temperature, steam inlet rate		

simulation studies can effectively solve this problem. The numerical simulation study of CLC technology opens up a novel path for future industrialization, and its prospects are relatively bright.

The CLC process has been highly developed in the past decades, with the fuels evolving from gaseous fuels to solid fuels and the OCs evolving from single-component carriers to multicomponent composite carriers. The development process of the CLC technology can be roughly summarized into five main directions of research: 1) the design and preparation of OCs, 2) the design of reactors, 3) the kinetics thermodynamics calculation, 4) the model simulation, and 5) the extension research of the CLC technology.[43−46] Among them, the design and preparation of OCs have been the most central issues in the CLC process. The OCs play the dual roles of the transfer of oxygen and heat in the CLC process, which are the key factors determining whether the oxygen reduction reaction in the CLC process can proceed smoothly. The relevant requirements for efficient OCs are summarized in Figure 4. From the viewpoint of CLC technology development, key problems and challenges still exist in the screening and design of high-performance OCs because the OC exerts the most important role of the CLC technology. As the transfer medium of lattice oxygen and heat in the CLC process, the OC can also exert a certain catalytic role in the reactions of gasification, reforming, and water vapor shift, *etc.* Its physicochemical performance directly determines the storing and transferring efficiency of the lattice oxygen and heat during the process, which affects the reaction performance and the thermal stability of the whole CLC system as well as the conversion degree of the fuel, the capture efficiency of CO_2, and the cost of system operation. Therefore, the research and development of high-performance OCs are the hot point and difficulty of CLC technology.

3. DESIGN OF STABLE OXYGEN CARRIER

3.1. Thermodynamic Perspective. During the CLC process, the OCs are the key part and have become a hot research topic in this field. The OCs are usually porous solids with low transport resistance within the particle, the particle surface, and the external environment. In general, the OCs should have three functions: (i) the generation of oxygen ions, electrons, or holes, (ii) the facilitation of the diffusion in the lattice phase, and (iii) the supplement of active sites for the surface reactions, as shown in Figure 5.[47,48] In the reduction process, the OC contacts the fuel, and the O^{2-} on the surface is generated in the carrier ligands to react with fuel to form H_2O and CO_2, thus forming a chemical potential difference on the surface and inside the support, which induces more O^{2-} to the surface. Moreover, the electrons transfer to the center of particles to balance the charge. When the reduced OCs are exposed to air, the electrons migrate to the surface to gain electrons from the O_2. The O^{2-} ligands were generated to refill the formed oxygen voids in the reduction process, and thus, the OC is reoxidized.[49] The ability to form the oxygen ions and oxygen vacancies during the CLC reaction mainly relies on the thermodynamic properties of the material and can also be modified by the doping of the material. Once the O^{2-} or vacancies are formed, the ions diffusion from the phase to the surface in the OCs will determine the release and replenishment rate of lattice oxygen.[50] The diffusion rate of lattice oxygen is not only determined by the crystal structure but also influenced by the doping, which is manifested macroscopically

https://doi.org/10.1021/acs.iecr.4c03713
Ind. Eng. Chem. Res. XXXX, XXX, XXX−XXX

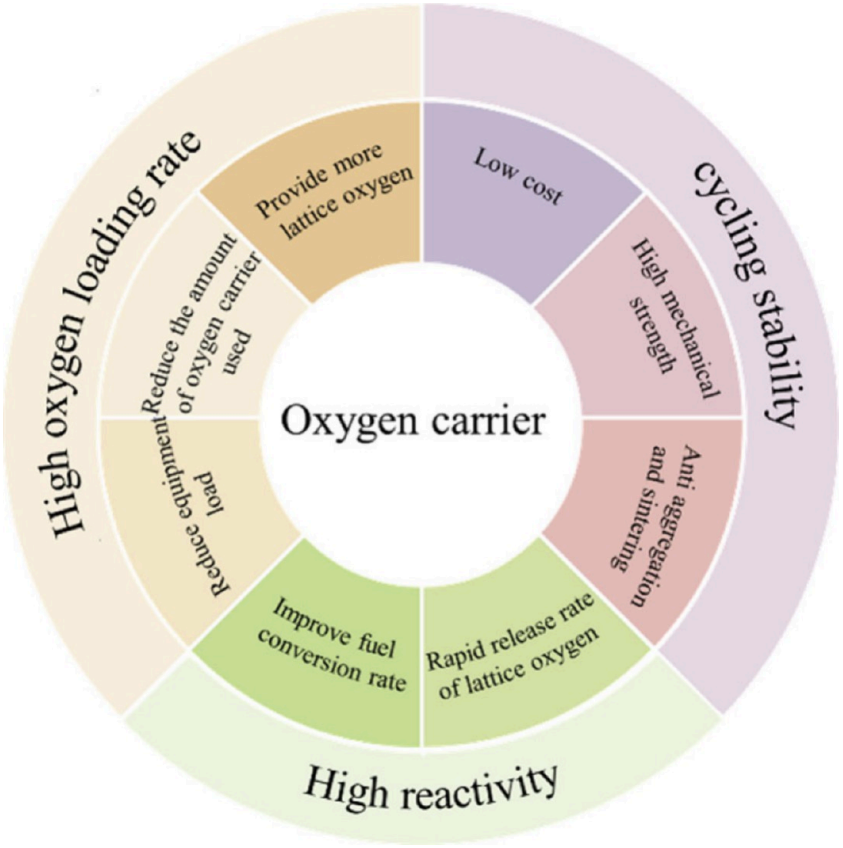

Figure 4. Requirements for efficient OCs in the CLC process.

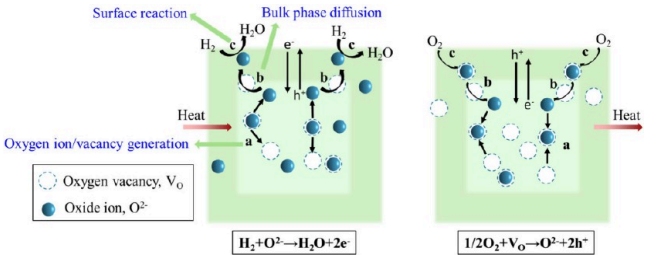

Figure 5. Oxygen transfer mechanism of OCs during the reducing and oxidizing processes.

in the kinetic properties of the material. When the O^{2-} diffuses to the OC surface, the O^{2-} will effectively combine with reactants at specific active sites to complete the reaction. Owing to this reason, the OCs should have excellent thermodynamic and fast kinetics in the CLC process.

The lattice oxygen is generally found in the transition metal oxides, chalcocite, spinel, and so on.[51−53] The transfer process of lattice oxygen in solid materials is an important aspect of the CLC reaction system and also needs to be explored in depth. This process is coupled with the interfacial reaction, and the type, amount, transformation, and transfer of reactive oxygen species are of great significance. Based on the results of the CLC process, the OCs have three kinds of reactive oxygen species, namely, surface lattice oxygen ($O_{s\text{-}latt}$), bulk lattice oxygen ($O_{b\text{-}latt}$), and adsorbed oxygen (O_{ads}), which are derived from the active sites (metal oxides, oxygen vacancies, *etc.*) of OCs. The O_{ads} originates from the dissociated oxygen generated by the activation of chemisorbed O_2 on the active sites of OCs, which can lead to overoxidation of the products. The O_{ads} is chemically adsorbed on an oxygen vacancy. This oxygen atom is not located in the crystal lattice but is bound to the oxygen vacancy when the oxygen vacancy is usually employed as a reaction site. The lattice oxygen is normally arranged in the lattice of metal oxides as a part of the stoichiometric ratio of the material. $O_{s\text{-}latt}$ and $O_{b\text{-}latt}$, totally referred to as the lattice oxygen, are stored within the metal oxides, which are capable of achieving selective oxidation. The relevant studies have reported the participation of $O_{s\text{-}latt}$ and $O_{b\text{-}latt}$ during the CLC reaction, and the migration of $O_{b\text{-}latt}$ is indirectly demonstrated by the kinetic and pulse techniques.[54] The studies on the migration transformation of lattice oxygen from metal oxides and the mutual coupling mechanism of the lattice oxygen-interfacial reaction in the CLC reaction system have also been gradually investigated. Up to now, it is recognized that the oxygen reduction (i.e., the release and restoration of lattice oxygen) of OC takes place at the surface, where the lattice oxygen at the surface is consumed by the fuel to create large oxygen vacancies (OVs), and $O_{b\text{-}latt}$ is driven by the concentration gradient of oxygen (the oxygenation potential) for the migration to the surface for filling the OVs. The formation process of OVs can be understood from the lattice structure of the metal oxides. In the metal oxides, oxygen atoms usually form stable bonds with other metal atoms. Under certain conditions (such as high temperatures), the oxygen atoms in the crystal lattice may detach from their positions and leave a vacancy. The OVs play an important role in the CLC process, which can introduce additional energy levels into the metal oxides as specific reaction sites for certain molecules. In addition, the OVs can facilitate the changes in the chemical rate, which is dependent on the charge transfer of

https://doi.org/10.1021/acs.iecr.4c03713
Ind. Eng. Chem. Res. XXXX, XXX, XXX−XXX

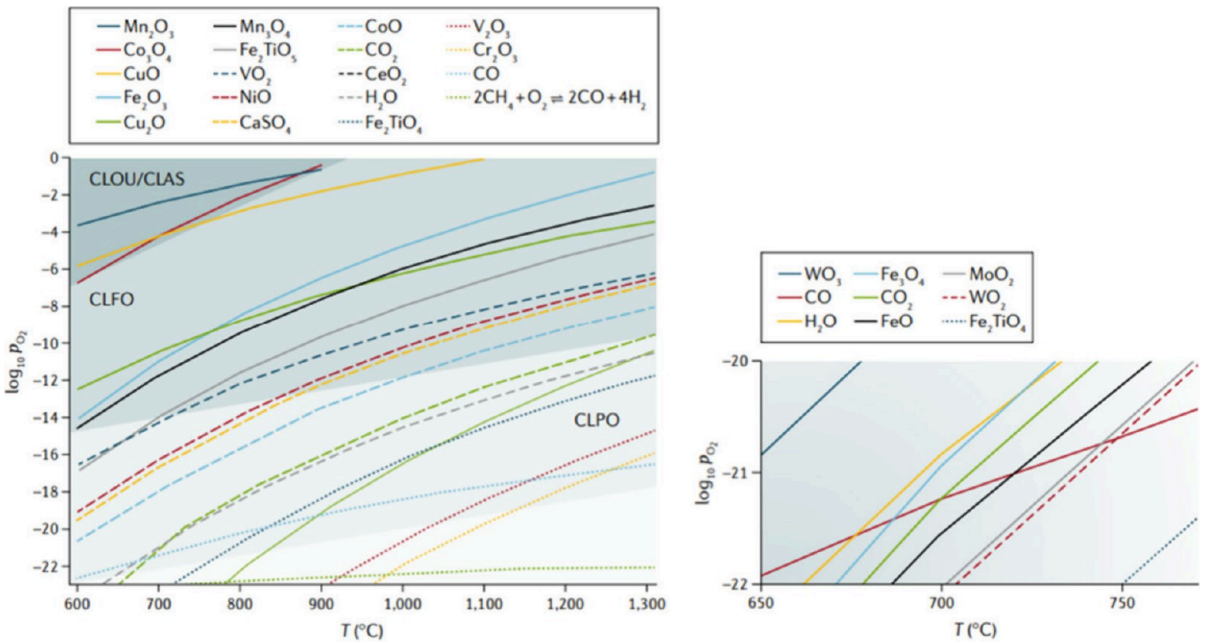

Figure 6. Ellingham diagram of metal oxides and typical OCs.[55] Reproduced with permission from ref 55. Copyright 2017 Wiley.

electrons or holes. The oxygen vacancies can also enhance the conductivity of the material, which is particularly important for catalytic processes.

The process of lattice oxygen restoration involves the adsorption of oxygen mediators on the surface of OC and the cleavage of O^{2-}, which are transported inward along the concentration gradient to gradually restore lattice oxygen. Moreover, the processes of ion diffusion, surface reaction, and structural evolution have a distinct influence on the properties of OCs. As the transfer medium of lattice oxygen during the CLC process, the high-performance OC is the premise and foundation of continuous and stable operation for industrial application of this technology. The OC not only supplies the lattice oxygen but also transfers the heat needed for the reaction in the CLC process. It also enhances the slow gasification in the CLC process of solid fuel. Therefore, the acquisition of high-performance OCs is the key point to the large-scale practical utilization of the CLC technology and also determines the economy of CO_2 capture and high efficiency of system energy utilization. In addition, the OCs with high performance are essential for full conversion of solid fuels. Compared with the gaseous fuel CLC technology, the solid fuel CLC technology has higher requirements on the performance of OCs: 1) higher reactivity, trying to avoid the emissions of unreacted products after the pyrolysis gasification of solid fuel, 2) higher oxygen-carrying capacity, thus reducing the transfer rate of OC between two reactors and the storage capacity in the FR, 3) excellent chemical stability, 4) outstanding physical properties, including the fluidization, abrasion resistance, crushing resistance, sintering resistance, and agglomeration resistance, 5) environmental friendliness, (thus the preparation and application process will not cause secondary pollution), and 6) economically feasible, cheap, and easy to obtain materials. Moreover, the magnetic properties and the density of the OCs are also of concern, thus facilitating the separation of OCs from unburned residues.

In terms of thermodynamic properties and the degree of conversion of carbonaceous fuel by the OCs, the oxidation process can be categorized into complete and partial oxidation, which converts the fuel to CO_2/H_2O and CO/H_2, respectively, and is mainly determined by the OVs that can be produced by the material, as reflected in the thermodynamic equilibrium diagrams. Figure 6 shows which oxides can be utilized for the complete oxidation process and which are suitable for the partial oxidation process. For the CLC process, the fuel should be converted as completely as possible to accomplish a higher combustion degree and CO_2 capture effect, therefore, the OCs that fulfill the complete oxidation conditions are more suitable for the CLC process. For complete oxidation, the equilibrium oxygen partial pressure of OC should be above the equilibrium oxygen partial pressure line for combustion of CO and H_2. Therefore, the oxides of Mn, Fe, and Cu, in which equilibrium partial pressure curves are in the upper part of the complete oxidation region, are suitable for the complete oxidation process and completely convert the fuel to CO_2 and H_2O. The most oxidizing agents are Mn_2O_3, Co_3O_4, and CuO, which are suitable for the CLOU process because of the release of O_2, even at intermediate temperatures. In contrast, the equilibrium oxygen partial pressure values of $CaSO_4$, NiO, and CoO are located at the bottom of the fully oxidized region, which is close to the combustion curves of CO and H_2, so these materials can also be employed in the complete oxidation process, but incomplete conversion of fuels may occur. Based on this, the domestic and foreign scholars' research on OCs mainly focuses on the OCs that meet the conditions of complete and partial oxidation, *i.e.*, metal oxides of Fe, Mn, Cu, Co, Ni, and $CaSO_4$.

Based on the energy band theory and molecular orbital theory, the thermodynamic conditions are first explored, in which the solid-phase catalysts can undergo the oxidation of lattice oxygen. Taking the single metal oxides as the example, the orbital coupling leads to the formation of the M−O band (O 2p band), which embodies the properties of oxygen ligands, the M−O* antibonding band (M nd band), and the properties of metal centers.[56−58] The variation between the two energies can be referred to as the charge-transfer energy. Meanwhile,

https://doi.org/10.1021/acs.iecr.4c03713
Ind. Eng. Chem. Res. XXXX, XXX, XXX−XXX

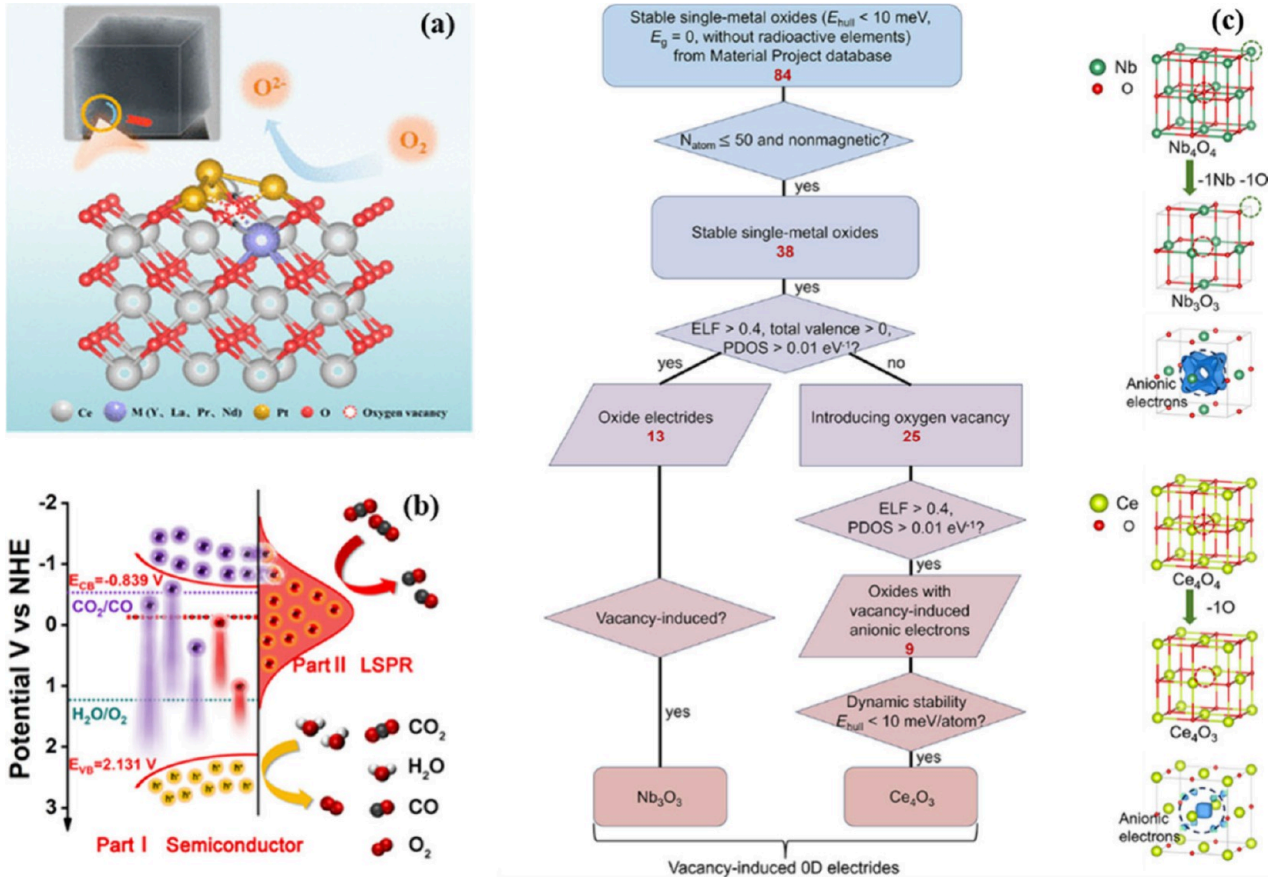

Figure 7. Role of electron transfer in the OVs.[65−67] (a) Localized electronic perturbation effects at the interface Pt/Ce-Ov-M asymmetric OV sites. (b) Self-coupling of intrinsically excited photogenerated electrons and plasma hot electrons in MoO_2-based photocatalysts. (c) High-throughput screening process for OV-induced anionic electron-type electronic compounds. Reproduced with permission from ref 65. Copyright 2024 American Chemical Society. Reproduced with permission from ref 66. Copyright 2022 Elsevier. Reproduced with permission from ref 67. Copyright 2024 American Chemical Society.

the M−O* band can further conduct the Mott−Hubbard splitting owing to electron repulsion inside the metal d orbitals. The formed electrons occupy the low Hubbard-band (LHB) and the empty state of the upper Hubbard-band (UHB), respectively, and the difference in the energy between the two can be defined as the electron repulsion energy.[59] For materials with high covalent metal−oxygen bonds, the charge transfer energy becomes smaller and the electron repulsion energy becomes larger, which causes the LHB of the metal to dive below the O 2p band. In this situation, when the oxidation reaction occurs, the electrons in the oxygen ligand are preferentially lost, and the oxidation of lattice oxygen occurs from the perspective of thermodynamically. At the same time, if the O 2p band is shifted upward because of high covalency, then the lattice oxygen after oxidation will participate directly during the production of oxidation products. Hence, the energy band and the interaction position of metal centers and oxygen ligands in the material are utilized as effective methods to measure the oxidation degree of lattice oxygen, in principle.

From a thermodynamic point of view, metal oxides exhibit various behaviors in the process of complete oxidation and partial oxidation. The oxidation−reduction of O 2p orbital holes in Li-rich manganese batteries is a well-known phenomenon. Nevertheless, such an anion redox process leads to oxygen formation, resulting in the instability of structure due to unstable O 2p holes. Guanglei Cui's group put forward that the oscillating nonisothermal sintering technology was employed to stabilize lattice oxygen in the $Li_{1.2}Mn_{0.54}Ni_{0.13}Co_{0.13}O_{2-x}$ by suppressing the oxygen formation during charging.[60] The prepared catalysts delivered a capacity retention of 87.6% after 600 cycles at 1.0 C and exhibited excellent performance at elevated temperatures. Compared with the conventional constant-high-temperature sintering, it reduced the intrinsic OV number of Li-rich manganese oxides and oxygen formation during charging. The samples prepared by oscillating the nonisothermal sintering showed rather slow voltage attenuation and good cycle stability, which provided valuable guidance for the stabilization of lattice oxygen and the improvement of structural stability from oxide cathodes during the electrochemical energy storage. Yudau Huang and co-workers showed dual roles by the introduction of the Fe into the Mo-based materials to inhibit complete dissolution.[61] The Fe increased the metal abundance of material and promoted chemical kinetics. The Fe after doping reduced the d-band center and activated the oxygen nonbonding state, thus realizing the thermodynamic favorable unit-point lattice oxidation. Fe-Mo_2C@CN had good electrocatalytic oxygen evolution reaction (OER) performance, and it was demonstrated that the OER of Fe-Mo_2C@CN obeyed with the unit point mechanism of lattice oxidation. The dual role of Fe improved the OER process from kinetics and thermodynamics, respectively. The introduction of Fe not only reduced the dissolution of Mo and improved the conductivity but also reduced the d-band center, filled the M−O

https://doi.org/10.1021/acs.iecr.4c03713
Ind. Eng. Chem. Res. XXXX, XXX, XXX−XXX

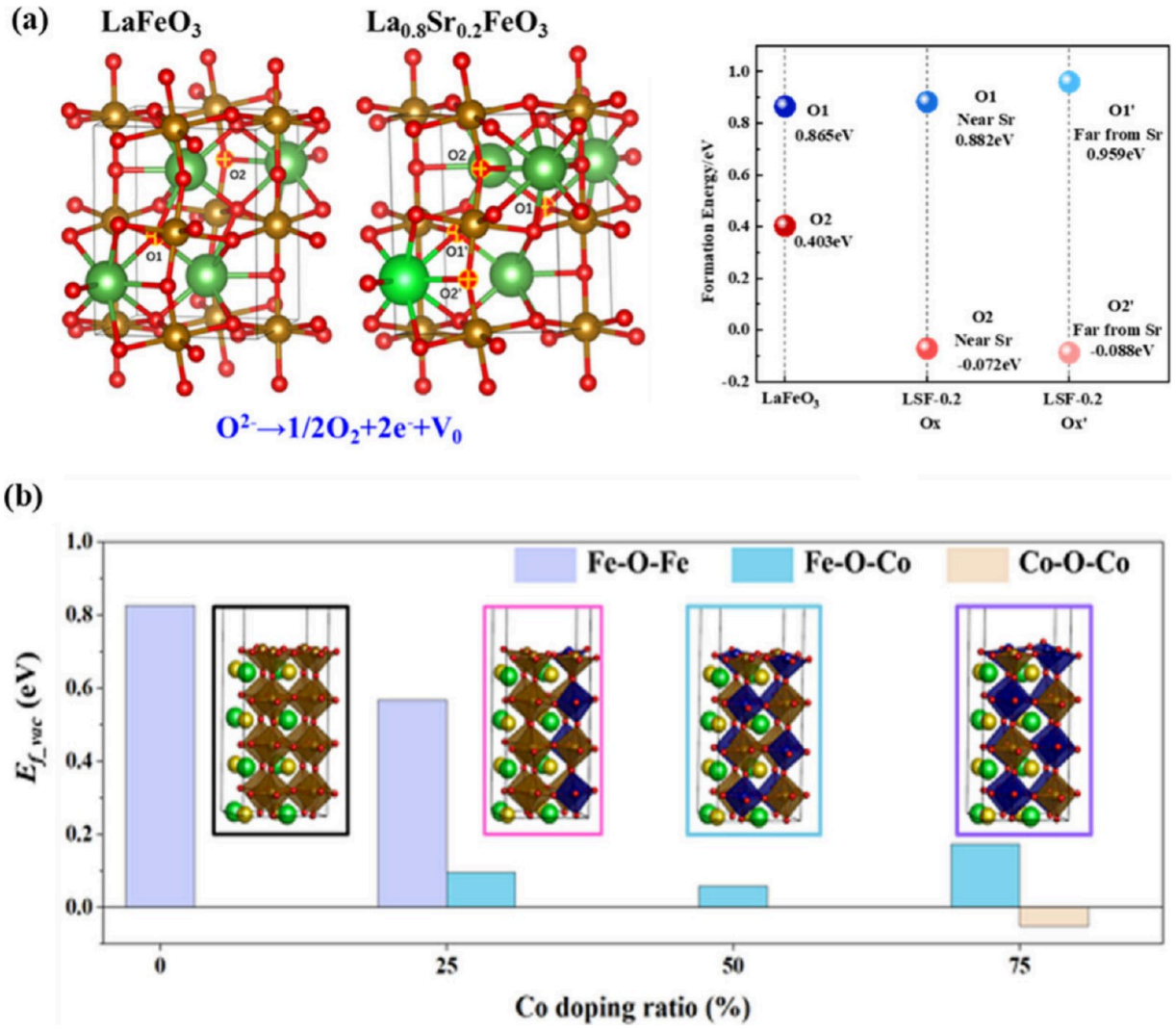

Figure 8. Required energy barrier for formation of the OVs and the doping of metals. (a) Calculation of the OVs formation energies for $LaFeO_3$ and $La_{0.8}Sr_{0.2}FeO_3$. (b) Surface OV formation energy (E_{f_vac}) for the $Pr_{0.6}Sr_{0.4}Co_xFe_{1-x}O_3$ (PSC_xF) model.[71,72] Reproduced with permission from ref 71. Copyright 2024 American Chemical Society. Reproduced with permission from ref 72. Available under a CC-BY 4.0 license. Copyright 2021 Chen, H. J. et al.

antibonding orbitals, and promoted the activation of lattice oxygen. At the same time, it also had good electrocatalytic properties and stability as an anode of total hydrolyzed water. This work paved a foundation for the study of the reaction mechanism of Fe-based catalysts in the OER process and provided certain references for other electrocatalysts in the case of the mechanism of lattice oxidation.

During the CLC process, as the OC participates in the reaction, the oxygen atom is removed from lattice oxygen in the metal oxides at the designed reaction conditions, and the OVs are correspondingly formed ($O^{2-} = 1/2O_2 + O_V + 2e$). The OVs are present in all metal oxides and significantly impact the structures and performance. Hence, the primary purpose of regulating the OVs is the enhancement of structural stability and oxygen ion transportation ability of OCs by adjusting the crystal structure around the OVs and electronic structure of the transition metals around the OVs to obtain the better catalytic reaction performance. In general, the types of OVs are closely related to their formation process, and various formation methods can cause different types or a mixture of the OVs. The common formation methods and the elements involved are shown in Figure S2.[62,63] The formation of OV defects mainly occurs in two stages: the treatment during the synthesis of materials and surface treatment after the synthesis of materials. With the deepening and development of research, regulation of OVs has become an effective strategy to optimize the performance of the catalyst. At present, the regulation strategies of the OVs are all dependent on the formation mode, which mainly includes the regulation of temperature and atmosphere, the doping of atoms, the ligands or other defects, the concentration reaction of the solution, and the pressure. Furthermore, the process of material synthesis and regulation refers to thermodynamics and kinetics. The thermodynamic analysis can predict the formation of OVs and the changes in the properties of materials at the thermodynamic equilibrium, while the kinetics enable the understanding of the dynamic processes in which these changes occur. The discussion on the thermodynamics of generating the OVs is conducted to provide a theoretical basis for its regulation.

According to the Gibbs−Helmholtz formula ($\Delta G = \Delta H + T\Delta S$), ΔG, ΔH, T, and ΔS are the variations in the Gibbs free energy, enthalpy, temperature, and change in entropy,

https://doi.org/10.1021/acs.iecr.4c03713
Ind. Eng. Chem. Res. XXXX, XXX, XXX−XXX

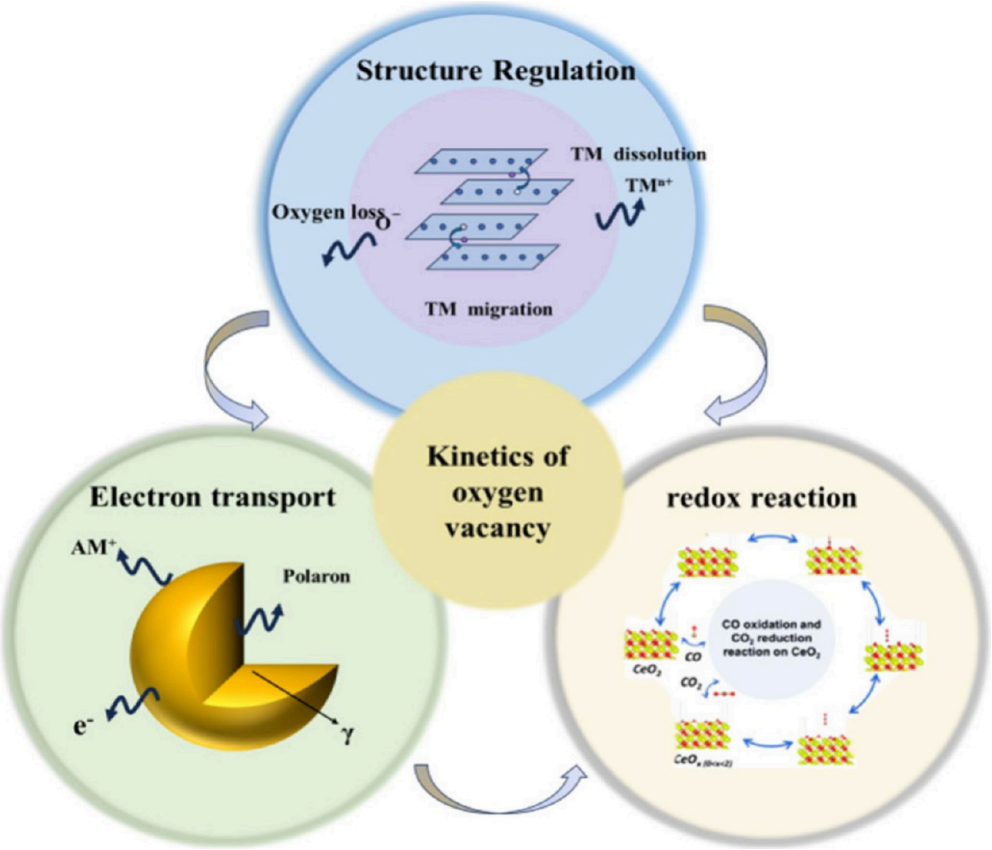

Figure 9. Effect of the Kinetics on the Formation of OVs.

respectively. The generation reaction of the OVs in the OCs can be described via the following formula: $MO_2 = MO_{2-x} + x/2O_2 + xO_V$. The $\Delta S > 0$ indicates that the formation of OV is easier to reduce the ΔG. As the formation energy of O_V is usually positive ($\Delta H > 0$), whether the OVs are generated or not relied on the comparison of ΔH and $T\Delta S$.[64] The generation of the OVs is a thermodynamically spontaneous reaction, which explains why the OVs are prevalent in the OCs. The formation energy of the OVs with a function of temperature and Le Chatelier's principle further indicates that the generation degree of the OVs can be artificially altered by regulating the temperature, the partial pressure of ambient oxygen, and the oxygen atom coordination environment. Therefore, the possibility of the OVs formation is positively related to the ambient temperature of the OC, explaining the loss of lattice oxygen during the calcination at high temperature. The difficulty of the OVs formation depends on the interaction strength of the O atoms with the surrounding cations, i.e., the coordination degree of O atoms and strength of M−O bonds, as shown in Figure 7. The strength of the M−O bond can also be regulated (e.g., the elemental doping), and the formation energy of the OVs is varied corresponding. Therefore, although all the OCs can form the OVs, only the OCs with low degree of O coordination and/or the weakened M−O bonds are likely to generate the OVs.

Generally, the introduction of the OVs results in variations in the electronic structure, including the valence state, energy band structure, and so on, which is the primary reason for the formation of the OVs in the solid OCs from the perspective of thermodynamic properties. The most distinct effect of the OVs for electronic structure of OCs is the destruction of the charge balance in the solid materials, and the weakening of oxidation state also accelerates the generation of OVs shown in Figure 8. Fang Song's team. described that the effect of surface OVs on the capacity of electron transport capacity of NiFe layered double hydroxide (NiFe LDHs) in the OER reaction was studied.[68] The OV barely regulated the catalytic activities but lowered the transportation resistances with more than 1 order of magnitude. Furthermore, the electronic structure of TiO_2 was changed to promote the electronic transportation of NiFe LDHs in the OER. Thus, its catalytic potential was released, and the photocatalytic performance of TiO_2 was affected. The surface OV enhanced the charge transfer ability of NiFe LDHS and enhanced its OER catalytic activity. Jiangshan Qu et al. reported that the dynamic evolution and the role of the OVs in the CeO_2 nanocrystals have been studied at the atomic level using the environmental transmission electron microscope.[69] The formation and filling of OVs would lead to lattice distortion and the shift of the cerium atom position, which would affect the redox performance and catalytic activity of CeO_2. Zhen Chen's and Yayu Wang's group provided insights into these microscopic defects and their effects on the material properties by means of advanced imaging techniques.[70] The OVs and self-doping ligand cavities in $La_3Ni_2O_{7-\delta}$ were successfully visualized using multiple electron transmission coherence imaging (MEP) combined with electron energy loss spectroscopy (EELS). The OVs were mainly located at the inner top corner position and led to significant electronic structure changes. In addition, $La_3Ni_2O_{7-\delta}$ exhibited strong charge transfer properties, and the self-doped holes were mainly distributed in the inner top corner and planar oxygen positions. The required energy barrier for the formation of the

https://doi.org/10.1021/acs.iecr.4c03713
Ind. Eng. Chem. Res. XXXX, XXX, XXX−XXX

OVs can be effectively simulated with the input of other energy to facilitate the formation of the OVs generation, such as electrical, optical, magnetic, mechanical, and so on. Yanguang Chen's group investigated that the Sr doping to $LaFeO_3$ generated more OVs were formed, and thus, the density of states (DOS) of $La_{1-x}Sr_xFeO_3$ was calculated. The Fermi level was located at 0 eV, and the band gap of $La_{0.8}Sr_{0.2}FeO_3$ was 0.429 eV, which was smaller than that of $LaFeO_3$ (0.828 eV) and $SrFeO_3$ (0.674 eV) by 0.399 and 0.245 eV, respectively.[71] At the same time, the valence band was mainly composed of the O 2p orbitals, and the guide band was contributed by Fe 3d orbitals. The doping of a certain amount of Sr (x = 0.2) reduced the band gap relative to the Fermi level and also facilitated the charge transfer and the transition of electron valence band and guide band. The doping of Sr accelerated the formation of the OVs, and enhanced the rate of charge transfer, which was more conducive to methane redox.

In view of the effect of intrinsic OVs on the anion redox-mediated OVs, the existence of intrinsic OVs makes the study of the anion redox-mediated OVs more complicated. However, it is not clear whether the intrinsic OVs stimulate or inhibit the formation mediated by the anion redox and whether the surface or bulk intrinsic OVs have a certain effect on the generation and evolution of the OVs by anion redox. Based on the previous studies, the effect of intrinsic OVs on the anion redox-mediated OVs can be analyzed dialectically according to the preparation and spatial distribution of intrinsic OVs. In the process of synthesis, the excess bulk OVs produced by high temperature usually lead to the reconstruction of the structure and the generation of the OVs mediated by the redox reaction of bulk anions. When the oxide is in a certain condition, the higher oxygen concentration in the crystal lattice indicates that the possibility of releasing the O_2 is much greater. The reduction of the oxygen concentration will restrict the release of O_2, which is unfavorable to the generation of the OVs. Moreover, the degree and direction for the effect of intrinsic OVs on the anion redox-mediated OVs (inhibition/promotion) are also related to the content of intrinsic OVs. Thus, the design of the proper distribution and concentration of intrinsic OVs for the relevant reactions is of significance. In addition, further exploration of the mechanism of dynamic effect of intrinsic OVs is on the way.

3.2. Kinetics Perspective. The thermodynamic analysis can predict thermodynamic equilibrium states such as the formation of OVs and the changes resulting from the material properties, but it cannot identify the dynamic processes in which these changes occur. Hence, there is a need for studying the formation of OV and evolution kinetics, such as the transportation dynamics (including the transportation of the transition metals, the diffusion of the ions, the transportation of the electrons, the transportation of the phonon), the phase change dynamics, and the chemical kinetics, shown in Figure 9. For the synthesis of OCs, the thermodynamic phase diagram usually acts as the starting point and combined with the experiment as the guidance. However, most of the time, the calculations show that the thermodynamic stable phase cannot be synthesized in the actual synthesis, but some metastable phases are synthesized. The tracing of the synthesis process by *in situ* experiments can reveal the existence of multiple nonstationary mesophase in the reaction process, but there is no single criterion that can determine whether a particular reaction path is fully thermodynamic or kinetic or if the two interact intricately. Moreover, it has been difficult to systematically and quantitatively understand the interaction between thermodynamics and kinetics, which is mainly due to 1) the initial reaction phase transition process being still unknown and 2) the reaction energy being difficult to track and measure as the reaction progresses. Therefore, the ability to interpret and predict these unstable intermediates is particularly important for the development of computational materials-based science. Recently, the *in situ* synchrotron radiation X-ray diffraction and ab initio calculations by Gerbrand Ceder and Wenhao Sun's group, Laurence Berkeley National Laboratory, USA, were employed to investigate the nonequilibrium reaction paths of layered metal oxides with sodium groups.[73] The interaction between the thermodynamics and kinetics during the synthesis reaction is further discussed. It was revealed that the formation of the first phase consumed the most reaction energy and was the template for a series of topotactical phase transitions. A physical model was put forward to indicate the first-phase nucleation at the interface of the reaction salt, which had the largest negative reaction energy and was not restricted by the composition of the reaction salt. This mechanism was well suited to solid-state synthesis, because of the strong thermodynamic driving force. For a low-temperature synthesis, such as the hydrothermal reaction, the reaction was more affected by the size-dependent thermodynamics and competitive nucleation kinetics. This work showed that the thermodynamics and kinetics are closely related. In the multistage crystallization process, the fast kinetics was caused by a large thermodynamic force and the small one by a slow kinetic force, thus requiring a high temperature to facilitate the reaction. Based on the mechanism of the interfacial reaction between the phases that were not affected by the component, the first phase required for the design could be predicted by careful selection of the reactive salt, and the subsequent reaction path could be determined.

The diffusion of the OVs in the metal oxides can be studied via the kinetic lattice Monte Carlo (KLMC) model. the present method employs a database of the activation energy of the OVs transport, and various transport pathways of the OVs can be calculated using first-principles calculations. Since the first-principle calculations reveal significant vacancy−vacancy exclusion, Pratik P. Dholabhai et al. investigated the importance of the effect by simulating and not conducting repulsive interactions.[74] At first, the vacancy concentration and conductivity strengthened with the enhancement of the doping concentration. A dopant concentration of ∼15−20% was found to be optimal for achieving the maximum ionic conductivity. At higher concentrations, however, the vacancies interfered with and repelled each other. The dopant trap vacancies resulted in the "traffic jams" that reduced conductivity, consistent with experiment results. Meanwhile, the simulated effective activation energy of the vacancy migration was enhanced by the increase in the doping concentration. The current methodologies, including the mixed first-principles calculations and KLMC models, have provided a powerful basic tool to predict the optimal doping concentration of cerium-based materials. Aravind Asthagiri's team utilized density functional theory (DFT) calculations to explore the initial thermal reduction process of the PdO (101) surface under the formation kinetics of the OVs.[75] The defect-free PdO (101) surface consisted of the discordant Pd (Pd_{cus}) and O atoms (O_{cus}) arranged in parallel. The basic process of O_{cus} vacancy formation, the diffusion of oxygen atoms along Pd_{cus}, and various oxygen formation pathways were studied by

https://doi.org/10.1021/acs.iecr.4c03713
Ind. Eng. Chem. Res. XXXX, XXX, XXX−XXX

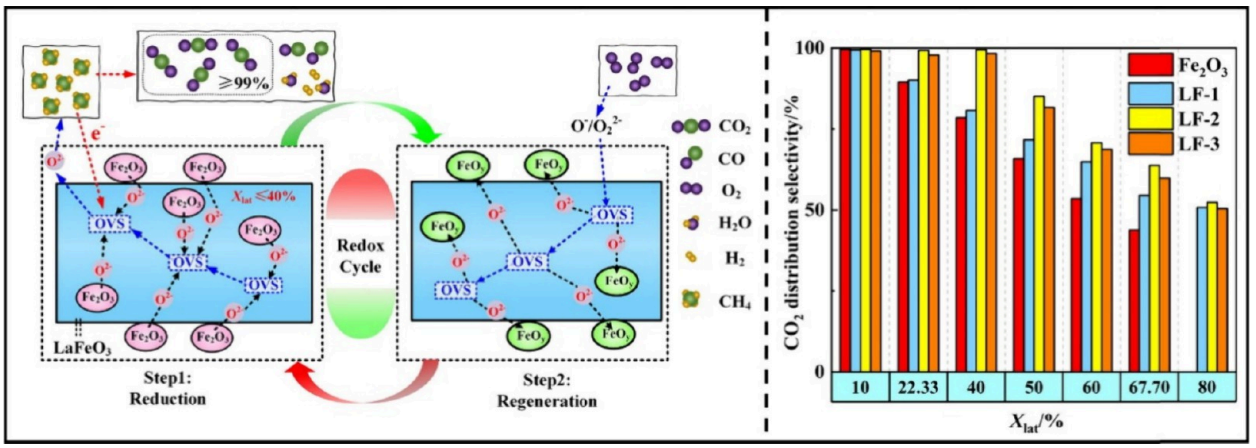

Figure 10. Strategies for regulating the generation of bulk-phase and surface-conducted OVs.[81] Reproduced with permission from ref 81. Copyright 2023 Elsevier.

DFT. Since the OVs were generated during the process of surface reduction, the DFT calculations showed that the existence of the OVs strongly affected the barrier of the adjacent surface. The barrier to the formation of OVs was reduced by ∼50%, compared with adjacent OVs. In the presence of the OVs, the oxygen barrier was formed along the Pd_{cus} decreased from 1.54 to 0.81 eV on the surface of the defect-free PdO (101). Moreover, the presence of the O_{cus} vacancies led to stronger oxygen binding for the Pd_{cus}. On the surface of PdO (101), the strong neighborhood effect was also favorable for the growth of the OVs and increased the thermal reduction rate of the surface.

Jiagang Wu's group investigated the transportation kinetics of the OVs in $BiFe_{0.95}Mn_{0.05}O_3$ films by using temperature-dependent leakage current, electric field, and temperature-dependent impedance spectroscopy.[76] $BiFe_{0.95}Mn_{0.05}O_3$ had abnormal leakage behavior, and different leakage behavior of $BiFe_{0.95}Mn_{0.05}O_3$ and pure $BiFeO_3$ was studied by the temperature-dependent impedance spectroscopy under various states. The analysis of impedance spectra at a high-resistance state showed that first ionization of the OVs was the reason for the dielectric relaxation and conductivity of $BiFe_{0.95}Mn_{0.05}O_3$ in the temperature range 294−474 K, but in the low-temperature range 294−374 K, the first ionization of OVs was the origin of dielectric relaxation and conductivity of $BiFe_{0.95}Mn_{0.05}O_3$. $BiFeO_3$ exhibited similar dielectric relaxation and electrical conductivity, and the short-range motion of OVs played an important role in the high-temperature range of 374−474 K. The analysis of diverse impedance spectra showed that the abnormal leakage behavior of $BiFe_{0.95}Mn_{0.05}O_3$ was related to the migration kinetics of the OVs, which was obviously different from that of $BiFeO_3$. Yi Jiang et al. studied the electrochemical reduction behavior of oxygen at the lanthanum manganese oxide (LSM) electrode.[77] The kinetics of the OVs formation observed in the alternating current impedance and potential step experiments was studied, and the formation kinetics of the OVs was the primary reason for reverse hysteresis of cyclic voltammetry and the improvement on the electrochemical activity of oxygen reduction at the cathode-polarized LSM electrode. The potential step experiment showed that the concentration of the OVs increased exponentially with time when the LSM was in the cathodic polarization state. The rate-limiting step of the OVs generation was the formation step, and the cathodic current produced by OVs reaction was contributed significantly to the total reduction current. Yiming Yan and co-workers successfully introduced abundant OVs into the manganese dioxide system by the complex-induced chemical precipitation method.[78] The enhanced conductivity and the local electric field formed around the OVs accelerated charge transfer and significantly improved capacitance and rate capability. The symmetric MnO_2 supercapacitors had higher energy density (54.2 Wh·kg^{-1}) and power density (3279.6 W·kg^{-1}) than other MnO_2-based supercapacitors, which paved the way for effective fine-tuning of bulk electron configurations and chemical kinetics.

3.3. Generation and Regulation of Stable Oxygen Carriers and Oxygen Vacancies. The core of the CLC process is to utilize the lattice oxygen in the OC with the replacement of molecular oxygen to realize partial oxidation of fuel to prepare the relevant chemicals. Thus, the OC exerts the role of transforming the lattice oxygen and reaction heat in the reaction process, which is the key to realize the whole reaction process. The systematic description of effects of intrinsic OVs on the thermodynamics, including the micro and macro aspects (e.g., electron, crystal, structure, phase structure, *etc.*) from the viewpoint of the stabilization by a mixed OC is favorable for understanding the structure−activity relationship of intrinsic OVs in the OCs, which can provide the guiding opinions for the design of the intrinsic OVs to achieve the efficient properties. The realization of high-stability OCs can be achieved by means of core−shell structure, the introduction of electronic additives, the composition of mixed OCs, and other methods.

For the OCs, the redox-mediated generation of the OVs in the bulk phase is mainly obtained by means of doping the bulk phase, the design of the gradient structure, the preparation of the single-crystal structure, the reduction of the embodied OVs, the arrangement and design of oxygen atoms, and the disordering of the cation. The generation of the OVs via the anionic redox-mediated usually occurs during an anionic redox reaction; i.e., the lattice oxygen in the transition metal oxides undergoes a specific redox reaction. Specifically, when the lattice oxygen (O^{2-}) is oxidized to generate high-valent oxygen species (O^{n-}, $0 \leq n < 2$), some oxygen species cannot be reversibly reduced to O^{2-} due to side reaction of O^{n-}, including the release of the oxygen, thus the OVs are generated correspondingly.[79,80] The occurrence of anionic oxidation reactions in the transition metal oxides usually depends on two

https://doi.org/10.1021/acs.iecr.4c03713
Ind. Eng. Chem. Res. XXXX, XXX, XXX−XXX

conditions: 1) a higher charging voltage to simulate the O 2p electrons and 2) the tops of the O 2p orbitals to locate in the Fermi energy level. The intrinsic OVs and anion redox-mediated generated OVs both exist in the form of bulk OVs and surface OVs. By regulating the concentration and transfer rate of the OVs, the stability of OCs is improved to perform the specific oxidation reactions. Currently, more researchers have proposed numerous effective strategies for regulating the generation of bulk-phase and surface-conducted OVs, as shown in Figure 10. Among them, the main methods include the employment of the core−shell structure, the introduction of electronic additives, surface doping, the surface reconstruction, the surface coating, the composition, and other interfacial strategies to realize.

3.3.1. The Doping of the Electronic Additives. The monometallic OCs are generally dominated by the oxides containing the transition metal elements, such as Fe_2O_3, MnO_2, CuO, *etc.* (shown in Figure S3), where primarily the outermost electron layer of the transition metal ions has a strong ability to gain or lose the electrons for leading to the transition metal oxides with variable valence states.[82] Various transition metal oxides have different oxygen-carrying capacities and catalytic activity, so they have diverse effects on the CLC process, which can be employed for production on a large scale due to the low price and abundant reserves. However, these OCs exhibit the following disadvantages: being harmful to the environment, having a lower migration rate of lattice oxygen resulting in serious deposition of carbon, being easier to sinter at high temperatures (which results in the inability to maintain the storage of massive reactive lattice oxygen in multiple high-temperature cycles), having lower release and recovery ability of lattice oxygen, having poor thermal stability at high temperatures (which is not conducive to efficient migration of lattice oxygen in multiple cycles), having high-cost consumption, being unstable at high temperatures, and having active components reacting with the inert component to form stable oxides with low reactivity (which leads to a decrease in its reactivity). Although the monometallic OCs have more drawbacks and different mobilization rates of lattice oxygen, OCs are still important in the CLC process.

The oxygen species in the metal oxide are generally categorized according to their activity into electrophilic and nucleophilic oxygen species. The electrophilic oxygen species include O^-, O_2^{2-} (perovskites), and O_2^- (superoxides), which are generally categorized as nonselective oxygen species due to higher activity and electron affinity.[83] In contrast, lattice oxygen (O^{2-}) is usually considered a nucleophilic oxygen species and classified as a "selective" oxygen species during catalytic oxidation reactions. However, such a categorization may be oversimplified because massive oxygen species depend on the types, the reaction conditions, and the degree of reduction of the oxides. Recent evidence suggests that the lattice oxygen can be converted dynamically to electrophilic oxygen during the CLC process and the doping of the metals is an effective method to strengthen the activity or selectivity of OCs. The doping of monometallic oxides using other cations can result in various types of solution mixtures. Two trivalent metals can generate the corundum solid solutions, and trivalent and divalent metals can produce the spinel solvents. Finally, the interactions between two divalent metal oxides can produce a solid rock salt solution. The generation of solid solutions changes its coordination environment of reactive metal centers and activity of lattice oxygen. Therefore, the composited metal oxides usually have higher reactivity than monometallic oxides, which can overcome the drawbacks of monometallic oxides owing to the interaction effects of multiple metallic elements.

Jinglong Gong's group reported that a series of the Al_2O_3-supported $MoO_3-Fe_2O_3$ catalysts with different Fe/Mo molar ratios were prepared using the impregnation method, and the coupling effect of surface acid catalysis and lattice oxygen selective oxidation on the $MoO_3-Fe_2O_3$ redox catalyst was studied.[84] The experimental results showed that the coupling strategy achieved 49% propane conversion and 90% propylene selectivity in 300 redox cycles. The atom-dispersed Mo resulted in the introduction of additional acid sites (Mo−OH) to promote the conversion of the propane. At the same time, the Mo effectively regulated the activity of lattice oxygen and external diffusion rate, so that original over-reactive oxygen species could be utilized for selective oxidative dehydrogenation. The yield of propylene was significantly increased by the enhancement of surface acid sites and the modification of lattice oxygen after the metal Mo was doped in the isolation state. Haibo Zhao's group reported that the lignite and its coke were employed as the gasification raw materials, and the cement-bonded iron ore (Fe_{100}@C), the red mud, the cement-bonded Fe ore and Cu ore ($Cu_{20}Fe_{80}$@C), the cement-bonded red mud and Cu ore ($Cu_{10.9}Red_{89.1}$@C) were used as the OCs.[85] The red mud and Cu20Fe80@C OCs were better candidates, and H_2/CO ratios of 4.03 and 2.36 were attained. The cyclic redox tests showed that both Cu20Fe80@C and red mud OCs could maintain a stable syngas yield within the ranges 1.25−1.29 and 1.08−1.14 N m^3/kg of coal. By comparing the three OCs, a shorter reaction time of $Cu_{20}Fe_{80}$@C showed the superiority as an OC for the CLC process of coal gasification, and the higher equilibrium constant also indicated a stronger catalytic effect than the other two OCs. The group of Chuan Shi and Ding Ma proposed that the utilization of the transition metal carbide as a new type of oxygen storage material was to construct a low-temperature "$MoC_x \rightarrow MoC_xO_y$" chemical looping and composite it chemically with the traditional "oxygen storage body" to obtain a novel type of oxygen storage material, which broke through the traditional oxidized component as an oxygen storage material, and developed a Ni-(α-MoC)/Al_2O_3 catalyst with both low-temperature high activity and cycle stability.[86] The stable cycle for the highly selective synthesis of CH_4 to syngas and the regeneration of CO_2 reduction were realized. The reaction temperature was significantly reduced by 200−300 °C, and during the 1140 cycles, the reactivity and selectivity of the catalyst to syngas remained basically unchanged, showing excellent cycle stability.

The OC plays an important role in the CLC process for the CO_2 capture technology. Although the doping OCs exhibit excellent reaction performance, the phase separation is an important factor that causes the failure of OCs in the oxidation−reduction cycle. In order to explore the rapid phase separation mechanism of the ilmenite OC, Chen et al. illustrated that the distribution of OC phases and elements, the surface shell morphology, and the internal structure and evolution of the OC phases were investigated during the particle oxidation.[87] The migration of Fe from interior to surface of the particles occurred in the oxidation stage during the CLC process with relatively high temperature (>900 °C) and high oxygen concentration (>5.0 vol %) for regeneration.

https://doi.org/10.1021/acs.iecr.4c03713
Ind. Eng. Chem. Res. XXXX, XXX, XXX−XXX

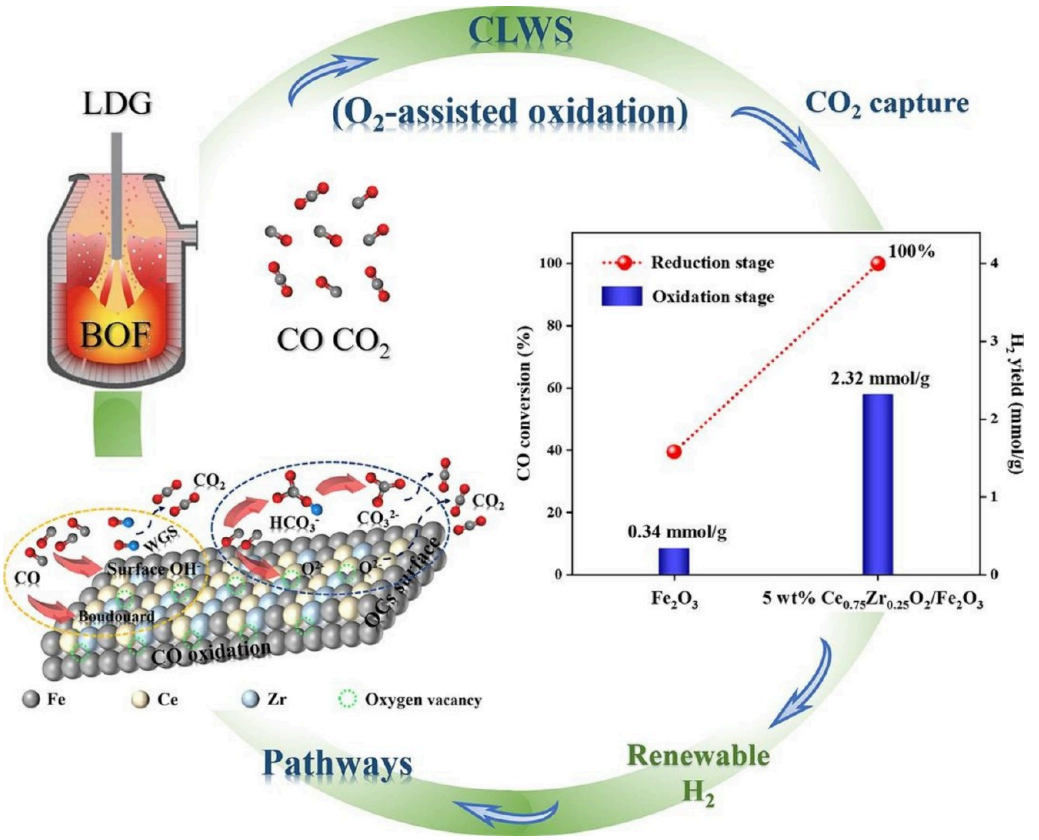

Figure 11. Effect of the composition materials on the CLC process.[89] Reproduced with permission from ref 89. Copyright 2023 Elsevier.

In this stage, the formation of the surface shell layer immediately triggered the rapid separation between the uniformly distributed Fe-containing phase and the TiO_2 phase in the OC. The shell layer formed on the surface of the OC was the double-layer structure (pure Fe layer/iron oxide layer). The outermost metal Fe played a dissociative role in the gas-phase oxygen, and the obtained ionic oxygen was conducted through the shell layer and the TiO_2 phase to take part in the oxidation reaction. The intense oxidation exotherm and the sharp increase in the local gas-phase pressure provided the impetus for the rapid migration of the molten Fe phase. Song et al. investigated that the pathways of lattice oxygen migration and transformation in the $NiFe_2O_4$ were studied based on *in situ* environmental transmission electron microscopy (*in situ* ETEM).[88] During the reduction process, the gas−solid reaction interface was usually fixed on the surface of the OCs. The Ni atoms first freed themselves from the spinel structure and gradually agglomerated on the surface of the oxygen-carrying particles. Finally, the spherical granular Ni monomers were formed, and lattice oxygen migrated extremely fast during this step. With the continuous progress of reaction, the Fe−O bond gradually started to break, the Fe atoms were detached from the oxygen-carrying particles, and eventually, the dumbbell-shaped Fe monomers were formed, in which the migration of lattice oxygen was slow. A stable oxide layer consisting of lattice oxygen and metal cations (Fe) was generated on the surface of the OC in the reduced ending state. The metal oxide−metal interface continuously migrated to the bulk phase, and the layer of metal oxide gradually became thicker. Moreover, the concentration gradient of lattice oxygen simulated the migration of O^{2-}; thus, the regulation of oxidative properties from oxidizing medium was realized to inhibit the separation of OC phase.

By introducing the metal oxides as the OC for cyclic regeneration between the reduction and oxidation reactors during the CLC process, the explosion risk related to the employment of pure oxygen can be avoided, and the corresponding reaction performance can also be substantially improved. Therefore, the development of OCs with strong redox activity, high mechanical properties, and good stability at higher temperatures is the key to the CLC process. Among various metal oxides, the oxides of transition metals, such as Ni, Fe, Cu, and Co are considered to be suitable OC materials for CLC technology. However, some of the properties from single metal OC make it difficult to meet the requirements of the process. These single metal OCs are usually loaded on inert carriers or added with other metal components to improve the corresponding comprehensive CLC reaction performance. The doping of electronic additives in OCs has great potential applications in CLC technology. The doped OCs can be studied in depth in terms of various preparation methods, metal substitutions, and other aspects.

3.3.2. The Employment of the Composition Materials. In the FR, the oxidation utilization of fuel is realized with the help of lattice oxygen in the metal oxide, and then, in the AR, the lattice oxygen of the reduced metal oxide is supplemented to complete the cycle. The CLC technology avoids direct contact between fuel and air, eliminates the release of harmful gases, and saves energy required for gas separation. The core of CLC technology is the OC, which can be widely utilized for *in situ* capture of CO_2 in the power generation process, partial oxidation to produce high-purity CO/H_2, selective oxidation to produce chemicals, ammonia, and other processes. Metal

https://doi.org/10.1021/acs.iecr.4c03713
Ind. Eng. Chem. Res. XXXX, XXX, XXX−XXX

oxides should have a certain bulk phase structure and OVs to facilitate ion transportation. For example, in the case of CeO_2 with a fluorite structure (face-centered cube), the (110) surface after reduction will produce an in-plane or split OV. During the oxidation process of FeO_x, the transition between FeO−Fe_3O_4 and Fe_2O_3 occurs, and the corresponding crystal structure also changes significantly. Fe ions migrate to the surface, resulting in a change in the morphology of the OC. The metal oxides such as Fe_2O_3, Co_2O_3, NiO, CuO, and MnO_2 contain abundant lattice oxygen and usually act as OCs. The particle scale of OC is a vital influence on the transfer of lattice oxygen, and lattice oxygen is easily transferred when the particle size of OCs is smaller. However, it is also prone to sintering, which leads to its poor structural integrity. The composition of other materials (the multiple metal oxides or the inset supports) is one of the modification methods that regulate the transfer of lattice oxygen in the OC. On the one hand, the composition can increase the amount of the available lattice oxygen, as shown in Figure 11. On the other hand, the transfer rate of lattice oxygen is also facilitated. Thus, the reactivity of lattice oxygen is improved to a great degree, which provides significant ideas for improving the transfer rate of lattice oxygen of transition metal oxides. By the composition of OC with other supports, not only can the transfer rate of the lattice oxygen in the OC be improved, but also the sintering of OC can be prevented, which is favorable the maintenance of structural integrity.

The general formula for the perovskite is ABO_3, where A is a lanthanide or alkaline earth metal ion and B is usually a transition metal ion. For example, La, Sr, Ca, Ba, and Ce are common elements in the A-site, and Fe, Ni, Co, Mn and Al are common elements in the B-site. Both A and B sites can be partially substituted by other metal ions with similar radii while the crystal structure basically keeps unchanged state. Thus, the perovskite materials are more suitable for the study of catalytic properties. Currently, perovskite is widely employed in the CLC process and other related research fields. According to the primary strategy of the catalyst design, it provides a reference for synthesis of high-efficiency catalysts: 1) the selection of B-site elements, which determines the catalytic activity, 2) the regulation of valence and vacancy through the selection of the A-site elements via the partial replacement, 3) the interaction effect of the constituent elements, especially for the replacement of B-site elements, 4) the increase of the specific surface area through the formation of small particles or dispersion on the carriers, and 5) the preparation of high activity catalysts by the addition of noble metals and appropriate regeneration. The preparation of pure perovskite oxides or the integration of metal oxides undergoes a long period of calcination at high temperature (>800 °C), which can result in a small specific surface area, and the raw materials can only reach the outer surface as a catalyst. The employment of a porous structure will enhance the specific surface area and thus improve the catalytic activity. During the CLC process, a common strategy for the application of perovskite OCs is to improve the reaction performance of perovskite by partially replacing the A- or B-site ions, which usually generates the OVs and improves the oxygen-carrying and oxygen-releasing capacity of perovskite.

Xing Zhu's group prepared $LaBO_3$ (B = Fe, Co, Ni, Cr, Mn, Al, Cu, V) perovskite oxides by the sol−gel method and investigated the reactivity and feasibility of perovskite oxides at various redox atmospheres.[90] The effects of the structural and thermal stability of various B-site elements on the properties of oxygen storage and redox behavior were compared. From the perspective of thermodynamics, the equilibrium partial pressures of metal oxides at various temperatures could be predicted based on the Ellingham diagrams, and to a certain extent, the oxygen partial pressures reflected the degree of difficulty in releasing lattice oxygen and the oxidizing activity of metal oxides. Ni, Co, and Mn oxides exhibited higher oxygen releasing rates at the temperatures of 350−550 °C with respective activation energies of 27.4, 44.4, and 69.1 kJ/mol. The required Gibbs free energy and enthalpy change for the reduction of the transition metal oxides were consistent with the V_2O_5 > Co_3O_4 > Fe_2O_3 > NiO > CuO > MnO_2 law, and the lower Gibbs free energy implied that the reaction was much easier to carry out and release oxygen. Correspondingly, the equilibrium oxygen partial pressure of metal oxides could be directly obtained to judge the releasing capacity of the oxygen. In addition to being a criterion for the releasing capacity of lattice oxygen, it could also be utilized to analyze the reoxidation capacity (the recovery capacity of lattice oxygen) of the metal or the reduced state metal oxides. The more easily an OC lost the lattice oxygen thermodynamically, the more difficult it was to recover the reduced state by oxidation. By comparison, the $LaFeO_3$ was suitable for the partial oxidation of the chemical looping for the CH_4/CO_2 cracking with a high reduction temperature, while the $LaCrO_3$ and $LaAlO_3$ were located in a $CH_4/CO/H_2$ atmosphere and were not capable of supplying the oxygen. This work provided a valuable reference for the future development of more active and stable chemical looping reaction oxides.

Zhen Zhao's group demonstrated that the design and synthesis of a bifunctional metal codoped high-efficiency carbon soot oxidation catalyst by replacing the A-site ions of $LaCoO_3$ using an alkali metal with stronger electron donating ability and the metal cerium with higher oxygen storage and discharge ability, which exhibited the outstanding reaction performance for the carbon soot particles catalytic combustion.[91] Due to the doping of potassium ions, more OVs appeared on the surface of catalyst to enhance the adsorption and activation of molecular oxygen, while the doping of the Ce^{3+} into the A-site enhanced the storage and release capacity of oxygen through the redox cycling reaction between Ce^{4+} and Ce^{3+}. The highly efficient oxidation of the carbon fume catalyst showed higher stability under various conditions and also exhibited stronger sulfur resistance and water resistance in the catalytic oxidation process of carbon fume. What is more, K and Ce codopant-modified La-Co-based perovskite catalysts were beneficial for practical applications in the catalytic reaction of diesel soot combustion owing to easier synthesis, lower cost, higher activity, and better stability. $La_{0.9}Ce_{0.05}K_{0.05}CoO_3$ possessed higher catalytic activity for soot combustion at 269, 309, and 342 °C, and in the presence of 10% H_2O, the temperature was significantly reduced to 327 °C. Yujun Zhu's and Junjiang Zhu's group illustrated that the performance of the perovskite catalysts prepared by selective etching, sol−gel, and coprecipitation methods was compared for the application to the catalysis of volatile organic compounds (VOCs), and the catalytic activity was explored for simultaneous removal of VOCs at the atmosphere of NO/H_2O.[92] A series of characterizations revealed that the preparation method had a great influence on the crystal size, specific surface area, redox capacity, oxygen mobility, and content of Co^{3+} in the $LaCoO_3$ oxides. The catalyst with a La/

https://doi.org/10.1021/acs.iecr.4c03713
Ind. Eng. Chem. Res. XXXX, XXX, XXX−XXX

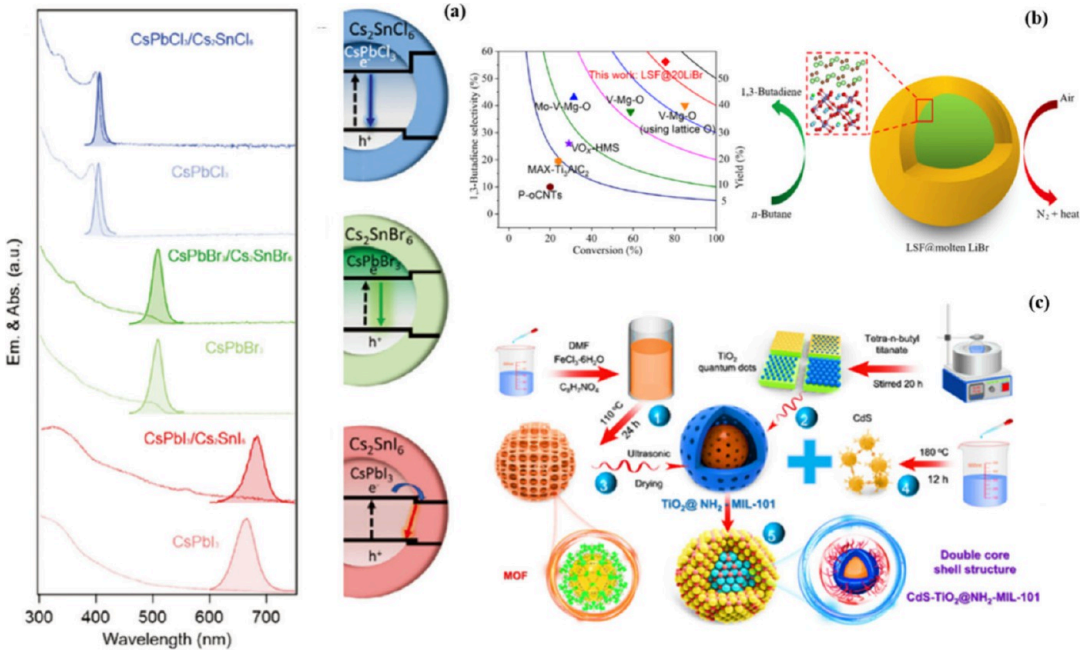

Figure 12. Preparation methods of the core−shell structure OC. (a) The preparation process of $CsPbX_3/Cs_2SnX_6$ (X = Cl, Br, and I) core/shell-type perovskite nanocrystals. (b) The effect of melt $LiBr@La_{0.8}Sr_{0.2}FeO_3$ for dehydrogenation of *n*-butane. (c) The process of CdS-TiO_2@NH_2-MIL-101 composition material.[95−97] Reproduced from ref 95. Available under a CC-BY 4.0 license. Copyright 2023 Lin, H. J. et al. Reproduced from ref 96. Available under a CC-BY 4.0 license. Copyright 2022 Gao, Y. F. et al. Reproduced from ref 97. Available under a CC-BY 3.0 license. Copyright 2024 Huang, Y. F. et al.

Co molar ratio of 2.0 and etched for 30 min was chosen as the most active catalyst, even in the presence of H_2O, and exhibited 100% ethyl acetate (EA) conversion at 220 °C. In particular, the role of NO in the reaction depended on the reaction temperature below or above 160 °C, whether the oxidation of NO to NO_2 occurred or not, which guided a novel strategy for the simultaneous removal of EA and NO, even for pollutants with more complex compositions.

The key to CLC conversion process is concentrated on the utilization of OC. Transition metal oxides readily transfer lattice oxygen into the reactant for the oxidation reaction and regulate the selectivity and distribution of products.[93] To avoid sintering, the perovskite acts as a carrier for OCs to form the composition of oxides. Although the perovskite cannot supply enough lattice oxygen for complete oxidation, it can be a "conductor" for the transportation of lattice oxygen in the OC due to its high thermal stability and excellent transportation properties. At the same time, by regulation of the composition of metal ions in the perovskite, the transfer rate of the O^{2-} in the OC can be improved. Yanguang Chen's group reported that the MOF precursors method was employed to prepare the $LaFeO_3$ with better textural parameters and tunable morphology.[81] The transformation process of lattice oxygen and gas product distribution of a single Fe_2O_3 OC and the composition Fe_2O_3−$LaFeO_3$ with different mass ratios were investigated during five cycles of CLC. The actual lattice oxygen conversions of Fe_2O_3−$LaFeO_3$ composition oxides were above 80% and higher than that of Fe_2O_3 (76.71%), suggesting that the incorporation of perovskite improved the conversion of lattice oxygen in the Fe_2O_3 OC. Dingshan Cao et al. prepared and screened the perovskite with various A site elements (La, Sr), various B site elements (Co, Fe), and various loading compounds (CeO_2, ZrO_2, Al_2O_3, and SiO_2) and utilized them for the CH_4 chemical looping steam reforming reaction.[94] The yield of hydrogen was higher for the metal La at the A-site and remained around 2 for the metal Fe at the B site (suitable for Fischer−Tropsch synthesis). In addition, the highest purity hydrogen was observed with the loading of CeO_2, and the CeO_2 could provide the lattice oxygen for the generation of the syngas in the CH_4 oxidation stage and increase the yield of the hydrogen in the water vapor reduction stage. Therefore, $LaFeO_3$−CeO_2 was screened as the optimal OC. When the WHSV was 11.79 h^{-1}, the CO selectivity of $LaFeO_3$−CeO_2 was over 98%, the H_2/CO ratio of syngas was 2, and H_2 purity was about 95%. The sample was able to recover its original crystalline phase after 10 cycles. Despite the slight aggregation of the sample that appeared during the reaction process at high temperature, it still showed stable reaction properties during the cycles.

3.3.3. The Construction of Core−Shell. Based on the introduction of composition materials, the dispersion of OC in the other supports is not suitable to be controlled due to its structural constraints. The core−shell structure further improves the dispersion degree of OC, and the composite oxides with the core−shell structure are prepared by the sol−gel method or the hydrothermal synthesis method, as shown in Figure 12. The composite oxides with OC as the core and other supports as the shell layer are synthesized, and the transfer rate of the lattice oxygen in the OC can be improved with the assistance of shell layer. At the same time, the sintering of OC in the redox process can also be effectively inhibited by high scale-composition-structure matching, and the regulation of lattice oxygen transfer in the OC can be realized.

The construction of the core−shell OC is favorable for mass transfer during the CLC technology.[98] Professor Fanxing Li, North Carolina State University, had studied oxygen-poor ODH using lattice oxygen from the core−shell structure of the

https://doi.org/10.1021/acs.iecr.4c03713
Ind. Eng. Chem. Res. XXXX, XXX, XXX−XXX

"perovskite@melting LiBr" redox catalyst.[96] The molten LiBr acted as a potent promoter to improve the redox active perovskite oxides, namely, $La_{0.8}Sr_{0.2}FeO_3$, for chemical looping-oxidative dehydrogenation (CL-ODH) of *n*-butane. The CL-ODH technology, using the metal oxides with excellent redox capacity as the solid medium (OC), effectively suppressed the excessive oxidation phenomenon brought about by the direct introduction of oxygen and improves the yield of olefins. At operating conditions, the redox catalyst consists of a molten LiBr layer overlaid on a solid $La_{0.8}Sr_{0.2}FeO_3$ substrate. The characterization and ab initio molecular dynamics showed that hydrogen peroxide species generated on $La_{0.8}Sr_{0.2}FeO_3$ reacted with molten LiBr to generate the active atom Br, which acted as an intermediate for C−H bond activation. At the same time, the molten LiBr inhibited the formation of nonselective CO_2, and the yield of butadiene was 42.5%. The design strategy of the redox catalyst can be employed for the CL-ODH reaction of isobutane conversion to isobutene and other low-carbon alkanes. Xing Zhu et al. proposed to prepare $(Ca/Mn)_{1-x}O$@ FeO_2 core−shell structure catalyst of ethylbenzene to styrene via the oxidative dehydrogenation.[99] The $KFeO_2$ shell was utilized for the activation of ethylbenzene, and the CaO−MnO solid solution with cation defect in the bulk phase was employed for reversible lattice oxygen acquisition and supply. The conversion of ethylbenzene was 97%, the selectivity of styrene was 94.2%, and the conversion of hydrogen was nearly 100%. The reaction route of oxidative dehydrogenation from ethylbenzene to styrene on the FeO_2 shell was C−H bond breaking → β-H bond breaking → styrene desorption. The C−H bond on C is activated as the speed control step of the process.

Jinlong Gong's group at Tianjin University developed an enhanced chemical looping dehydrogenation of propane to propylene, which was catalyzed by a nano core−shell redox catalyst.[100] The core−shell structure redox catalyst combined the dehydrogenation catalyst with solid OC in the same particle, and the structure was two-/three-layer vanadium oxide modified by CeO_2. Via *in situ* spectroscopy, chemical kinetics, and theoretical calculations, it proposed a dynamic "donor−acceptor" process of lattice oxygen, in which oxygen from CeO_2 generated the O^{2-} and then cooperatively transitioned through the interface. The diffusion transferred to the dehydrogenation catalytic site of vanadium oxide could stabilize the vanadium oxide species on the surface, achieve quasi-static oxygen coverage, and avoid overoxidation of the catalytic reaction or cracking of hydrocarbons. During 300 cycles of long-term dehydrogenation−oxidation cycles, the selectivity of propane to propylene and the yield of propylene still maintained 93.5% and 43.6%, respectively, with energy savings of 45%. Arya Shafiefarhood et al. investigated that a core−shell Fe_2O_3@$La_xSr_{1-x}FeO_3$ redox catalyst was prepared by the sol−gel method.[101] During the partial oxidation of CH_4, the activity of the core−shell redox catalyst was 200 times that of the inert catalyst. At high temperature (900 °C), the core−shell structure and activity of the redox catalyst also showed excellent stability over 100 redox cycles. In addition, the reactivity and product selectivity of the core−shell material was better than that of the multiple redox cycles, and the resistance of carbon formation using the composite sample with the same carrier was also enhanced. The increased activity could be due to a nanoscale Fe_2O_3 core (50 nm), which provided more available lattice oxygen via a mixed conductive shell (10 nm), resulting in a lower amount of carbon deposition using the core−shell redox catalyst than the composite sample.

Xianglei Yin et al. prepared the syngas and hydrogen by the chemical looping steam of the CH_4 reforming reaction, and they proposed a Fe@Ce OC with a core−shell structure, i.e., Fe_2O_3 nanocores covered by Ce shells.[102] The OC combined the advantages of high ionic conductivity from metallic Ce with the high oxygen storage capacity of Fe_2O_3. By comparing the activity of uniformly mixed Fe−Ce OCs and core−shell structured Fe@Ce OCs on a fixed bed, the experimental results demonstrated that the Fe@Ce OC exhibited higher yields of syngas and H_2, the selectivity of CO, and the conversion of CH_4 during a longer CH_4 reduction process, compared with Fe−Ce OC. The CeO_2 shell layer was able to provide more selective oxygen ions, which promoted the transportation of O^{2-} between the Fe_2O_3 nanocore and the surface of the Ce shell layer. In addition, a further increase occurred in the selectivity of CO and the conversion of CH_4 with a increase in the number of cycles of the reforming reaction, which was attributed to the gradual improvement in the proportion of the $CeFeO_3$ phase (one of the primary components in the oxidized Fe@Ce OC) as the cycles proceeded and had a higher transfer capacity of O^{2-} than that of the Fe@Ce OC that had not undergone oxidation and reduction. Moreover, the excellent conductivity of the O^{2-} via the CeO_2 shell layer also improved the carbon buildup resistance of the Fe@Ce OC, enabling the generation of syngas (H_2/CO close to 2) with higher quality and H_2 with higher purity. The amount of carbon deposition using the Fe@Ce was only 28.7% as much as that of Fe-Ce.

The chemical looping provides a favorable platform for converting fuels and oxidants in a clean manner with a high efficiency. The key of the technology is the metal oxide material that oxidizes the fuel, providing a reduced material that can be reoxidized to accomplish the loop. Jinlong Gong's and Liangshi Fan's group[103] in collaboration with Stanford University, summarized the recent advances in the redox chemistry of OC in the chemical looping. The motivation was the requirement of efficient materials and energy conversion programs. With the development of novel areas of the CLC process, the team focused specifically on state-of-the-art CLC systems, along with issues and guidelines on the construction of novel OC and chemical looping reactions. Fanxing Li and Christoph R. Müller's group reviewed the progress and development tendency of the chemical looping beyond combustion. In order to expand the application of chemical looping in the field of energy conversion and high-value conversion other than combustion, the general design principles, the advantages and challenges of the process, the construction strategy of OC (oxygen storage catalyst), and the redox reaction mechanism were elaborated in detail.[18] At the same time, the existing cases and research progress were comprehensively introduced, and the outlook and prediction of the potential new system were also looking. In many cases, energy consumption and CO_2 emissions are reduced by an order of magnitude. In recent years, significant progress has been conducted in the construction and manufacture of OC and its incorporation into chemical looping reactors for generating various chemicals.

3.4. The Characterization Techniques of Oxygen Vacancy. The concept of OV was first introduced in 1960[104] for the mechanism study of gas interaction with solid metal oxides. Specific external environments (e.g., high temperature) cause oxygen detachment from the lattice,

https://doi.org/10.1021/acs.iecr.4c03713
Ind. Eng. Chem. Res. XXXX, XXX, XXX−XXX

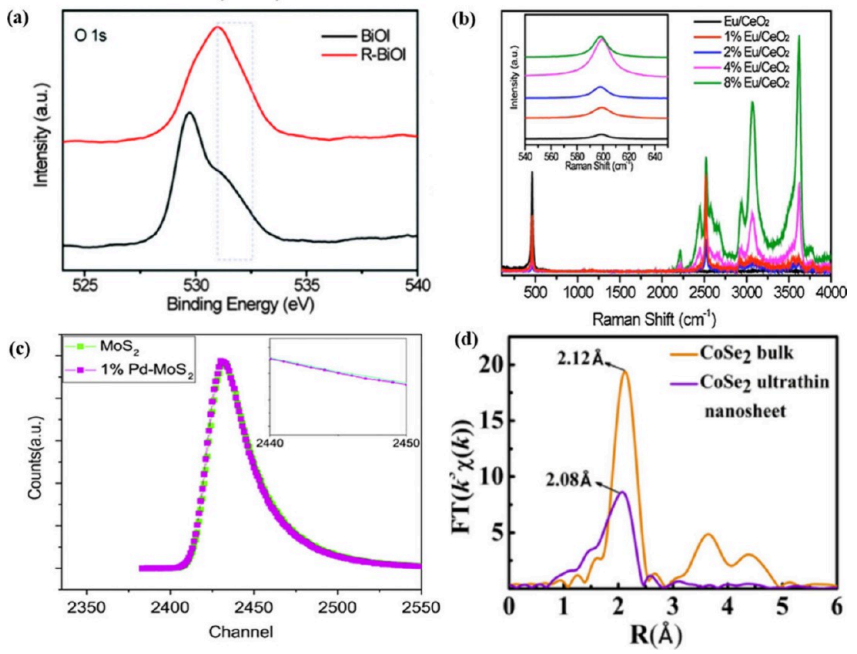

Figure 13. Characterization methods and results of the OV. (a) The O 1s XPS. (b) The Raman spectra. (c) The PALS spectra. (d) The XAFS spectra. Reproduced with permission from ref 105. Copyright 2016 Royal Society of Chemistry. Reproduced with permission from ref 106. Copyright 2016 Elsevier. Reproduced from ref 107. Available under a CC-BY 4.0 license. Copyright 2018 Luo, Z. Y. et al. Reproduced from ref 108. Copyright 2014 American Chemical Society.

leading to oxygen defect and the formation of OVs, and the defect equation can be expressed as shown: $MO_x - \lambda O_{lattice} = V_0 + MO_{x-1} + \lambda/2O_2$. In short, the OV is defects formed when the oxygen of the metal oxide lattice is removed from one oxygen atom. In the case of metal oxides, OV is a type of defect (point defect). The electronegativity of other elements is generally smaller than oxygen; thus, the loss of oxygen is equivalent to taking away an oxygen atom plus two positively charged electrons−holes. If the two electrons and holes are bound in the OV, the OV is generally positively charged. The metal oxides cause a deficiency of the element oxygen under the conditions (such as reduction) to lead to the formation of OV. The defects are mainly of several types: anionic vacancies, cationic vacancies, aberrations, and vacancy combinations. The introduction of OV affects the light absorption properties, geometry, electronic structure, and surface properties, of materials, providing novel ideas for applications and mechanisms. For the catalysis, the OV plays an important role, mainly in the following aspects: 1) the introduction of extra energy levels in the material, 2) the specific reaction sites for certain molecules in the catalytic process, which can act as an electron scavenger and then convert the attached oxygen to a superoxide radical, 3) a change in the chemical rate, which is dependent on the charge transfer from electrons or holes, and 4) the improvement of the electrical conductivity in the material.

At present, the characterization methods for the OV primarily include X-ray photoelectron spectroscopy (XPS), Raman spectroscopy, electron paramagnetic spectroscopy (EPR), positron annihilation lifetime spectroscopy (PALS), the Synchrotron X-ray absorption fine structure (XAFS), Scanning transmission electron microscope (STEM), DFT calculation, and others. The XPS technique is one of the most widely employed methods for surface analysis. It can be applied to most solid materials to provide the chemical state and valuable quantitative information from the surface property of the material, which achieves the surface to a depth of ∼10 nm. In general, the defects in the materials would change the bonding energy from the perspective of the shifted peaks or emerging peak. Therefore, XPS can be an effective method to detect the oxygen atoms or unsaturated sites in the defective materials compared to the defect-free materials. The OV was determined by O 1s XPS spectra as shown in Figure 13(a).[105] The peak at 529.5 eV was linked to lattice oxygen, and the peak at 531.5 eV came from the oxygen chemisorbed in the OV, respectively. This also indicated that the OV is stabilized by the adsorbed oxygen, which is a typical feature of the defect-rich oxides. This phenomenon can also be seen in the O 1s XPS spectra of other defective metal oxides. Raman spectroscopy is an analytical tool for studying the structure of molecules to obtain the information about their vibrations and rotations. Various chemical bonds have their vibrational modes that determine the changes between the energy levels. The variation in the energy levels of molecular vibration generates the Raman shifts. Therefore, the Raman shifts are correlated with the lattice vibrational modes, which can be utilized to explore the structural properties of the materials. The defects in the materials, especially the metal oxides, can affect the vibrational modes, leading to Raman shifts or the appearance of new peaks. The Raman spectra in Figure 13(b)[106] revealed the presence of OV in the structure of the doped cerium oxide nanosheets. The doped cerium oxide nanosheets showed a peak at 600 cm^{-1}, compared to that of the cerium oxide nanosheets, indicating the generation of OV.

Electron paramagnetic spectra (EPR) is a direct and advanced technique for detecting and characterizing the OV, which provides the information about the fingerprints of the unpaired electrons on the surface, and is a common method to identify single electron capture with considerable sensitivity. More importantly, these techniques can be informative as to

https://doi.org/10.1021/acs.iecr.4c03713
Ind. Eng. Chem. Res. XXXX, XXX, XXX−XXX

whether the sample is a liquid or a solid. EPR spectra are based on the fact that paramagnetic samples (with one unpaired electron) all absorb electromagnetic radiation in the right magnetic field. This phenomenon may occur at specific frequencies depending on the following equation: $h\nu = g\beta B$, where h is the Planck's constant, ν is the frequency, g is a constant, β is the Bohr magneton, and B is the applied magnetic field. The g value depends on the nature of free radicals and the g value of OV is ∼2.00. To date, EPR is a common technique for identifying the presence of OV. Taking the WO_3 for example, the WO_3 with OV had a representative EPR signal at $g = 2.002$, revealing the electron trapping on the OV. EPR spectra are a direct and effective method for determining the presence of OV. Although the EPR technique can directly identify the presence of defects, it cannot differentiate the types of defects, e.g., anionic vacancies, cationic vacancies, *etc.* In addition, it cannot confirm that the defect is in the volume or on the surface of the material. Therefore, the Positron annihilation lifetime spectroscopy (PALS) can directly measure the unoccupied volume of molecules of subnanometer size. A positron is injected into the material and then tested for length of time until it is annihilated by one of the electrons in the gamma-ray-producing material. The lifetime of a positron is a measure of the local electron density at the point of annihilation. Positrons preferentially react in regions of low electron density (vacancy and micropores), which is utilized to detect the type of defect and the relative concentration of defects based on the positron lifetime. PALS has the following advantages: 1) it is extremely sensitive to defects and microstructural changes at the atomic scale, 2) it does not damage the sample and can take the initiative to find defects, and 3) slow positron technology has energy adjustability to conduct the in-depth analysis of defective or structurally inhomogeneous samples. As shown in Figure 13(c),[107] after 1 wt % palladium was doped with molybdenum disulfide, the relaxation time of lattice defect t_1 and vacancy defect t_2 were significantly prolonged. t_1 changed from 183.6 to 206.2 ps, and t_2 changed from 355.5 to 384.6 ps. The increase in the relaxation time revealed the enhancement of defective dimension. In addition, the strength of relaxation time is also improved, which means that the defect content in the doped material is significantly higher than that in the undoped molybdenum disulfide material.

XAFS, an X-ray absorbing fine structure based on synchrotron radiation, has been widely employed in many scientific fields such as chemistry, environmental science, and materials, providing a powerful method for determining the electronic structure and the presence of OV. XAFS can provide structural information such as oxidation states, bond length and type, and atomic coordination number. Thus, they can be utilized to study the defects, atomic coordination numbers, and more structural information. In addition, a qualitative level of defect can be obtained by observing the distance of adjacent migrating coordination atoms and their peak intensities. In Figure 13(d),[108] the Co defects on the surface of $CoSe_2$ ultrathin nanosheets was verified and the Fourier transform curve of the bulk $CoSe_2$ showed the nearest CoeSe coordination with a main peak of 2.12 A. However, the peak intensity of ultrathin $CoSe_2$ nanosheets decreased and shifted 0.04 A toward low direction, which was attributed to the disordered surface structure of ultrathin nanosheets, as well as the loss of coordination accompanied by the formation of Co defects. The STEM has been utilized to characterize the structure of nanomaterials, which directly images the atomic structure. The atomic number and the arrangement of each atom can be observed in the crystal structure through STEM, which makes it play an important role in a wide range of applications such as surface science, materials science, and life science. However, this technique can only be observed in the localized areas of the material's surface. The investigation on the overall defects of the material is too limited because it requires a very thin sample for beam electron transport. Other than the above characterization methods, the DFT is a computational method for studying the electronic structure of materials. It is a quantum mechanical model for the study of atoms and molecules. Electron density can be predicted by using a general function. As a result, DFT is a general method utilized in physics, computational chemistry, and materials. With the broadening of the relevant research, more and more advanced techniques are applied in the exploration of OV.

4. CAPTURE AND UTILIZATION OF CO_2

4.1. Comparison of Various CO_2 Capture Techniques.

As the front end of the CCUS technology, the CO_2 capture is the basis of the utilization and storage of CO_2 and also the most expensive stage of CCUS technology. On the basis of the mechanism of CO_2 capture, many CO_2 capture technologies have been developed at various stages of research and application. According to the combustion process and combustion mode, CO_2 capture technology mainly includes precombustion capture, postcombustion capture, oxygen-enriched combustion, and CLC. The precombustion capture is a technology that separates CO_2 from the fuel or fuel-to-gas before combustion. It requires high treatment gas pressure, high CO_2 concentration, and low impurities, which is mainly employed in the IGCC. The postcombustion CO_2 capture is a technology in the separation and recovery of CO_2 from the tail gas after dust removal and desulfurization in the combustion process, which is widely utilized in the industry, power plant, and other scenarios. Based on the existing power plant boiler system, the oxygen-enriched combustion employs O_2 instead of air and regulates the characteristics of combustion and heat transfer in the furnace with a large proportion of flue gas circulation (70%) to directly obtain the flue gas with a higher concentration of CO_2 (up to 80%).[109] Some of the flue gas is re-enttered into the furnace. Thus, a technology that collects CO_2 to capture, store, or recycle CO_2 at a lower cost need to be established. The CLC process is a technology that employs solid OCs (metal oxides, *etc.*) to transfer oxygen from air to fuel for combustion, as mentioned above, which avoids contact between the fuel and atmosphere and realizes the separation of CO_2 in the combustion process.

In detail, the suitable processes for postcombustion CO_2 capture include chemical solution absorption, chemical adsorption, physical adsorption, and membrane separation. Solution absorption, solid adsorption, membrane separation, low-temperature fractionation, and so on are utilized for the precombustion methods of CO_2 capture. For the oxygen-enriched combustion technology, it can be applied to CO_2 capture in coal-fired power plants, which can be decomposed into atmospheric oxygen-enriched combustion and pressurized oxygen-enriched combustion. Pressurized oxygen-enriched combustion is a new technology that raises the pressure of the combustion system to 10−15 bar on the basis of atmospheric oxygen-enriched combustion and recovers the enthalpy of moisture in the flue gas to improve the efficiency of

https://doi.org/10.1021/acs.iecr.4c03713
Ind. Eng. Chem. Res. XXXX, XXX, XXX−XXX

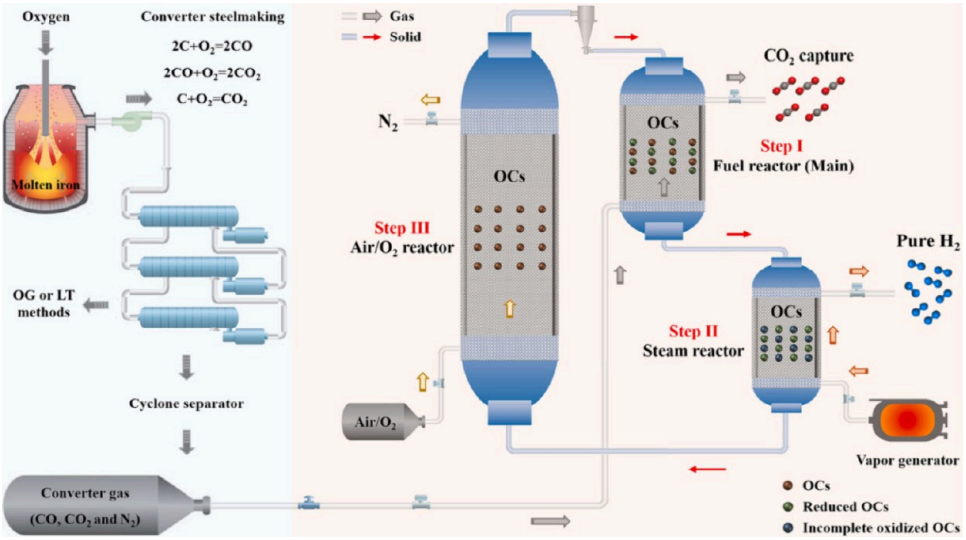

Figure 14. H_2 generation and CO_2 capture via the chemical looping water splitting of LDG.[89] Reproduced with permission from ref 89. Copyright 2023 Elsevier.

carbon capture system.[110] Besides the above three CO_2 capture technologies, CLC technology is a novel CO_2 capture technology, which is considered one of the most optimal options for the reduction of the costs for CO_2 capture. It can be divided into two types: iG-CLC and CLOU. The iG-CLC employs H_2O and CO_2 to convert fuel into H_2, CO, and other combustible volatiles, which then undergo solid oxidation with OCs such as iron ore. The CLOU employs OCs (such as CuO) that can release gaseous oxygen, which can enhance the combustion of solid fuels and improve carbon conversion and CO_2 capture.

According to four kinds of CO_2 capture routes (precombustion CO_2 capture, postcombustion CO_2 capture, oxygen-enriched combustion, and the CLC technology), every technical route and methods have their advantages and disadvantages, shown in Table S1.[111] As the CLC technology does not require oxygen production from air separation, it can directly produce high-concentration CO_2 flue gas without nitrogen, which reduces the energy consumption, the cost of CO_2 capture, and the net efficiency loss of the system. Therefore, compared with oxygen-enriched combustion technology, the CLC technology will not enrich SO_2, SO_3, and other corrosive gases, not easily cause the corrosion of the equipment and pipeline, and not easily cause combustion instability, furnace flame out, and other failures. The technology is usually utilized for the low-carbon combustion of coal but can also be utilized for biomass, petroleum coke, natural gas, and other fuels. At the same time, it is employed in coal-fired power plant projects. At present, more research into this technology has entered the semiindustrial or small-scale test period. In the future, we should focus on the research and development of OCs with high stability, high activity, and low cost to design and develop highly efficient and scientific CLC reactors and other devices, which improve the corresponding process design, construction, and other technologies to promote the realization of commercial application.

The concept of calcium looping technique (CaL) was first proposed in 1999.[112] For this method, CO_2 reacts directly with CaO to form solid calcium carbonate, which can be conveniently separated from other gases. The basic reversible reaction in this process is carbonation, which releases heat (exothermic), while the reverse reaction, called calcination reaction, can absorb heat (endothermic). The limestone ($CaCO_3$) employed in this process is harmless, readily available, and more cost-effective than the amine normally employed for washing during the postcombustion carbon capture.[113] In addition, the spent adsorbent could be reused for secondary applications. Although the adsorbent is recovered and reused for CO_2 capture, it is noteworthy that the reversibility of the core reaction decreases with each cycle, causing the decrease for the capacity of adsorbent. The main causes of this process are sintering and wear. After the first cycle, the capacity of the adsorbent is reduced by 15−35%, depending on the various reaction conditions, and this capacity loss is reduced in each cycle. Other natural materials such as dolomite ($CaMg(CO_3)_2$), oyster shells, and eggshells are also investigated, which is economically feasible to utilize these materials in the CaL cycle.[114] However, it is unlikely that these residues will be produced in the quantities required for commercial implementation of CaL as the process requires a large amount of adsorbent.

4.2. CO_2 Capture and Utilization via the CLC Technology. The huge amount of greenhouse gases generated by burning fossil fuels has led to climate problems such as global warming. To alleviate greenhouse gas emissions, the conversion of the captured carbon into the high-value-added products or energy could accelerate the shift from fossil fuels to clean energy. The main ways to utilize CO_2 resources are as follows: 1) starting from the source: reducing the use of carbon-containing fossil energy and developing the zero-carbon new energy, thereby reducing the rate of carbon emission, and 2) starting from the end: capture, storage, and resource utilization of CO_2. At present, the utilization of CO_2 resources includes chemical, biological, and geological resource utilization. Some of the chemical utilization modes have been industrialized, and the physical and geological utilization modes are still in the early stages. Among these methods, the CLC technology is the more clean and efficient way to generate the hydrogen-rich syngas and realize CO_2 *in situ* capture. The CO_2 is captured by an indirect mineralization reaction through the chemical looping reaction, and the captured CO_2 can be utilized to prepare high-value-added

https://doi.org/10.1021/acs.iecr.4c03713
Ind. Eng. Chem. Res. XXXX, XXX, XXX−XXX

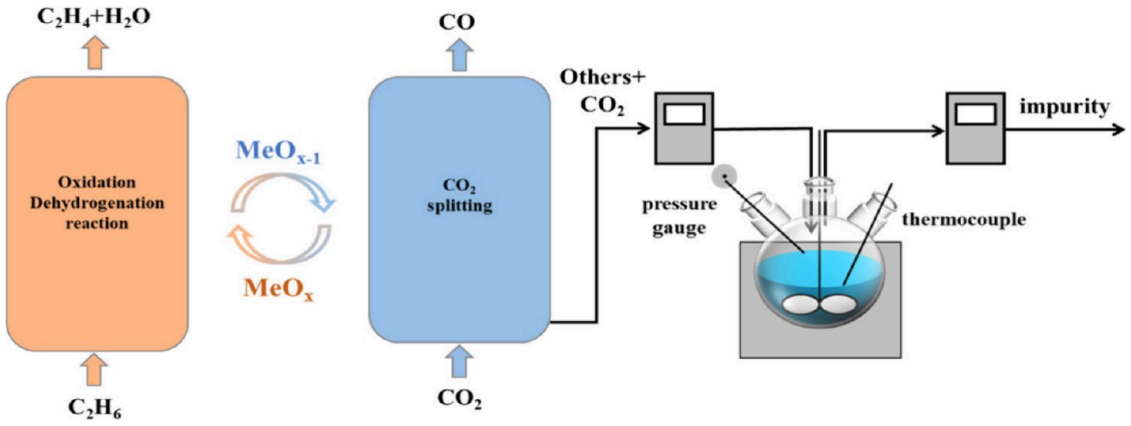

Figure 15. Splitting and adsorption of CO_2 during the CLC process.

chemicals. The technology provides large-scale, low-cost CO_2 capture, and lower storage solutions to achieve the reduction of CO_2 emissions, bulk solid waste reduction, and resource recycling. At the same time, high-value-added green products are generated correspondingly, which can be widely employed in the construction, plastic, paper, paint, and other industries and exhibit better technical and economic value.

The chemical looping process can easily achieve CO_2 capture without additional energy consumption to power the converter gas into green energy. Meanwhile, the method of producing pure H_2 by chemical looping is vital and attractive in many research fields and provides an economical and effective way to utilize industrial byproducts. Kongzhai Li's group proposed to utilize the Linz−Donawitz converter gas (LDG) as a reducing agent, and high-purity H_2 and CO_2 capture by the LDG under relatively mild (650 °C) conditions were achieved by coupling a three-stage chemical looping reactor: the FR, the steam reactor, and the AR (Figure 14).[89] Lower cost, efficient, and environmentally friendly OC was one of the key technologies to implement the technology. The Fe_2O_3 could act as an environment-friendly material that could participate in the gas conversion process of chemical looping. However, the defects of pure Fe_2O_3 limited the rapid and stable reaction. Therefore, a low-cost and high-performance composite OC modified with a small amount of $Ce_{0.75}Zr_{0.25}O_2$ solid solution was designed. 5 wt % $Ce_{0.75}Zr_{0.25}O_2$ solid solution was sufficient to optimize the activity, and the excess of the carrier could decrease the conversion rate of CO and the yield of H_2 to 100% and 2.32 mmol·g^{-1} at 650 °C, respectively. The addition of an air-oxidation-assisted water decomposition process could make the reduced OC fully regenerate and show a stable cycling capacity. The concept of chemical looping to the conversion process of the converter gas was applied, and the problem of massive carbon emission was solved in the process of traditional converter gas treatment. The CO in the converter gas was converted into high-purity H_2 with important industrial value by water vapor transformation reaction, and meanwhile, the CO_2 capture was realized. The OC showed excellent oxygen storage, releasing, and cycle stability when utilized in the converter gas thermochemical conversion. Compared with the traditional converter gas direct combustion or the single treatment mode of power generation, the proposed chemical looping reforming of converter gas to realize the generation of H_2 and self-capture of CO_2 provided a novel scheme for multiway utilization of industrial exhaust gas and had high industrial application potential.

Gulf of Tonkin University Professor Haiyan Zhang and Hunan University Professor Zhiwu Liang have introduced the redox metal oxides coupled with absorbents to form an absorbent−OC reaction model and a novel chemical looping of CO_2 capture and *in situ* reverse water gas conversion process was constructed.[115] The feasibility of the Prussian blue-derived Ca−Fe materials employed in the new process was verified by a series of experiments, and the capture−conversion reaction of Ca−Fe materials with different iron contents was investigated. The CO could be produced in the isothermal CO_2 capture and the conversion stage of the Ca−Fe material, which was attributed to reoxidation of CO_2 and the reverse water gas conversion of Fe, respectively. At 650 °C, the catalyst exhibited better CO spatiotemporal yields (238.25 mmol·S^{-1}·$kg_{Fe_2O_3}{}^{-1}$ and 3.00 mmol·S^{-1}·$kg_{CaO}{}^{-1}$) and a better CO yield (142.95 mmol·S^{-1}·$kg_{Fe_2O_3}{}^{-1}$ and 1.80 mmol·S^{-1}·$kg_{CaO}{}^{-1}$) without performance decay. The reasons for the excellent properties were concentrated on this: 1) the CO formation rate was enhanced by high Fe dispersion, and 2) the thermal stability was enhanced by t-ZrO_2 and $CaZrO_3$, which supplied a novel method for the construction of dual-functional materials in the process of CO_2 capture and *in situ* transformation.

The conversion and utilization of greenhouse gas CO_2 is the focus of international research, but CO_2 has strong stability, high bond energy, and thermodynamic decomposition temperature of nearly 2000 °C. How to realize the activation of CO_2 and the production of the chemicals under mild conditions is a bottleneck problem. To this end, Hao Zhang's team, in collaboration with Xin Tu's team of the University of Liverpool, UK and Hai Zhang's team of the Shanghai Jiao Tong University, reported a novel plasma-chemical looping coupling strategy for the conversion of CO_2.[116] It combined rotating arc plasma with OC to transform CO_2 into oxygen-free CO at a mild temperature. Through systematic experimental and theoretical studies, including DFT calculations, the key role of interaction between activated CO_2* and OV in this synergistic effect has been revealed. A new type of plasma-chemical looping CO_2 splitting (PCLCS) system was developed, which integrated rotating arc plasma with $Ce_xZr_{1-x}O_2$ OC, and CO_2 could be effectively converted to oxygen-free CO at a mild temperature (320 °C). Meanwhile, this technology achieved an impressive CO_2 conversion of 84% and a CO yield of 1.3 mmol of g^{-1}. Owing to the instantaneous on/off characteristics of the plasma, the proposed PCLCS

https://doi.org/10.1021/acs.iecr.4c03713
Ind. Eng. Chem. Res. XXXX, XXX, XXX−XXX

system could be powered by renewable energy in intermittent and decentralized manners, and it was expected to be a viable solution to the enormous challenge of converting CO_2 into clean CO.

Luis Pérez-Magueda et al. prepared the Mg-calcite with the formula of $Ca_{1-x}Mg_xCO_3$ by a precipitation-based method to capture CO_2 and thermal chemical energy storage in the CaL process.[117] The samples with the Ca:Mg molar ratios of 0.5:0.5 and 0.55:0.45 were pure phases, whereas the samples with the Ca:Mg molar ratios of 0.7:0.3, and 0.8:0.2 were composed of two phases. Furthermore, the aragonite phase was shown only in the samples prepared with calcium. The microstructure of magnesium-containing samples consisted of nanocrystals, which were aggregated into spherical particles, while the aragonite samples by precipitation showed a typical rod shape. Multicycle testing showed that the enhancement in the MgO content for calcined samples caused a decrease in the effective conversion rate, compared to the Fumiishi phase. Meanwhile, the samples with higher MgO showed an effective conversion value of ~0.5 after 20 cycles, improving the properties from aragonite as well as natural dolomite tested under the same conditions.

4.3. Preparation of the Chemicals via the CO_2 Capture and Activation Technology. *4.3.1. The Releasing and Concentration of CO_2.* Most utilization technologies of CO_2 (storage or value-added) require the concentrated stream of CO_2. Nevertheless, traditional combustion technologies generate low CO_2 concentrations in flue gas with the requirement of a large quantity of energy to concentrate CO_2. In contrast, the flue gas from the CLC process provides a pure CO_2 stream after the condensation of the cocomponent H_2O, as shown in Figure 15. Ravindra Gudi's group proposed the improvement process to endow multigeneration (energy and chemical production) and CO_2 high-value utilization during the CLC technology.[118] The design modifications for gasifier and FR separation, the employment of the hydrogen separators, the relevant separators, and partial/complete flue gas recovery had all led to various CLC-based poly generation schemes, and the effectiveness of these schemes to the above goals was also analyzed, and the methanol production rate (12.01−67.9 kg/h), dimethyl ether (DME) production flow rate (9.56−48.37 kg/h), relative profit/CO_2 emission (7.77−56.69%), and relative CO_2 emission reduction (4.62−25.96%) were achieved correspondingly. Based on the performance indicators of operational cost analysis, i.e., relative profit/CO_2 emissions, it had been employed to measure the poly generation schemes as a stand-alone version of the traditional CLC technology and chemical (methanol and DME) production processes. The effects of operation conditions, such as the ratio of syngas to FR, flue gas cycle ratio, and the ratio of syngas to water gas shift reaction, on the performance of the scheme were evaluated. Moreover, the simulation in Aspen Plus also proved the effectiveness of the proposed scheme. Haibo Zhao's group investigated the chemical looping reactions of Ce-modified $SrFeO_{3-\delta}$ OC to oxidative dehydrogenation of ethane and the CO_2 cracking were studied.[119] Over 39 cycles of redox testing, the conversion rate of the ethane reached 29%, and the selectivity of ethylene reached 82% on $0.2Ce/SrFrO_3$, with a CO production of 0.25 $mmol{\cdot}g^{-1}$ in the subsequent CO_2 cleavage step. The $Fe^{2+}/(Fe^{3+} + Fe^{4+})$ ratio decreased, and the reactive oxygen species ratio increased on the near surface of Ce-modified samples, which was the primary reason for the enhancement of $0.2Ce/SrFeO_3$ activity in the ethane oxidative dehydrogenation reaction. DFT calculations further showed that the improvement of oxidative dehydrogenation activity of $0.2Ce/SrFrO_3$ was due to a decrease of the formation energy from surface OV after the promotion of Ce. In addition, the ethylene selectivity of the CO_2 regenerated samples was better than that of the O_2 regenerated samples, which was owing to the larger diffusion resistance of lattice oxygen from bulk to surface. $0.2Ce/SrFeO_3$ catalyst successfully promoted the valorization of ethane and CO_2 via the oxidative dehydrogenation of ethane coupled with the splitting of CO_2 in a chemical looping manner.

The chemical looping rearrangement of CH_4 for CO_2 capture is a novel means of utilizing CH_4 and CO_2. Yane Zheng's and Yuhao Wang's group reported an outstanding $LaFe_{0.8}Co_{0.15}Cu_{0.05}O_3$/Silicalite-1 OC that efficiently converted CH_4 and utilized CO_2 at lower operating temperatures.[120] At 800 °C, the $LaFe_{0.8}Co_{0.15}Cu_{0.05}O_3$ exhibited a higher reaction rate of CH_4 (7.0×10^{-7} $mol{\cdot}(g{\cdot}s)^{-1}$), the selectivity of CO (84.2%), and the yield of CO (0.045 $mol{\cdot}g^{-1}$). The activity of $LaFe_{0.8}Co_{0.15}Cu_{0.05}O_3$ decreased rapidly with multiple redoxing cycle. The employment of Silicalite-1 improved the activity of $LaFe_{0.8}Co_{0.15}Cu_{0.05}O_3$ during the redoxing cycle. Under the condition of heating, $LaFe_{0.8}Co_{0.15}Cu_{0.05}O_3$ grew on the edge of Silicalite-1, and the nanoparticles were uniformly dispersive on the surface, improving the thermal stability and reactivity of OC. Moreover, the interface between Silicalite-1 and $LaFe_{0.8}Co_{0.15}Cu_{0.05}O_3$ played a vital role, in which the textural structure of the Silicalite-1 decreased the mass transfer limitation of the interface. Thus, Silicalite-1 had a higher selectivity for adsorbing the CH_4 and CO_2, which generated high reaction activity. Except for gas fuel, coal is the primary ingredient for the preparation of methanol to ease the supply and demand. The traditional coal-to-methanol process has a low energy efficiency because of high consumption for energy in the separation of air and the capture of CO_2. In order to decrease the energy consumption and CO_2 emission to improve the efficient utilization of energy, Huairong Zhou's group designed and analyzed a new coal-to-methanol process, which integrated the chemical looping air separation and chemical looping hydrogen.[121] The interaction of chemical looping air separation technology removed the air separation device and reduced energy consumption to some degree. The integration of chemical looping hydrogen technology could remove the device of water gas conversion, enhance the CO_2 concentration, and decrease the energy consumption of the CO_2 capture. The chemical looping hydrogen technology also produced the hydrogen to regulate the ratio of hydrogen to carbon in syngas. The energy consumption of the chemical looping air separation process and chemical looping hydrogen process was reduced by 41% and 89%, respectively, by comparison with traditional air separation and coal-to-methanol process. In contrast with the traditional coal-to-methanol process, the process improved the energy efficiency by 18% and reduced CO_2 emissions by 45%.

At present, many adsorbent materials, such as basic solvents, amines, and metal organic frameworks (MOFs), can remove CO_2 from ultradilute gases such as flue gas and air (~400 ppm). However, the regeneration of CO_2 adsorbents usually requires a large amount of energy. Therefore, it is particularly important to develop adsorbents that can capture CO_2 efficiently and achieve low energy consumption regeneration. Qing He's group employed an ultrafan solution to capture CO_2 directly from low-concentration CO_2 gas (i.e., simulated flue

https://doi.org/10.1021/acs.iecr.4c03713
Ind. Eng. Chem. Res. XXXX, XXX, XXX−XXX

gas, exhaled gas, and dry air).[122] About 6.4 mol of CO_2 could be captured by 1.0 mol of ultrafan, and CO_2 was released to regenerate ultrafan adsorbent at ambient pressure and room temperature by magnetic stirring. In addition, for CO_2 capture and releasing from different gas sources, the adsorption−desorption performance of the ultrafan remained unchanged after 5−20 cycles. Meanwhile, the release of CO_2 could be collected through a simple device, and the concentration was up to 83%. The mechanism of the CO_2 adsorption by ultrafan, as a pseudo particle, was clarified by theoretical calculation. As a pseudo particle, an ultrafan could react with CO_2 through the transition state of the six-membered ring with low activation energy. The phase transition was also important for the capture and release of low-energy CO_2. The ultrafan solution was the first to propose a solution for CO_2 capture, mechanical releasing, and concentration system for CO_2 at room temperature that could be utilized to capture CO_2 from rarefied gases under environmental conditions and release CO_2 at low energy consumption. The study provides guidance for the further development of sophisticated CO_2 capture materials and advanced atmospheric negative carbon technology and supplies a feasible strategy for reducing the amount of CO_2 in the atmosphere and for the post conversion of the concentrated CO_2. In addition, the nanocatalysts improved the desorption of CO_2 and decreased the energy requirement of solvent regeneration. Ozge Yuksel Orhan's and Hulya Yavuz Ersan's group investigated the adsorption−desorption properties of nonaqueous triblend amines (MEA, MDEA, and PZ).[123] The catalysts included HZSM-5, H-ferrite (FER), H-zeolite (MOR), γ-Al_2O_3, TiO_2, MgO, and In_2O_3. Compared with the blank test, the addition of catalysts significantly improved the desorption performance of three mixed amine and reduced the energy consumption. Moreover, when the amount of the catalyst was lower, the desorption efficiency was higher. As 0.125 g of catalyst was employed, the reduction order of CO desorption heat load performance was as follows: MgO (70.9%) > In_2O_3 (80.2%) > HZSM-5 (84.1%) > Al_2O_3 (84.2%) > FER (87.1%) > MOR (88.4%) > TiO_2 (89.7%). Besides, HZSM-5 had the highest desorption factor of 42.5 mol/kJ·min with the desorption rate of 23.7 mol/min, which provided desorption properties of nonaqueous amine mixtures with energy-saving catalysts and strengthened the potential as the outstanding materials in the carbon capture and storage applications and the enhancement of energy efficiency.

4.3.2. The Fundamentals of the Coupled Olefins Technology. The CLC technology is the combustion of traditional fuel in a direct contact manner with air, which is divided into the gas−solid reaction by the action of OC, and the oxygen from the atmosphere is transferred to fuel by an oxygen-carrying agent. By comparison with traditional combustion technology, the CLC technology can realize the utilization of energy cascade, and the separation of combustion and regeneration space makes it exhibit the function of near-zero energy consumption and internal separation of CO_2. Under this background, the CO_2 capture, activation, and resource integration can be realized through an economical and feasible hydrogenation process in series as the high-purity CO_2 capture is condensed in the exiting flue gas of FR. The coupling of CO_2 capture and catalytic conversion in the CLC technology provides a novel idea for carbon emission reduction and resource utilization. The CLC technology has characteristics of CO_2 internal separation and can realize CO_2 capture at a low cost. Through analyzing the principle of the coupling technology and the application of the complicated OCs, especially the feasibility to produce low-carbon olefin in detail, the application of CO_2 capture and conversion with the assistance of the CLC technology exerts a potential value, as shown in Figure 16. What is more, the activation and resource

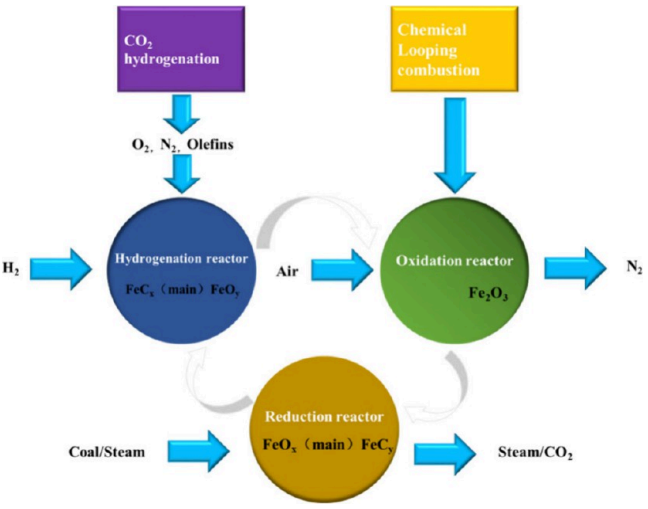

Figure 16. Production of olefin coupled with the CLC technology.

utilization of CO_2, a byproduct of coal chemical process, also provide a theoretical reference. The design of OC dual-function catalyst particles is the key to realizing this technology. The development of an efficient and stable OC can be utilized to improve the conversion and yield of low-carbon olefin via CO_2 hydrogenation. The investigation of the mechanism is still the focus and difficulty of future research.

Qingjie Guo's and Yurong He's group developed a bifunctional OC with higher catalytic activity and oxygen mobility, which played a decisive role in the CO_2 conversion to light olefins by the CLC technology.[124] $K/La_yCo_xFe_{1-x}O_3$ (x = 0, 0.2, 0.4, 0.6, y = 0.2, 0.4, 0.8) catalysts with OV-active metal biactive sites were established by the synergistic strategy of Co doping and La defects, and the releasing of oxygen and catalytic performance were also evaluated. $K/La_{0.4}Co_{0.4}Fe_{0.6}O_3$ exhibited higher oxygen mobility and the reduced state was utilized directly for CO_2 conversion to light olefins. The selectivity of light olefins was ∼30%, and the conversion rate of CO_2 was 36%. The synergistic effect of Co doping and La defects increased the OVs and accelerated the growth of the dissolved CoFe alloy under the reduction conditions of the CLC technology. *In situ* DRIFTS revealed a formate−methoxy mechanism and the dynamic equilibrium of the reverse water-gas shift (RWGS) Fischer−Tropsch synthesis (FTS) pathway. The OV promoted the transformation of CO_2 through the formic acid pathway, as the metal phase changed the distribution of products by the variation of intermediates evolution. Co_7Fe_3 and OV on $K/La_{0.4}Co_{0.4}Fe_{0.6}O_3$ promoted the generation of CH_x and the coupling of C-C by various intermediates, which improved the selectivity of light olefins. Meanwhile, Qingjie Guo's and Jianli Zhang's group studied catalytic performance of $K/LaFeBO_3$ (B = Cu, Zr, Al, Mn, Ni, and Zn) catalysts by the sol−gel and impregnation methods for CO_2 conversion to light olefins.[125] With the introduction of Cu and Zn, the particle size decreased with the increase of Fe dispersion, as the exposed alkaline centers increased with the desorption temperature decreasing of hydrogen. The mobility

https://doi.org/10.1021/acs.iecr.4c03713
Ind. Eng. Chem. Res. XXXX, XXX, XXX−XXX

of oxygen in the perovskite had a great effect on the catalytic performance and the selectivity of the olefin. While Fe at the B site was replaced by Zn and Cu, the mobility of oxygen and the selectivity of olefin increased significantly. The lattice oxygen in the surface with lower binding energy preferentially formed olefins, and the increase of the oxygen diffusion rate led to the enrichment of lattice oxygen species in the surface, thus increasing the yield of olefin.

The oxidative dehydrogenation of propane (ODP) with CO_2 to propylene has attracted more and more attraction in the past years due to its features of CO_2 utilization, higher yield, and the avoidance of overoxidation. Nevertheless, this process is endothermic and undergoes the burning of fuels to meet thermal needs, resulting in significant CO_2 emissions. C. Sumana's group put forward a new eco-friendly propylene production method for the first time, which combined the ODP-CO_2 technology with the CLC technology and had double benefits of inherent CO_2 capture and utilization.[126] In addition, the process was self-sustainable by recycling residual heat energy and producing steam for the generation of power. The steady whole-plant simulation model of the CLC-ODP-CO_2 joint scheme was established by using Aspen software. For the ratio of CO_2 and propane, a strict sensitivity analysis process was also carried out to screen the operation temperature, pressure, and molar flow of OCs, leading to a maximum propylene yield of 79.1%. The total energy analysis results of the CLC-ODP-CO_2 method showed that the net thermal efficiency of the scheme was 73.48%. Muhammad Aziz's group proposed a carbon-negative olefin and green hydrogen cogeneration system using the solar energy and biomass via the chemical looping, which provided a new way for high-value-added conversion of solar energy and biomass.[127] The whole system consisted of two parts: the biomass to olefin (BTO) and the photovoltaic to hydrogen (PVHP). Solar energy was utilized to generate green hydrogen for taking advantage of excess CO_2 and reaching zero CO_2 emissions in the formation process. The annual output of ethylene and propylene was 4550−5500 tons, and the energy efficiency of the BTO subsystem was 55%−65%. In terms of technical and economic effects, rice straw was the best biomass feed, and the cost could be acquired within 8.5 years. In the future, as the development of photovoltaic technology leads to the reduction of cost, the system will show an outstanding economy.

During the process of oxidative dehydrogenation (ODH) of light alkanes, chemical looping technology has become a promising approach that provides an opportunity to significantly reduce the emissions and the energy consumption for the ethylene and propylene production industries. The higher yields of olefin can be achieved via the CLC process by the regulation of material requirements (e.g., electronic and geometric structure) to prevent from the total conversion of alkanes to CO_x. Christoph R. Müller's group summarized the nucleophilic oxygen species and the electrophilic oxygen species, which promoted the peroxidation of CO_x products in the selective reaction of alkenes.[128] To reduce the generation of CO_x and enhance the selectivity of olefin, the modification and regulation methods of catalyst materials were discussed in depth. At present, common techniques primarily include bulk and surface doping and the deposition of coatings. In terms of the consumption of energy and the intensity of CO_2, the techno-economic evaluation of CL-ODH system predicts the energy savings of >80%, compared with existing production processes of olefin, such as the steam cracking or dehydrogenation.

In essence, the system has the following advantages: 1) the internal separation of CO_2, without the need for external separation device for CO_2 capture, 2) the cycle utilization of OC in the FR after reaction, 3) the OC preactivation in the FR, which shortens the induction period of the reaction in the catalytic reactor, and 4) the direct capture of CO_2 from the CLC technology and its conversion into the high-value-added chemicals, which improves the environmental protection and economic benefits of fuel combustion. The technology can make solid fuel burn and realize CO_2 activation by regulating the ratio of lattice oxygen/fuel/gasifier and utilizing the phase transformation and mass transfer of an iron-based compound. Meanwhile, both the heat and high-value-added olefins are acquired. The excellent performance of OV for oxygen storage and transportation is expected to improve the performance of catalyst and reduce the surface deposition carbon in the AR oxidation. Moreover, the releasing energy can be utilized for the circulation system heating.

4.3.3. The Preparation of the Coupled Methanol Technology. As the world transitions toward a low-carbon economy, the development of multiple ways to reduce CO_2 emissions is important. Chemical looping technology, a low-carbon technology, considered as a breakthrough for efficient conversion of fuel and the capture and storage of CO_2, has been successfully tested in pilot plants in many countries. Furthermore, the conversion of the captured CO_2 into methanol is regarded as an effective way to reduce CO_2 emissions (shown in Figure 17) and the resulting methanol

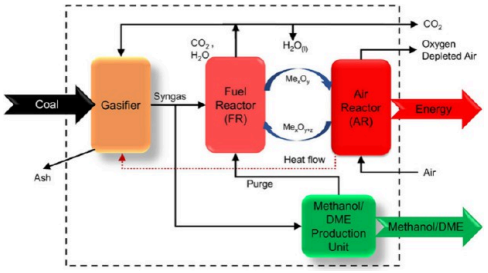

Figure 17. Valorization of CO_2 to methanol during the CLC technology of coal.[118] Reproduced with permission from ref 118. Copyright 2022 American Chemical Society.

can serve as a convenient hydrogen storage energy carrier. Muhammad Aziz's group focused on the utilization of the produced CO_2 in the process of converting the microalgae (a potential fuel) into the methanol chemicals.[129] The specific focus was to maximize the energy recovery and convert the microalgae into methanol via two-stage integration. The Aspen Plus software was employed to simulate the production of 42 t of methanol using 60.1 mt·h^{-1} CO_2 and 8.2 mt/H H_2, which consisted of four modules: drying, chemical looping gasification, syngas chemical looping, and the synthesis of methanol. The energy efficiency was 45−51%, which was comparable to the generation process of the methanol from CO_2-based methanol after concentration and the biomass synthesis gas. The separated CO_2 by chemical looping technology was employed for the preparation of methanol to obtain a negative carbon value. In addition, the process of propane to propylene will generate large amounts of hydrogen and hydrocarbons, not only wasting energy but also leading to

https://doi.org/10.1021/acs.iecr.4c03713
Ind. Eng. Chem. Res. XXXX, XXX, XXX−XXX

emissions of CO_2, if burned directly for heating. For solving these problems, Dong Xiang's group developed a new process for producing the propylene and methanol from the propane.[130] First, hydrogen in the product gas was obtained via PSA and extraction technologies. Then, the heat and high-purity CO_2 were obtained by burning the remaining hydrocarbons via the chemical looping process, which eventually reacted with hydrogen to form the methanol. The exergy efficiency of the process was enhanced from 77.61% to 80.18%, the direct capture rate of CO_2 was 98%, and the utilization rate was ~40%. The process was superior to the traditional process in the exergy efficiency and CO_2 capture but inferior to the traditional process in the investment.

Methanol is considered a vital chemical raw material in the industry, which exhibits great potential to replace gasoline and diesel as automobile fuel. The production of methanol from biomass is a green production method, while the economy and environmental feasibility depend on the generation technology and geographical environment. Nurin Wahidah Mohd Zulkifli's group proposed a method of producing the carbon-negative methanol, which was integrated four modules: bagasse pyrolysis, physical activation, chemical looping, and methanol synthesis.[131] Three schemes of coproduction for methanol and biochar, coproduction of methanol and activated carbon, and coproduction of methanol and activated carbon with multi hydrogen and activated carbon were established in the Aspen Plus software. The evaluation system was demonstrated to quantitatively assess carbon, energy efficiency, economy, and environmental benefits of three scenarios. The addition of hydrogen effectively improved the methanol yield, thereby enhancing the carbon utilization efficiency and energy efficiency, which presented remarkable environmental benefits with low GWPs of −1631.18 and −710.28 kg CO_2-eq/t methanol. On the other hand, the utilization of coke oven gas to prepare methanol requires additional carbon and results in the waste of hydrogen resources. Jiancheng Wang's group employed a combination of coke oven gas chemical looping reforming and pulverized coke CLC technology to solve the problems of high intensification and low hydrocarbon utilization in the process.[132] The CO_2 produced by the pulverized coke CLC technology was recovered into the coke oven gas chemical looping reforming, and the CH_4 in the coke oven gas was reformulated to change the H/C ratio of syngas and produce massive methanol. The utilization ratio of hydrogen and carbon was 85.4% and 63.9%, respectively, and the exergy efficiency was 77.5%. The system had less complexity, and massive CO_2 was recycled to generate the value-added chemicals.

Liang-Shi Fan's group took the advantages of the modularization strategy from the quantitative chemical looping reducer and employed two or more parallel operations of the reducer to increase the production of syngas, which was beyond the reach of a single reducer reactor or the conventional process.[133] The capture and utilization of CO_2 were utilized as the raw materials for a chemical looping system using the Fe−Ti composite oxide to improve the production capacity of coal-based chemicals. The simulation results in the Aspen Plus software were verified by experiments in a small reducer reactor, and the modular simulation was extended to the industrial-scale methanol and the acetic acid production plant. The chemical looping modularization had shown that the coal consumption could be reduced by up to 25% in a basic coal gasification process, compared to if a single chemical looping reducer was employed with the replacement of modularization method, the consumption of coal could be reduced by 15% for the production of 10,000 tons of methanol a day. With the interaction into a commercial-scale acetic acid production plant, the process could be regarded as a CO_2-neutral or negative system, in which the process consumed much more CO_2 than it produced. For the coal chemical process with large scale, the methanol, formic acid, acetic acid, and oxalic acid all had potential yield.

4.3.4. The CLC Technology for Other Chemicals. The CLC technology for CO_2 capture and conversion is the key to the utilization of CO_2. During the process of CLC technology, gasification, and reforming, the introduction of the fluidized bed reactor and fixed bed reactor should be considered for various types of fuels (including biomass and gaseous fuels). Thus, the sustainability should be universally emphasized in the CLC technology studies for coal, natural gas, and so on. The conversion of captured CO_2 to methanol, formic acid, and other chemicals should be further discussed in the process for the CLC technology and fixed-bed reactors. The major CLC technologies through the capture of CO_2 and the relevant reaction process of carbon conversion are conducive to the selection of appropriate clean energy technologies for specific processes. In the area of carbon capture and transformation, the CLC technology combined with the hydrothermal processes is viable and sustainable, which leads to more clean energy technologies via the employment of coal, natural gas, biomass, and so on.[134] By means of the chemical looping process, Nadi Braidy's group reported that $NiFe_2O_4$ acted as the catalyst and magnetic heating was employed to induce the self-controlled heating medium. Thus, the technical feasibility of a new method for efficient reduction of CO_2 produced by RWGS was accomplished.[135] First, at ~400 °C, the Ar/H_2 mixture flowed on the catalyst for 1 h to produce the OVs (δ). Then, under similar conditions, the Ar/CO_2 mixture flowed over the active catalyst $NiFe_2O_{4-\delta}$ to produce the CO and replenish oxygen. The effects of the heating mode (conventional heating or induction heating), the added amount of gas, and cycle times on the performance of the catalyst were studied. The catalyst maintained its activity in several cycles (1.37 ± 0.07 $\mu mol \cdot g^{-1}$ $NiFe_2O_4$), but its activity decreased slowly under the action of H_2. The formation of (Ni, Fe) clusters on the surface of Ni ferrite nanoparticles was due to the separation of metal atoms absorbed from the octahedral position of Ni-spinel. The change of the chemical structure had an outstanding effect on the activity of the catalyst and the total CO production. The induced heating could heat the catalyst shortly, but the temperature distribution of the catalyst bed was less uniform, resulting in the reduction of the superheated area in the catalyst bed. Finally, the simultaneous entry of H_2 and CO_2 allowed for higher CO production, compared with the chemical looping, reaching 7.74 ± 0.67 $\mu mol \cdot g^{-1}$ of $NiFe_2O_4$ in 1 h experiments.

The chemical looping dry reforming of methane is a promising process for the highly efficient utilization of methane and the production of CO_2 from syngas, which provides a suitable H_2/CO ratio for Fischer−Tropsch synthesis. The key problem of the chemical looping dry reforming of methane is to find a stable and high reactive OC. Yinhe Liu's group employed the hydrothermal and calcination methods to prepare polyhedral NiO/Fe_2O_3 composite OCs, and the performance of NiO/Fe_2O_3 was evaluated in a fixed bed reactor.[136] The yield of the synthesis gas from Fe_2O_3-0.6Ni was

https://doi.org/10.1021/acs.iecr.4c03713
Ind. Eng. Chem. Res. XXXX, XXX, XXX−XXX

the highest at 750 °C, reaching 90.25%, and the molar ratio of H_2/CO in the reductant was ∼2. In addition, under a reducing atmosphere, the Ni_3Fe alloy was generated instead of Ni and Fe, so the resistance of coke was improved remarkably. The energy barrier of the dehydrogenation process (*CH_3 released *H to form *CH_2) of pure Fe_2O_3 was 2.64 eV, higher than that of NiO/Fe_2O_3 composite compounds (2.64 eV) by the DFT calculation. The introduction of NiO to Fe_2O_3 was beneficial to the dehydrogenation of CH_4, which provided the guideline for the design of OCs with better coke resistance capability during the CH_4 chemical looping dry reforming. Via the utilization of CO_2, the greenhouse gas emission reduction strategy to CO_2 storage has been widely concerned. The fossil fuel power plants, as a single sector, are major emitters of CO_2. The CLC technology is an inherent CO_2 capture technology and can also be employed for the production of H_2. The captured CO_2 and produced H_2 can be utilized as the reactants during the synthesis of various chemicals. Venkata Suresh Patnaikuni's group discussed four conditions of the CO_2 utilization in the coal direct CLC unit to produce four valuable products,[137] containing the methanol, formic acid, methane, and DME. Comprehensive assessments also included energy, ecological, exergy, economic, and life cycle analyses. The coal direct chemical looping device for synthesizing formic acid was the most advantageous choice, and the CO_2 utilization rate was 100%.

Zhiwu Liang's and Bo Jin's group reported a crystal construction strategy to regulate the strong electron interactions of Fe_2O_3/ZrO_2 by theoretical calculations and the reactivity assessments.[138] By comparison with *t*-ZrO_2, *m*-ZrO_2 had a strong electron interaction strength with Fe_2O_3 and Fe, generated more OVs, and transported more electrons to promote the H_2 and CO_2 activation, which reduced the redox energy barrier. This strategy made the time-averaged CO space-time yield (560) of Fe_2O_3/m-ZrO_2 twice as high as that of Fe_2O_3/t-ZrO_2. There was a positive interaction between the electron interaction strength and the yield of CO, which provided guidance for the rational design of efficient catalysts for thermochemical and redox reactions. The efficient utilization of CO_2 is the key point to limiting the global climate change. CO is an important feedstock for the synthesis of chemicals, and it can be generated by the decomposition of CO_2. At present, the thermochemical routes are the energy-intensive and require high-operating-temperature process. Fanxing Li's group reported a hybrid redox process (HRP) for the conversion of CO_2−CO via the employment of lattice oxygen-deficient redox catalyst at low temperatures (<700 °C).[139] The lattice oxygen of the redox catalyst was restored during the decomposition of CO_2 and was subsequently employed to convert CH_4 to prepare the syngas via the chemical looping. This cyclic redox process was operated at significantly lower temperatures than many industrial waste heat sources, thus efficiently utilizing waste heat for CO_2 conversion. The metal rhodium (0.5 wt %)-promoted lanthanum-modified cerium (1:1) was an effective catalyst. The complete conversion of CO_2 was reached using the Rh-promoted $LaCeO_{4-x}$, with the yield of syngas >83% at lower temperature. The metal La improved the intrinsic low-temperature redox performance of CeO_2, and the metal Rh significantly improved the surface catalytic performance for CH_4 activation. The efficient redox catalysts and HRP schemes offer a potentially attractive pathway for the utilization of CO_2, industrial waste heat, and the conversion of CH_4 for CO_2 emissions.

Vincenzo Spallina and co-workers employed the bimetallic NiFe LSF (LaSrFe) perovskite for hydrogen application via the chemical looping.[140] The interaction of FeNi bimetallic and $La_{0.6}Sr_{0.4}FeO_3$ (LSF-641) material showed only a 2% decrease in oxygen capacity over 20 redox cycles while exhibiting better resistance to carbon deposition using three-stage chemical looping with alternating hydrogen reactions in the temperature range of 500−900 °C. The H_2 yield of the bimetallic NiFe modified LSF increased by 20 compared to LSF-641. Iron-doped nickel produced more stable and efficient OCs, and the OCs coupling with LSF exhibited better redox cycling. Alessandro Longo's and Stavros A. Theofanidis's group illustrated a CO_2-assisted dehydrogenation of ethane (CO_2-ODHE) carbon-atom economic process for selective utilization of CO_2-ODHE to produce the ethylene via the Fe_2O_3.[141] The C_2H_6 (reduction step) and CO_2 (oxidation step) feedstocks were fed into a fixed-bed reactor (CO_2-ODHE-CL) via a chemical looping cycle at 600 °C to obtain constant ethane and CO_2 conversions (∼17.6%) and the selectivity of C_2H_4 (∼75%) in the reduction step. The lattice oxygen mobility acted as a descriptor of the material employed during the CO_2-ODHE-CL, and the lower mobility accelerated the breakage of the C−H bond during the reduction step and thus increased in the selectivity, i.e., the production of C_2H_4. The formation of a spinel-like arrangement between Mg and Fe stabilized the lattice oxygen, thus minimizing the C−C bond breakage during the CO_2-ODHE-CL. Binjian Nie's group reported that the chemical looping-based ammonia synthesis (CLAS) provided a sustainable alternative to the formation of ammonia through a chemical looping process, in which the hydrogen reacted with nitrogen-containing solids (called "nitrogen carriers") at near-ambient pressure.[142] The nitrogen carrier was regenerated in a N_2 atmosphere during the separation. The nitrogen support materials for the CLAS process were analyzed, and the material screening and fabrication techniques were summarized. Also, the strategies to reduce energy consumption and increase ammonia production at the reactor and system level were introduced, which provided the better foundation for the CLAS technology.

5. OUTLOOK AND PERSPECTIVE

The CLC technology coupled with the capture and utilization of CO_2 can realize the emission reduction and resource utilization of carbon, which is a vital and attractive prospect but also challenging. The future opportunities of the CLC technology are mainly focused on the lower cost of CO_2 capture and the promising prospects of high-value utilization (CLC gasification and the production of sustainable chemicals). However, the disadvantages of the CLC technology are mainly reflected in the following aspects: relatively low combustion efficiency, high fuel requirements, and relatively complex process flow. In view of the key technical challenges facing the coupled CO_2 capture and utilization in the CLC technology (the cost and performance of OCs, the regulation of heat and mass transfer between the reactor and the OCs, the optimization of reactor design theory, and manipulation, *etc.*), the way to skillfully take advantage of CO_2 capture for the production of chemicals and construct a well-stable OC are the keys to realize the CO_2 capture and resource utilization in the CLC technology.

https://doi.org/10.1021/acs.iecr.4c03713
Ind. Eng. Chem. Res. XXXX, XXX, XXX−XXX

The stable OCs exhibit better CLC performance, and the reduced OCs exported from the FR can become the active phase structure of the activated CO_2, which is expected to realize the purpose of directional conversion to produce sustainable chemicals and fuels. However, this coupling technology still needs a lot of fundamental research. The introduction of multiple strategies, such as the doping of the metal elements, the construction of OVs at the surface interface and the intrinsic body, the reduction of the energy barrier, and the regulation of the OV content improve the contact of the interface, the construction of the chemical interfaces, and realize the reduction of reaction barriers in the decisive step of reactant adsorption, the conversion of reaction intermediates, and the desorption of reaction products. The rational design of novel catalysts with targeted orientation can be achieved through the composition interaction between the metal-OCs and the introduction of the core−shell structure. This approach enhances the adsorption capacity of the catalysts for reactants and intermediates throughout the reaction process. Consequently, the overall activity of the catalysts in the oxidation and hydrogenation reactions will be improved, representing a promising avenue for further investigation in the long term.

■ ASSOCIATED CONTENT

Supporting Information

The Supporting Information is available free of charge at https://pubs.acs.org/doi/10.1021/acs.iecr.4c03713.

Illustration of the CLC process for the CO_2 storage (Figure S1), the formation of the OVs for various metal oxides (Figure S2), the commonly employed OCs and oxygen species types (Figure S3), and comparison of various CO_2 capture technologies (Table S1) (PDF)

■ AUTHOR INFORMATION

Corresponding Authors

Yanguang Chen − *College of Chemistry & Chemical Engineering, Northeast Petroleum University, Daqing 163318, China;* orcid.org/0000-0002-4431-9473; Email: ygchen79310@126.com

Shouliang Yi − *Department of Civil and Environmental Engineering, University of Pittsburgh, Pittsburgh, Pennsylvania 15261, United States;* orcid.org/0000-0001-8305-6322; Email: shouliang.yi@hotmail.com, shouliang.yi@pitt.edu

Authors

Yanan Zhang − *College of Chemistry & Chemical Engineering, Northeast Petroleum University, Daqing 163318, China*

Hongjing Han − *College of Chemistry & Chemical Engineering, Northeast Petroleum University, Daqing 163318, China;* orcid.org/0000-0002-3354-777X

Nini Zhu − *College of Chemistry & Chemical Engineering, Northeast Petroleum University, Daqing 163318, China*

Yu Che − *College of Chemistry & Chemical Engineering, Northeast Petroleum University, Daqing 163318, China*

Xiaodan Zhang − *College of Chemistry & Chemical Engineering, Northeast Petroleum University, Daqing 163318, China*

Yan Xue − *College of Chemistry & Chemical Engineering, Northeast Petroleum University, Daqing 163318, China*

Jitong Deng − *College of Chemistry & Chemical Engineering, Northeast Petroleum University, Daqing 163318, China*

Chunfei Wu − *School of Chemistry and Chemical Engineering, Queen's University Belfast, Belfast BT7 1NN, U.K.;* orcid.org/0000-0001-7961-1186

Haiying Wang − *College of Chemistry & Chemical Engineering, Northeast Petroleum University, Daqing 163318, China*

Complete contact information is available at: https://pubs.acs.org/10.1021/acs.iecr.4c03713

Notes

The authors declare no competing financial interest.

Biographies

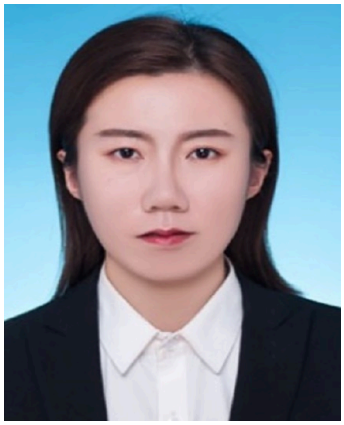

Yanan Zhang is an associate professor in the College of Chemistry and Chemical Engineering at the Northeast Petroleum University, China. Her current research is focused on cutting-edge research in the fields of catalytic material design and synthesis process regulation, direct catalytic conversion of oil and natural gas, and pollutant control and resource utilization. Her research outcome has been published in prestigious peer reviewed top journals such as *Journal of Hazardous Materials, Journal of Cleaner Production, Separation and Purification Technology*, and many others. She was an academic visiting scholar at the Agency for Science, Technology and Research (A*STAR) of Singapore in 2022-2023. As a core team member, she has participated in a number of national, provincial, and ministerial scientific research projects such as the National Natural Science Foundation of China, Heilongjiang Provincial Science Foundation for Outstanding Young Scholars, and Heilongjiang High-level Talent Project.

Hongjing Han is an associate professor in the College of Chemistry and Chemical Engineering, Northeast Petroleum University, China. She is mainly engaged in the basic and applied research on the design

https://doi.org/10.1021/acs.iecr.4c03713
Ind. Eng. Chem. Res. XXXX, XXX, XXX−XXX

and synthesis of catalytic materials, the control and conversion of pollutants and the treatment of oilfield wastewater. She presided over 1 National Natural Science Foundation youth project, participated in 2 National Natural Science Foundation, Provincial Outstanding Youth Science Fund and other provincial and ministerial funds and science and technology research projects. She has published more than 30 papers in *Journal of Hazardous Materials, Energy & Fuels, Journal of Rare Earths* and other journals.

Nini Zhu is a Ph.D. student in the College of Chemistry and Chemical Engineering of Northeast Petroleum University, China. She received her master's degree in chemical Engineering and technology from Northeast Petroleum University in 2023. She is currently working on enhancing the flow of shale oil.

Yu Che is a Ph.D. student in the College of Chemistry and Chemical Engineering, Northeast Petroleum University, China. She is currently working on the synthesis of catalysts and catalytic conversion of biomass.

Xiaodan Zhang is a Ph.D. student at the College of Chemistry and Chemical Engineering, Northeast Petroleum University, China. She is currently working on the catalytic crack of shale oil.

Yan Xue is a Master student at the College of Chemistry and Chemical Engineering, Northeast Petroleum University, China. She is currently working on the catalytic crack of shale oil.

Jitong Deng is a Ph.D. student in the College of Chemistry and Chemical Engineering, Northeast Petroleum University, China. She is mainly engaged in the catalytic oxidation of methane and enrichment of CO_2.

Chunfei Wu is a professor at Queen's University of Belfast, the editor of *Carbon Capture Science and Technology*, and the Managing Editor of *Biomass and Bioenergy* magazine. He has accumulated nearly 20 years of research experience in the field of energy and the utilization of waste materials. So far, he has published more than 200 papers in the field of thermal conversion of energy and waste (he has been cited more than 15,000 times, with an H-index of 70, according to Google Scholar). Dr. Wu is currently leading an EU Horizon Project (15

https://doi.org/10.1021/acs.iecr.4c03713
Ind. Eng. Chem. Res. XXXX, XXX, XXX−XXX

organizations, including the University of Liverpool, the University of Sydney, Huazhong University of Science and Technology, Zhejiang University, Xi'an Jiaotong University, the Institute of Thermophysics of the Chinese Academy of Sciences and the Dalian Institute of Chemistry).

Haiying Wang is a lecturer in the College of Chemistry and Chemical Engineering, Northeast Petroleum University, China. She conducted the academic visit at North Carolina State University during 2019–2020. She chairs a Petrochina Innovation Fund, as a principal member of the National Natural Science Foundation of China (NSFC), the Heilongjiang Science Foundation for outstanding young people, the Heilongjiang high-level talent program and other national, provincial and ministerial-level research projects. She has published 20 SCI papers in the *Journal of Applied Pyrolysis, Energy & Fuels, Journal of Rare Earths, etc.*

Yanguang Chen is currently a Distinguished Professor of Longjiang Scholar and the Dean of School of Chemistry and Chemical Engineering at the Northeast Petroleum University, China. He is the winner of Heilongjiang Outstanding Youth Fund and Heilongjiang Youth Science and Technology Award. His current research is focused on rational design and synthesis of catalytic materials, process engineering, and catalytic conversion of fossil energy. He presided 3 national-level projects and more than 10 provincial and ministerial-level projects; and has published more than 70 SCI papers in peer reviewed top journals such as *Journal of Hazardous Materials, Journal of Cleaner Production, Fuel, etc.* He won 7 provincial and ministerial-level scientific research awards and 3 provincial teaching achievements award. He is the inventor of more than 40 granted patents. He also serves as Deputy Secretary-General of Heilongjiang Petrochemical Standardization Technical Committee, Executive Director of Heilongjiang Chemical Engineering Society, and Director of Heilongjiang Energy and Environment Society.

Shouliang Yi is an Adjunct Professor in the Department of Civil and Environmental Engineering at the University of Pittsburgh, USA. He served as Principal Research Scientist and Team Lead at U.S. Department of Energy's National Energy Technology Laboratory. His current research focuses on creating sustainable solutions for key energy intensive separations, including point source carbon capture (PSCC), carbon dioxide removal (CDR), integrated carbon capture and utilization (ICCU), hydrogen production, biorefinery & bio-products, dye desalination, critical minerals recovery, renewable energy production, and other challenging gas/liquid separations toward carbon neutrality. He has published more than 90 peer-reviewed publications in prestigious journals and conference proceedings, including articles in *Science Advances, Nature Materials, Angewandte Chemie International Edition, Journal of Materials Chemistry A, Separation and Purification Technology, and Journal of Membrane Science*. He is the inventor of 12 patents (U.S., China, and PCT) in membrane materials and separation technologies. He also contributes numerous internal technical reports and presentations. He serves as an Editor of *Separation and Purification Technology* (Elsevier), Executive Editor-in-Chief of *Results in Engineering* (Elsevier), Associate Editor of *Carbon Capture Science & Technology* (IChemE & Elsevier) and *Industrial Chemistry and Materials* (RSC), and Editorial Advisory Board Member of a number of peer-reviewed international top journals. He is the recipient of numerous awards, including RINENG Distinguished Young Investigator Award for Excellence in Chemical Engineering (2022), Distinguished Investigator Award for Excellence in Carbon Capture Science & Technology (2023), IChemE Carbon Capture Outstanding Achievement Award (2024), and International Award for Outstanding Young Chemical Engineer (2024). He was elected to a Fellow of the Royal Society of Chemistry (FRSC) in 2022, and Vice President of International Association for Carbon Capture (IACC) in 2023.

■ ACKNOWLEDGMENTS

This work was financially supported by the National Natural Science Foundation of China (No. 21908021), the CNPC Innovation Fund (No. 2021DQ02-0701), the Chunhui Program Cooperative Research Project of the Ministry of Education of China (No. HZKY20220310), Project of Heilongjiang Outstanding Young Teachers' Basic Research Support Program (No. YQJH2023072 and YQJH2024047), the Guiding Innovation Fund of Northeast Petroleum University (No. 2021YDL-03), and the Northeast Petroleum University Talent Introduction Program (No. 13051202306).

https://doi.org/10.1021/acs.iecr.4c03713
Ind. Eng. Chem. Res. XXXX, XXX, XXX−XXX

REFERENCES

(1) Riebeek, H. (16 June 2011). "The Carbon Cycle". Earth Observatory. NASA. Archived from the original on 5 March 2016. Retrieved 5 April 2018.

(2) https://www.iea.org/data-and-statistics/charts/annual-change-in-energy-related-CO2-emissions-1900-2023. Last updated 25 Feb 2024.

(3) Gan, K. E.; Taikan, O.; Gan, T. Y.; Weis, T.; Yamazaki, D.; Schüttrumpf, H. Enhancing Renewable Energy Systems, Contributing to sustainable development goals of united nation and building resilience against climate change impacts. *Energy Technol.* **2023**, *11* (11), 2300275.

(4) Akashi, O.; Tatsuya, H. Technological feasibility and costs of achieving a 50% reduction of global GHG emissions by 2050: mid- and long-term perspectives. *Sustain. Sci.* **2012**, *7*, 139−156.

(5) Ding, H. B.; Dong, Y. Y.; Zhang, Y.; Wen, C.; Yang, Y. Mass, energy and economic analysis of supersonic CO_2 separation for carbon capture, utilization and storage (CCUS). *Appl. Energ.* **2024**, *373*, 123856.

(6) Ling, J. L. J.; Yang, W.; Park, H.; Lee, H. E.; Lee, S. H. A comparative review on advanced biomass oxygen fuel combustion technologies for carbon capture and storage. *Energy.* **2023**, *284*, 128566.

(7) Zhang, P. H.; Yin, P. Y.; Yang, L. F.; Cui, X. L.; Xing, H. B.; Suo, X. Recent advances and challenges in ionic materials for post-combustion carbon capture. *Carbon Capture Science & Technology.* **2024**, *11*, 100180.

(8) Richter, H. J.; Knoche, K. F. Reversibility of combustion processes. *ACS Symp. Ser.* **1983**, *235*, 71.

(9) High, M.; Patzschke, C. F.; Zheng, L.; Zeng, D.; Xiao, R.; Fennell, P. S.; Song, Q. L. Hydrotalcite-derived copper-based oxygen carrier materials for efficient chemical-looping combustion of solid fuels with CO_2 capture. *Energy Fuels.* **2022**, *36* (18), 11062−11076.

(10) Zhao, H. B.; Xin, T.; Ma, J. C.; Su, M. Z.; Wang, B. W.; Mei, D. F. Development of tailor-made oxygen carriers and reactors for chemical looping processes at Huazhong University of Science & Technology. *Int. J. Greenh. Gas Con.* **2020**, *93*, 102898.

(11) Pérez-Vega, R.; Abad, A.; Bueno, J. A.; García-Labiano, F.; Gayán, P.; Diego, L. F.; Adánez, J. Improving the efficiency of chemical looping combustion with coal by using ring-type internals in the fuel reactor. *Fuel* **2019**, *250*, 8−16.

(12) Adánez-Rubio, I.; Bararpour, S. T.; Abad, A.; Gayán, P.; Williams, G.; Scullard, A.; Mahinpey, N.; Adánez, J. Performance evaluation of a Cu-Based oxygen carrier impregnated onto ZrO_2 for chemical-looping combustion (CLC). *Ind. Eng. Chem. Res.* **2020**, *59* (15), 7255−7266.

(13) Huang, J. Q.; Liu, H.; Zhang, C. H.; Feng, B.; Wei, X. L.; Kang, R. N.; Wu, S. H. Study on the structural evolution and heat transfer performance of Cu supported on regular morphology CeO_2 in CO catalytic combustion and chemical looping combustion. *J. Clean. Prod.* **2023**, *417*, 138038.

(14) Ishida, M.; Jin, H. CO_2 recovery in a power plant with chemical looping combustion. *Energy Convers. Manage.* **1997**, *38*, S187−S192.

(15) Ahmed, I.; Lasa, H. D. Syngas chemical looping combustion using a highly performing fluidizable oxygen carrier. *Catal. Today* **2020**, *343*, 63−71.

(16) Kuang, C.; Wang, S. Z.; Luo, M.; Zhao, J. Mechanism analysis of coal with CuO in the in situ gasification chemical-looping combustion and in situ gasification chemical-looping with oxygen uncoupling process. *Energy Fuels.* **2021**, *35* (1), 618−625.

(17) Adánez-Rubio, I.; Pérez-Astray, A.; Mendiara, T.; Izquierdo, M. T.; Abad, A.; Gayán, P.; Diego, L. F. D; García-Labiano, F.; Adánez, J. Chemical looping combustion of biomass: CLOU experiments with a Cu-Mn mixed oxide. *Fuel Process. Technol.* **2018**, *172*, 179−186.

(18) Zhu, X.; Imtiaz, Q.; Donat, F.; Müller, C. R.; Li, F. X. Chemical looping beyond combustion-a perspective. *Energy Environ. Sci.* **2020**, *13*, 772−804.

(19) Hu, Q.; Shen, Y.; Chew, J. W.; Ge, T.; Wang, C.-H. Chemical looping gasification of biomass with Fe_2O_3/CaO as the oxygen carrier for hydrogen-enriched syngas production. *Chem. Eng. J.* **2020**, *379*, 122346.

(20) Zheng, A. Q.; Fan, Y. Y.; Wei, G. Q.; Zhao, K.; Zhen, H.; Zhao, Z. L.; Li, H. B. Chemical looping gasification of torrefied biomass using $NiFe_2O_4$ as an oxygen carrier for syngas production and tar removal. *Energy Fuels* **2020**, *34* (5), 6008−6019.

(21) Zhang, J.; Cui, Y.; Sima, W.; Zhang, Y. Q.; Gao, Y. M.; Wang, P. X.; Zhang, Q. Advances and challenges in oxygen carriers for chemical looping partial oxidation of methane [J]. *Catalysts.* **2024**, *14* (4), 246.

(22) Oh, D.; Colombo, F.; Nodari, L; Kim, J. H.; Kim, J. K.; Lee, S.; Kim, S; Kim, S; Lim, D. K.; Seo, J.; Mascotto, S.; Jung, W. C. Rocking chair-like movement of ex-solved nanoparticles on the Ni-Co doped $La_{0.6}Ca_{0.4}FeO_{3-\delta}$ oxygen carrier during chemical looping reforming coupled with CO_2 splitting [J]. *Appl. Catal. B-Environ. Energy.* **2023**, *332*, 122745.

(23) Zhang, J. R.; Yang, T. L.; Rao, Q.; Gai, Z. R.; Li, P.; Shen, Y. H.; Liu, M. K.; Pan, Y.; Jin, H. G. Enhancement of Fe/Ce oxygen carrier performance in chemical looping dry reforming of methane [J]. *Fuel.* **2024**, *366*, 131344.

(24) Tian, X.; Su, M.; Zhao, H. B. Kinetics investigation of copper ore oxygen carrier for chemical looping combustion [J]. *Fire.* **2024**, *7* (7), 245.

(25) Wang, X. J.; Chen, D. L; An, F. X.; Chen, J. J.; Shao, D. Y. Test operation of microwave-assisted chemical looping gasification for water hyacinth with a lean iron ore as oxygen carrier [J]. *Biomass Bioenerg.* **2024**, *183*, 107141.

(26) An, M.; Guo, Q. J.; Ma, J. J.; Hu, X. D. Chemical-looping gasification of coal with $CuFe_2O_4$ oxygen carriers: the reaction characteristics and structural evolution [J]. *Can. J. Chem. Eng.* **2020**, *98* (7), 1512−1524.

(27) Wang, Y.; Niu, P.; Zhao, H. Chemical looping gasification of coal using calcium ferrites as oxygen carrier [J]. *Fuel Process. Technol.* **2019**, *192*, 75−86.

(28) Wang, Y. N.; Bu, H. F.; Zhao, H. B.; Liu, K. L. Performance evaluation of inexpensive Cu/Fe-based oxygen carriers in chemical looping gasification of coal [J]. *Energy Fuels.* **2021**, *35* (19), 15513−15524.

(29) Zhang, K.; Han, X. T.; Zhang, C.; Wang, Y. F.; Wang, S. Q.; Li, W. D.; Zhang, Q. M. Fe-Ni composite oxygen carrier for chemical looping gasification with diverse fuels to produce syngas. *Int. J. Hydrogen Energy.* **2024**, *80*, 847−857.

(30) Pan, Q. H.; Ma, L. P.; Du, W.; Yang, J.; Ao, R.; Yin, X.; Qing, S. C. Hydrogen-enriched syngas production by lignite chemical looping gasification with composite oxygen carriers of phosphogypsum and steel slag. *Energy.* **2022**, *241*, 122927.

(31) Yang, R. H.; Wang, Z. X.; Cheng, M. Q.; Yang, Y. Y.; Huang, Z. C.; Cen, Q. H.; Zhao, Y. C.; Zhou, T.; Liu, Z. W.; Li, B. Chemical looping gasification of automotive paint sludge with red mud oxygen carrier for flammable gas production. *Chem. Eng. J.* **2024**, *497*, 154676.

(32) Liu, X. F.; Hu, J. J.; Zhao, S. H.; Wang, W.; Zhang, Q. G.; Yan, X. Y. Chemical looping co-gasification of wheat straw and lignite with calcium-enhanced iron-based oxygen carrier for syngas production. *Fuel Process. Technol.* **2022**, *227*, 107108.

(33) Luo, M.; Zhang, H.; Wang, S.; Cai, J. J.; Qin, Y. J.; Zhou, L. Z. Syngas production by chemical looping co-gasification of rice husk and coal using an iron-based oxygen carrier. *Fuel.* **2022**, *309*, 122100.

(34) Hedayati, A.; Soleimanisalim, A. H.; Linderholm, C. J.; Mattisson, T.; Lyngfelt, A. Experimental evaluation of manganese ores for chemical looping conversion of synthetic biomass volatiles in a 300 W reactor system. *J. Environ. Chem. Eng.* **2021**, *9* (2), 105112.

(35) Yan, J. C.; Sun, R.; Shen, L. H.; Bai, H. C.; Jiang, S. X.; Xiao, Y.; Song, T. Hydrogen-rich syngas production with tar elimination via biomass chemical looping gasification (BCLG) using $BaFe_2O_4/Al_2O_3$ as oxygen carrier. *Chem. Eng. J.* **2020**, *387*, 124107.

(36) Harichandan, A. B.; Shamim, T. CFD analysis of bubble hydrodynamics in a fuel reactor for a hydrogen-fueled chemical

https://doi.org/10.1021/acs.iecr.4c03713
Ind. Eng. Chem. Res. XXXX, XXX, XXX−XXX

looping combustion system. *Energy Convers. Manage.* **2014**, *86*, 1010−1022.
(37) Liu, Y.; Qin, L.; Cheng, Z.; Goetze, J. W.; Kong, F. H.; Fan, J. A.; Fan, L. S. Near 100% CO selectivity in nanoscaled iron-based oxygen carriers for chemical looping methane partial oxidation. *Nat. Commun.* **2019**, *10*, 5503.
(38) Donat, F.; Müller, C. R. CO_2-free conversion of CH_4 to syngas using chemical looping. *Appl. Catal. B-Environ. Energy.* **2020**, *278*, 119328.
(39) Guan, Y.; Liu, Y. H.; Lin, X. L.; Wang, B; Lyu, Q. Research progress and perspectives of solid fuels chemical looping reaction with Fe-Based oxygen carriers. *Energy Fuels.* **2022**, *36* (23), 13956−13984.
(40) Ji, J. Q.; Shen, L. H. Synergistic Effect of Calcium Oxide/$LaNi_{0.5}Fe_{0.5}O_3$ oxygen carriers on syngas production from algae chemical looping gasification. *Ind. Eng. Chem. Res.* **2022**, *61* (45), 16662−16672.
(41) Daneshmand-Jahromi, S.; Sedghkerdar, M. H.; Mahinpey, N. Synthesis, characterization, and kinetic study of nanostructured copper-based oxygen carrier supported on silica and zirconia aerogels in the cyclic chemical looping combustion process. *Chem. Eng. J.* **2022**, *448*, 137756.
(42) Ahmed, I.; Lasa, H. D. 110th anniversary: kinetic model for syngas chemical looping combustion using a nickel-based highly performing fluidizable oxygen carrier. *Ind. Eng. Chem. Res.* **2019**, *58* (8), 2801−2811.
(43) Qasim, M.; Ayoub, M.; Ghazali, N. A.; Aqsha, A.; Ameen, M. Recent advances and development of various oxygen carriers for the chemical looping combustion process: a review. *Ind. Eng. Chem. Res.* **2021**, *60* (24), 8621−8641.
(44) Chen, X.; Li, R.; Tao, Y.; Tong, Y. Q.; Li, A.; Mei, D.; Zhao, H. B. Engineering design and numerical design for chemical looping combustion reactor: A review. *Energy Reviews.* **2024**, *3* (3), 100100.
(45) Chen, X.; Zhao, H. B. A self-consistent design method of the autothermal dual circulating fluidized bed reactor for in-situ gasification chemical looping combustion of coal. *Carbon Capture Science & Technology.* **2024**, *13*, 100292.
(46) Lichtenberger, D. L.; Lynn, M. A.; Chisholm, M. H. Quadruple metal-metal bonds with strong donor ligands ultraviolet photoelectron spectroscopy of $M_2(form)_4$ (M = Cr, Mo, W; form = N, N′-diphenylformamidinate). *J. Am. Chem. Soc.* **1999**, *121* (51), 12167−12176.
(47) Gao, Y. F.; Haeri, F.; He, F.; Li, F. X. Alkali metal-promoted $La_xSr_{2-x}FeO_{4-\delta}$ redox catalysts for chemical looping oxidative dehydrogenation of ethane. *ACS Catal.* **2018**, *8* (3), 1757−1766.
(48) Thursfield, A.; Murugan, A.; Franca, R.; Metcalfe, I. S. Chemical looping and oxygen permeable ceramic membranes for hydrogen production-a review. *Energ. Environ. Sci.* **2012**, *5* (6), 7421−7459.
(49) Song, D.; Long, T.; Li, C. Q.; Li, Y.; Fan, M.; Lu, Y. H.; Zhou, Y. C.; Chen, H. T.; Lin, Y.; Huang, Z.; He, F. Micro-structure change and crystal-structure modulated of oxygen carriers for chemical looping: Controlling local chemical environment of lattice oxygen. *Fuel.* **2024**, *364*, 131087.
(50) Li, J. B.; Shu, C. Z.; Liu, C. H.; Chen, X. F.; Hu, A. J.; Long, J. P. Rationalizing the effect of oxygen vacancy on oxygen electrocatalysis in Li-O_2 battery. *Small* **2020**, *16* (24), 2001812.
(51) Hao, P. C.; Suo, Y. L.; Shi, R.; Zhang, J.; Li, B.; Yan, Z.; Wang, J.; Liu, B.; Wang, Z. Z.; Qiao, X. Preparation of novel C/N-Doped $LaFeO_3$ type perovskite for efficient photocatalytic degradation of sodium humate. *ACS Omega* **2023**, *8* (44), 41744−41754.
(52) Xiao, K.; Wang, Y.; Wu, P. Y.; Hou, L. P.; Liu, Z. Q. Activating lattice oxygen in spinel $ZnCo_2O_4$ through filling oxygen vacancies with fluorine for electrocatalytic oxygen evolution. *Angew. Chem. Int. Ed.* **2023**, *62* (24), No. e202301408.
(53) Wang, H. Y.; Han, H. J.; Sun, E. H.; Han, Y. J.; Zhang, Y. N.; Li, J. X.; Chen, Y. G.; Song, H.; Zhao, H. Z.; Kang, Y. Production of aryl oxygen-containing compounds by the pyrolysis of bagasse alkali lignin catalyzed by $LaM_{0.2}Fe_{0.8}O_3$ (M = Fe, Cu, Al, Ti). *Energy Fuels.* **2019**, *33* (9), 8596−8605.
(54) Nie, L.; Mei, D.; Xiong, H.; Peng, B.; Ren, Z.; Hernandez, X. I. P.; Delariva, A.; Wang, M.; Engelhard, M. H.; Kovarik, L.; Datye, A. K.; Wang, Y. Activation of surface lattice oxygen in single-atom Pt/CeO_2 for low-temperature CO oxidation. *Science.* **2017**, *358* (6369), 1419−1423.
(55) Yi, C.; Wei, F.; Yong, J. *Multiphase reactor engineering for clean and low-carbon energy applications*; Wiley, 2017.
(56) Gatteschi, D.; Sessoli, R.; Plass, W.; Müller, A.; Krickemeyer, E.; Meyer, J.; Sölter, D.; Adler, P. Giant clusters with unusual electronic and magnetic structures due to open shell metal centers embedded far apart from each other: spin frustration and antisymmetric exchange. *Inorg. Chem.* **1996**, *35* (7), 1926−1934.
(57) Comer, B. M.; Li, J.; Abild-Pedersen, F.; Bajdich, M.; Winther, K. T. Unraveling electronic trends in O* and OH* surface adsorption in the MO_2 transition-metal oxide series. *J. Phys. Chem. C.* **2022**, *126* (18), 7903−7909.
(58) Colabello, D. M.; Camino, F. E.; Huq, A.; Hybertsen, M.; Khalifah, P. G. Charge disproportionation in tetragonal La_2MoO_5, a small band gap semiconductor influenced by direct Mo-Mo bonding. *J. Am. Chem. Soc.* **2015**, *137* (3), 1245−1257.
(59) Eskes, H.; Oleś, A. M.; Meinders, M. B.; Stephan, W. Spectral properties of the Hubbard bands. *Phys Rev B.* **1994**, *50* (24), 17980.
(60) Zhang, Y. H.; Zhang, D.; Wu, L. R.; Ma, J.; Yi, Q.; Wang, Z.; Wang, X.; Wu, Z; Zhang, C.; Hu, N.; Haw, S. C.; Chen, J. M.; Hu, Z.; Cui, G. Stabilization of lattice oxygen in Li-rich Mn-based oxides via swing-like non-isothermal sintering. *Adv. Energy Mater.* **2022**, *12* (43), 2202341.
(61) Liu, Q. C.; Su, Q. H.; Cheng, W. H.; Ding, J.; Zhang, W. J.; Wang, J. L.; Wang, Y. G.; Wang, X. C.; Huang, Y. D. Dual role of Fe boost lattice oxygen oxidation of Mo-based materials from kinetics and thermodynamics. *Appl. Catal. B-Environ. Energy.* **2024**, *340*, 123188.
(62) Wang, Z.; Lin, R.; Huo, Y.; Li, H.; Wang, L. Formation, detection, and function of oxygen vacancy in metal oxides for solar energy conversion. *Adv. Funct. Mater.* **2022**, *32* (7), 2109503.
(63) Ye, K. H.; Li, K. S.; Lu, Y. R.; Guo, Z. J.; Ni, N.; Liu, H.; Huang, Y. C.; Ji, H. B.; Wang, P. S. An overview of advanced methods for the characterization of oxygen vacancies in materials. *Trend. Anal. Chem.* **2019**, *116*, 102−108.
(64) Zhang, Y. H.; Zhang, S.; Hu, N.; Liu, Y.; Ma, J.; Han, P.; Hu, Z.; Wang, X.; Cui, G. Oxygen vacancy chemistry in oxide cathodes. *Chem. Soc. Rev.* **2024**, *53* (7), 3302−3326.
(65) Yang, W.; Qi, F.; An, W.; Yu, H.; Liu, S.; Ma, P.; Chen, R.; Liu, S.; Lou, L. L.; Yu, K. Local electronic structure modulation of Interfacial oxygen vacancies promotes the oxygen activation capacity of Pt/$Ce_{1-x}MxO_{2-\delta}$. *ACS Catal.* **2024**, *14* (8), 5936−5948.
(66) Liu, X.; Yang, L.; Huang, M.; Li, Q.; Zhao, L.; Sang, Y.; Zhang, X.; Zhao, Z.; Liu, H.; Zhou, W. Oxygen vacancy-regulated metallic semiconductor MoO_2 nanobelt photoelectron and hot electron self-coupling for photocatalytic CO_2 reduction in pure water. *Appl. Catal. B-Environ. Energy.* **2022**, *319*, 121887.
(67) Yang, J.; Pan, J.; Deng, J.; Zhang, Y. F.; Li, Y.; Zhu, Y.; Wan, G.; Du, S. Vacancy-induced anionic electrons in single-metal oxides and their possible applications in ammonia synthesis. *J. Am. Chem. Soc.* **2024**, *146* (30), 21160−21167.
(68) Zhang, Y.; Wu, L. L.; Feng, R. H.; Wang, S.H.; Hsu, C. S.; Ni, Y. M.; Ahmad, A.; Zhang, C. C.; Wu, H. F.; Chen, H. M.; Zhang, Y.; Zhang, W.; Li, Y.; Liu, P.; Song, F. Oxygen vacancies unfold the catalytic potential of NiFe-layered double hydroxides by promoting their electronic transport for oxygen evolution reaction. *ACS Catal.* **2023**, *13* (9), 6000−6012.
(69) Qu, J.; Liu, W.; Liu, R.; He, J.; Liu, D.; Feng, Z.; Feng, Z.; Li, R.; Li, C. Evolution of oxygen vacancies in cerium dioxide at atomic scale under CO_2 reduction. *Chem Catal.* **2023**, *3* (10), 100759.
(70) Dong, Z.; Huo, M.; Li, J.; Li, J.; Li, P.; Sun, H.; Lu, Y.; Wang, M.; Wang, Y.; Chen, Z. Visualization of oxygen vacancies and self-doped ligand holes in $La_3Ni_2O_{7-\delta}$. *Nature* **2024**, *630*, 847−852.
(71) Deng, J.; Zhang, Y.; Han, H.; Zhang, Y.; Wang, H.; Gong, X.; Chen, Y. Characterization and performance of Sr and Co Doped

https://doi.org/10.1021/acs.iecr.4c03713
Ind. Eng. Chem. Res. XXXX, XXX, XXX−XXX

Fe_2O_3-$LaFeO_3$ quaternary perovskite composite oxides for efficient realization of CH_4 chemical looping conversion. *ACS Sustain. Chem. Eng.* **2024**, *12* (8), 3265−3278.
(72) Chen, H.; Lim, C.; Zhou, M.; He, Z.; Sun, X.; Li, X.; Ye, Y.; Tan, T.; Zhang, H.; Yang, C. Activating lattice oxygen in perovskite oxide by B-site cation doping for modulated stability and activity at elevated temperatures. *Adv. Sci.* **2021**, *8* (22), 2102713.
(73) Bianchini, M.; Wang, J.; Clément, R. J.; Ouyang, B.; Xiao, P.; Kitchaev, D.; Shi, T.; Zhang, Y.; Wang, Y.; Kim, H.; Zhang, M. J.; Bai, J. M; Wang, F.; Sun, W. H.; Ceder, G. The interplay between thermodynamics and kinetics in the solid-state synthesis of layered oxides. *Nat. Mater.* **2020**, *19* (10), 1088−1095.
(74) Dholabhai, P. P.; Anwar, S.; Adams, J. B.; Crozier, P.; Sharma, R. Kinetic lattice Monte Carlo model for oxygen vacancy diffusion in praseodymium doped ceria: Applications to materials design. *J. Solid State Chem.* **2011**, *184* (4), 811−817.
(75) Kim, M.; Pan, L.; Weaver, J. F.; Asthagiri, A. Initial reduction of the PdO (101) surface: role of oxygen vacancy formation kinetics. *J. Phys. Chem. C* **2018**, *122* (45), 26007−26017.
(76) Wu, J.; Wang, J.; Xiao, D.; Zhu, J. Migration kinetics of oxygen vacancies in Mn-modified $BiFeO_3$ thin films. *ACS Appl. Mater.* **2011**, *3* (7), 2504−2511.
(77) Jiang, Y.; Wang, S.; Zhang, Y.; Yan, J.; Li, W. Kinetic study of the formation of oxygen vacancy on lanthanum Manganite electrodes. *J. Electrochem. Soc.* **1998**, *145* (2), 373.
(78) Zhang, A.; Gao, R.; Hu, L.; Zang, X.; Yang, R.; Wang, S.; Yao, S.; Yang, Z.; Hao, H.; Yan, Y. M. Rich bulk oxygen Vacancies-engineered MnO_2 with enhanced charge transfer kinetics for supercapacitor. *Chem. Eng. J.* **2021**, *417*, 129186.
(79) Lai, L. D.; Zhou, H. Y.; Zhang, H.; Ao, Z. M.; Pan, Z. C.; Chen, Q. X.; Xiong, Z. K.; Yao, G.; Lai, B. Activation of peroxydisulfate by natural titanomagnetite for atrazine removal via free radicals and high-valent iron-oxo species. *Chem. Eng. J.* **2020**, *387*, 124165.
(80) Taube, H. Mechanisms of oxidation with oxygen. *J. Gen. physiol.* **1965**, *49* (1), 29−50.
(81) Deng, J. T.; Zhang, Y. J.; Wang, X. P.; Zhang, W.; Han, H. J.; Wang, H. Y.; Yuan, H. M.; Zhang, Y. N.; Chen, Y. G. Chemical looping conversion of methane via Fe_2O_3-$LaFeO_3$ calcined from LaFe-MOF precursor. *Chin. J. Chem. Eng.* **2023**, *62*, 225−237.
(82) Zheng, A. Q.; Fan, Y. Y.; Wei, G. Q.; Zhao, K.; Huang, Z.; Zhao, Z. L.; Li, H. B. Chemical looping gasification of torrefied biomass using $NiFe_2O_4$ as an oxygen carrier for syngas production and tar removal. *Energy Fuels.* **2020**, *34* (5), 6008−6019.
(83) Pfeifer, V.; Jones, T. E.; Vélez, J. J. V.; Arrigo, R.; Piccinin, S.; Hävecker, M.; Knop Gericke, A.; Schlögl, R. In situ observation of reactive oxygen species forming on oxygen-evolving iridium surfaces. *Chem. Sci.* **2017**, *8* (3), 2143−2149.
(84) Wang, X. H.; Pei, C. L.; Zhao, Z. J.; Chen, S.; Li, X. Y.; Sun, J. C.; Song, H. B.; Sun, G. D.; Wang, W.; Chang, X.; et al. Coupling acid catalysis and selective oxidation over MoO_3-Fe_2O_3 for chemical looping oxidative dehydrogenation of propane. *Nat. Commun.* **2023**, *14* (1), 2039.
(85) Wang, Y. N.; Bu, H. F.; Zhao, H. B.; Liu, K. L. Performance evaluation of inexpensive Cu/Fe-based oxygen carriers in chemical looping gasification of coal. *Energy Fuels.* **2021**, *35* (19), 15513−15524.
(86) Zhang, X.; Xu, Y.; Liu, Y.; Niu, L.; Diao, Y. N.; Gao, Z. R.; Chen, B. B.; Xie, J. L.; Bi, M. S.; Wang, M.; Xiao, D. Q.; Ma, D.; Shi, C.; et al. A novel Ni-MoC_xO_y interfacial catalyst for syngas production via the chemical looping dry reforming of methane. *Chem* **2023**, *9* (1), 102−116.
(87) Chen, L. Y.; Liu, D. C.; Xue, J.; Sun, Z. K.; Shen, L. H. Mechanism of phase segregation in ilmenite oxygen carriers for chemical-looping combustion. *Chem. Eng. J.* **2024**, *479* (479), 147921.
(88) Song, D.; Lin, Y.; Fang, S. W.; Li, Y.; Zhao, K.; Chen, X. F.; Huang, Z.; He, F.; Zhao, Z. L.; Huang, H. Y. Unraveling the atomic interdiffusion mechanism of $NiFe_2O_4$ oxygen carriers during chemical looping CO_2 conversion. *Carbon Energy.* **2024**, *6* (8), No. e493.
(89) Zuo, H. C.; Lu, C. Q.; Jiang, L.; Cheng, X. M.; Li, Z. Q.; Li, Y. L.; Li, D. Y.; Wang, H.; Li, K. Z. Hydrogen production and CO_2 capture from Linz-Donawitz converter gas via a chemical looping concept. *Chem. Eng. J.* **2023**, *477*, 146870.
(90) Jiang, Y. J.; Li, Z. S.; Zhu, T.; Li, D. F.; Wang, H.; Zhu, X. Oxygen storage characteristics and redox behaviors of lanthanum perovskite oxides with transition metals in the B-sites. *Energy & Fuels* **2023**, *37* (13), 9419−9433.
(91) Yu, D.; Wang, L. Y.; Zhang, C. L.; Peng, C.; Yu, X. H.; Fan, X. Q.; Liu, B.; Li, K. X.; Li, Z. G.; Wei, Y. C.; Liu, j.; Zhao, Z.; et al. Alkali metals and cerium-modified La-Co-based perovskite catalysts: facile synthesis, excellent catalytic performance, and reaction mechanisms for soot combustion. *ACS Catal.* **2022**, *12* (24), 15056−15075.
(92) Wang, S.; Zhu, J. J.; Carabineiro, S. A.; Xiao, P.; Zhu, Y. J. Selective etching of in-situ formed La_2O_3 particles to prepare porous $LaCoO_3$ perovskite for catalytic combustion of ethyl acetate. *Appl. Catal. A-Gen.* **2022**, *635*, 118554.
(93) Yan, J. C.; Zhang, L.; He, J.; Liu, M. X.; Lei, Z. P.; Li, Z. K.; Wang, Z. Z.; Ren, S. B.; Shu, H. F. Boosting chemical looping combustion performances of red mud with transition metal oxides. *Carbon Resources Conversion.* **2022**, *5* (2), 119−130.
(94) Cao, D. S.; Luo, C.; Wu, F.; Zhang, L. Q.; Li, X. S. Screening loaded perovskite oxygen carriers for chemical looping steam methane reforming. *J. Environ. Chem. Eng.* **2022**, *10* (2), 107315.
(95) Lin, H. J.; Li, S. Y.; Zhang, Y. C.; Chu, C.; MacSwain, W.; Meulenberg, R. W.; Qiao, Q.; Zhao, D.; Zheng, W. W. Epitaxial growth of lead-free double perovskite shell for $CsPbX_3/Cs_2SnX_6$ (X = Cl, Br, and I) core/shell perovskite nanocrystals with enhanced photoelectric properties and stability. *Adv. Funct. Mater.* **2024**, *34* (7), 2309480.
(96) Gao, Y. F.; Wang, X. J.; Corolla, N.; Eldred, T.; Bose, A.; Gao, W. P.; Li, F. X. Alkali metal halide-coated perovskite redox catalysts for anaerobic oxidative dehydrogenation of n-butane. *Sci. Adv.* **2022**, *8* (30), No. eabo7343.
(97) Huang, Y. F.; Tan, L.; Ma, H. Y.; Wang, X.; Huang, Y. Q.; Yin, J. P.; Liang, Z. W.; Luo, X. Novel double-layer core-shell photocatalyst CdS-TiO_2@NH_2-MIL-101: enhanced conversion of CO_2 and CH_4 at ambient temperature. *EES Catal.* **2024**, *2* (2), 675−686.
(98) Xu, K. L.; Liu, D. Y.; Feng, L.; Jin, J.; Xiong, Z. B.; Ni, M. G.; Liu, Z.; Liu, Q. Q.; Hou, F. X. Mercury removal by Co_3O_4@TiO_2@Fe_2O_3 magnetic core-shell oxygen carrier in chemical-looping combustion. *Fuel.* **2021**, *306*, 121604.
(99) Zhu, X.; Gao, Y. F.; Wang, X. F.; Haribal, V.; Liu, J. C.; Neal, L. M.; Bao, Z. H.; Wu, Z. L.; Wang, H.; Li, F. X. A tailored multi-functional catalyst for ultra-efficient styrene production under a cyclic redox scheme. *Nat. Commun.* **2021**, *12* (1), 1329.
(100) Chen, S.; Luo, R.; Zhao, Z. J.; Pei, C. L.; Xu, Y. Y.; Lu, Z. P.; Zhao, C. J.; Song, H. B.; Gong, J. L. Concerted oxygen diffusion across heterogeneous oxide interfaces for intensified propane dehydrogenation. *Nat. Commun.* **2023**, *14* (1), 2620.
(101) Shafiefarhood, A.; Galinsky, N.; Huang, Y.; Chen, Y. G.; Li, F. X. Fe_2O_3@ $LaxSr_{1-x}FeO_3$ core-shell redox catalyst for methane partial oxidation. *ChemCatChem.* **2014**, *6* (3), 790−799.
(102) Yin, X. L.; Wang, S.; Sun, R.; Jiang, S. X.; Shen, L. H. A Ce-Fe oxygen carrier with a core-shell structure for chemical looping steam methane reforming. *Ind. Eng. Chem. Res.* **2020**, *59* (21), 9775−9786.
(103) Zeng, L.; Cheng, Z.; Fan, J. A.; Fan, L. S.; Gong, J. L. Metal oxide redox chemistry for chemical looping processes. *Nat. Rev. Chem.* **2018**, *2* (11), 349−364.
(104) TOMPKINS, F. C. Superficial chemistry and solid imperfections. *Nature* **1960**, *186*, 3−6.
(105) Fan, W. J.; Li, H. B.; Zhao, F. Y.; Xiao, X. J.; Huang, Y. C.; Ji, H. B.; Tong, Y. X. Boosting the photocatalytic performance of (001) BiOI: enhancing donor density and separation efficiency of photo-generated electrons and holes. *Chem. Commun.* **2016**, *52*, 5316−5319.
(106) Huang, Y. C.; Long, B.; Tang, M. N.; Rui, Z. B.; Balogun, M. S.; Tong, Y. X.; Ji, H. B. Bifunctional catalytic material: An ultrastable and high-performance surface defect CeO_2 nanosheets for form-

https://doi.org/10.1021/acs.iecr.4c03713
Ind. Eng. Chem. Res. XXXX, XXX, XXX−XXX

aldehyde thermal oxidation and photocatalytic oxidation. *Appl. Catal. B: Environ.* **2016**, *181*, 779−787.
(107) Luo, Zh. Y.; Ouyang, Y. X.; Zhang, H.; Xiao, M. L.; Ge, J. J.; Jiang, Z.; Wang, J. L.; Tang, D. M.; Cao, X. Z.; Liu, C. P.; Xing, W. Chemically activating MoS_2 via spontaneous atomic palladium interfacial doping toward efficient hydrogen evolution. *Nat. Commun.* **2018**, *9*, 2120.
(108) Liu, Y. W.; Cheng, H.; Lyu, M. J.; Fan, S. J.; Liu, Q. H.; Zhang, W. S.; Zhi, Y. D.; Wang, C. M.; Xiao, C.; Wei, S. Q.; Ye, B. J.; Xie, Y. Low Overpotential in vacancy-rich ultrathin $CoSe_2$ nanosheets for water oxidation. *J. Am. Chem. Soc.* **2014**, *136* (44), 15670−15675.
(109) Qureshi, Y.; Ali, U.; Sher, F. Part load operation of natural gas fired power plant with CO_2 capture system for selective exhaust gas recirculation. *Appl. Therm. Eng.* **2021**, *190*, 116808.
(110) Hughes, R. W.; Lu, D. Y.; Symonds, R. T. Improvement of oxy-FBC using oxygen carriers: concept and combustion performance. *Energy Fuels.* **2017**, *31* (9), 10101−10115.
(111) Wienchol, P.; Szlęk, A.; Ditaranto, M. Waste-to-energy technology integrated with carbon capture-challenges and opportunities. *Energy* **2020**, *198*, 117352.
(112) Blaustein, M. P.; Lederer, W. J. Sodium/calcium exchange: its physiological implications. *Physiol. Rev.* **1999**, *79* (3), 763−854.
(113) Arcenegui-Troya, J.; Sánchez-Jiménez, P. E.; Perejon, A.; Moreno, V.; Valverde, J. M.; Pérez-Maqueda, L. A. Kinetics and cyclability of limestone ($CaCO_3$) in presence of steam during calcination in the CaL scheme for thermochemical energy storage. *Chem. Eng. J.* **2021**, *417*, 129194.
(114) Yadav, V. K.; Yadav, K. K.; Cabral-Pinto, M. M.; Choudhary, N.; Gnanamoorthy, G.; Tirth, V.; Prasad, S.; Khan, A. H.; Islam, S.; Khan, N. A. The processing of calcium rich agricultural and industrial waste for recovery of calcium carbonate and calcium oxide and their application for environmental cleanup: A review. *Appl. Sci.* **2021**, *11* (9), 4212.
(115) Jin, B.; Ouyang, T.; Zhang, Z. N.; Zhao, Y. L.; Zhang, H. Y.; Yao, W. X.; Huang, G. Q.; Liang, Z. W. Prussian blue derived Ca-Fe bifunctional materials for chemical looping CO_2 capture and in-situ conversion. *Sep. Purif. Technol.* **2023**, *320*, 123975.
(116) Long, Y. H.; Wang, X. Z.; Zhang, H.; Wang, K. Y.; Ong, W. L.; Bogaerts, A.; Li, K. Z.; Lu, C. Q.; Li, X. D.; Yan, J. H. Plasma chemical looping: unlocking high-efficiency CO_2 conversion to clean CO at mild temperatures. *JACS Au* **2024**, *4* (7), 2462−2473.
(117) Perejón, A.; Arcenegui Troya, J.; Sánchez Jiménez, P. E.; Diánez, M. J.; Pérez Maqueda, L. A. Magnesium calcites for CO_2 capture and thermochemical energy storage using the calcium-looping process. *Environ. Res.* **2024**, *246*, 118119.
(118) Pankhedkar, N.; Dwivedi, A.; Gudi, R.; Biswas, P. Intensified chemical looping combustion based polygeneration for CO_2 valorization to value-added chemicals (methanol and DME). *Ind. Eng. Chem. Res.* **2022**, *61* (32), 11861−11879.
(119) Tian, X.; Zheng, C. H.; Zhao, H. B. Ce-modified $SrFeO_{3-\delta}$ for ethane oxidative dehydrogenation coupled with CO_2 splitting via a chemical looping scheme. *Appl. Catal. B-Environ. Energy.* **2022**, *303*, 120894.
(120) Yuan, K.; Wang, Y. H.; Li, K. Z.; Zhu, X.; Wang, H.; Jiang, L. H.; Wei, Y. G.; Shan, S. Y.; Zheng, Y. E. $LaFe_{0.8}Co_{0.15}Cu_{0.05}O_3$ supported on Silicalite-1 as a durable oxygen carrier for chemical looping reforming of CH_4 coupled with CO_2 reduction. *ACS Appl. Mater. Interfaces.* **2022**, *14* (34), 39004−39013.
(121) Zhang, D. Q.; Duan, R. H.; Li, H. W.; Yang, Q. C.; Zhou, H. R. Optimal design, thermodynamic, cost and CO_2 emission analyses of coal-to-methanol process integrated with chemical looping air separation and hydrogen technology. *Energy.* **2020**, *203*, 117876.
(122) Li, A. M.; Liu, Y. C.; Luo, K.; He, Q. CO_2 capture in liquid phase and room-temperature release and concentration using mechanical power. *CCS Chemistry.* **2024**, *6*, 2882−2894.
(123) Orhan, O. Y.; Hugul, A.; Ulus, N.; Ersan, H. Y. Enhancing CO_2 desorption efficiency with non-aqueous catalyst-enhanced triblend amines. *Fuel* **2024**, *375*, 132458.
(124) Sun, X. N.; Guo, T.; An, M.; Guo, X. T.; Han, Z. H.; Zhai, D. D.; Ma, J. J.; Hu, X. D.; Zhang, J. L.; He, Y. R.; Guo, Q. J. The bifunctional oxygen carrier $K/La_yCo_xFe_{1-x}O_3$ for the production of C_2-C_4 olefins via CO_2 hydrogenation. *Int. J. Hydrogen Energ.* **2024**, *51*, 368−381.
(125) Ma, L. H.; Gao, X. H.; Zhang, J. L.; Ma, J. J.; Hu, X. D.; Guo, Q. J. Effects of metal doping on the catalytic performance of LaFe-based perovskites for CO_2 hydrogenation to light olefins. *Journal of Fuel Chemistry and Technology* **2023**, *51* (1), 101−110.
(126) Ruthwik, N.; Kavya, D.; Shadab, A.; Lingaiah, N.; Sumana, C. Thermodynamic analysis of chemical looping combustion integrated oxidative dehydrogenation of propane to propylene with CO_2. *Chem. Eng. Process.* **2020**, *153*, 107959.
(127) Chen, X. X.; Sun, Z.; Kuo, P. C.; Aziz, M. Carbon-negative olefins production from biomass and solar energy via direct chemical looping. *Energy.* **2024**, *289*, 129943.
(128) Oing, A.; von Muller, E.; Donat, F.; Müller, C. R. Material engineering solutions toward selective redox catalysts for chemical-looping-based olefin production achemes: a review. *Energy Fuels* **2024**, *38* (18), 17326−17342.
(129) Nurdiawati, A.; Zaini, I. N.; Aziz, M. Dual-stage chemical looping of microalgae for methanol production with negative-carbon emission. *Energy Procedia.* **2019**, *158*, 842−847.
(130) Xiang, D.; Li, P. P.; Xia, Y. Y. Conceptual design and techno-economic analysis of a novel propane dehydrogenation process integrated with chemical looping combustion and CO_2 hydrogenation. *Energ. Convers. Manage.* **2023**, *281*, 116820.
(131) Su, G. C.; Zulkifli, N. W. M.; Liu, L.; Ong, H. C.; Ibrahim, S.; Yu, K. L.; Wei, Y. F.; Bin, F. Carbon-negative co-production of methanol and activated carbon from bagasse pyrolysis, physical activation, chemical looping, and methanol synthesis. *Energ. Convers. Manage.* **2023**, *293*, 117481.
(132) Zhao, Y. X.; Zhao, Y. J.; Wang, J. C.; Bao, W. R.; Chang, L. P. Highly simplified and efficient process for methanol and ammonia synthesis from coke-oven gas and pulverized coke using chemical looping technology. *Int. J. Hydrogen Energ.* **2023**, *48* (99), 39330−39346.
(133) Kathe, M.; Sandvik, P.; Fryer, C.; Kong, F. H.; Zhang, Y. T.; Grigonis, G.; Fan, L. S. Coal refining chemical looping systems with CO_2 as a co-feedstock for chemical syntheses. *Energy Fuels.* **2018**, *32* (2), 1139−1154.
(134) Demirel, Y.; Matzen, M.; Winters, C.; Gao, X. Capturing and using CO_2 as feedstock with chemical looping and hydrothermal technologies. *Int. J. Energ. Res.* **2015**, *39*, 1011−1047.
(135) Castellanos-Beltran, I. J.; Perreault, L. S.; Braidy, N. Application of Ni-spinel in the chemical-looping conversion of CO_2 to CO via induction-generated oxygen vacancies. *J. Phys. Chem. C.* **2021**, *125* (13), 7213−7226.
(136) Guan, Y.; Liu, Y. H.; Song, H. C.; Wang, B.; Zhang, G. H.; Wang, Y. Y. High-reactive and coke-resistant polyhedral NiO/Fe_2O_3 oxygen carrier for enhancing chemical looping CH_4-CO_2 dry reforming. *J. Clean. Prod.* **2024**, *447*, 141490.
(137) Surywanshi, G. D.; Patnaikuni, V. S.; Vooradi, R.; Kakunuri, M. CO_2 capture and utilization from supercritical coal direct chemical looping combustion power plant-comprehensive analysis of different case studies. *Appl. Energ.* **2021**, *304*, 117915.
(138) Ouyang, T.; Jin, B.; Mao, Y.; Wei, D.; Liang, Z. W. Control of strong electronic oxide-support interaction in iron-based redox catalysts for highly efficient chemical looping CO_2 conversion. *Appl. Catal. B-Environ. Energy.* **2024**, *343*, 123531.
(139) Haribal, V. P.; Wang, X. J.; Dudek, R.; Paulus, C.; Turk, B.; Gupta, R.; Li, F. X. Modified ceria for "Low-Temperature" CO_2 utilization: a chemical looping route to exploit industrial waste heat. *Adv. Energy Mater.* **2019**, *9* (41), 1901963.
(140) Zaidi, A.; de Leeuwe, C.; Spallina, V. Bi-metallic Ni-Fe LSF perovskite for chemical looping hydrogen application. *Powder Technol.* **2024**, *436*, 119510.
(141) Tasioula, M.; Theofanidis, S. A.; de Clermont Gallerande, E.; Christodoulou, A.; Antzaras, A. N.; Delikonstantis, E.; Sahle, C. J.;

https://doi.org/10.1021/acs.iecr.4c03713
Ind. Eng. Chem. Res. XXXX, XXX, XXX−XXX

Longo, A.; Lemonidou, A. A. CO_2 utilization and on-purpose ethylene production: a chemical looping approach. *Appl. Catal. B: Environ. Energy*. **2025**, *362*, 124757.
(142) Guo, H. Z.; Harrison, A. R. P.; Gao, M. C.; Zhang, X. S.; Chen, Q. C.; Cui, Z. F.; Nie, B. J. Chemical looping based low-pressure ammonia synthesis. *Chem. Eng. J.* **2024**, *500*, 157321.

https://doi.org/10.1021/acs.iecr.4c03713
Ind. Eng. Chem. Res. XXXX, XXX, XXX−XXX